Grant Title: **3-D Coronal-Solar Wind Energetic Particle Acceleration (C-SWEPA) module**
Year 4 (2016) Report
PI: Nathan A. Schwadron
University of New Hampshire
8 College Road, Durham, NH 03824
Grant Number: NNX13AI75G

TABLE OF CONTENTS

I. C-SWEPA Objectives:

Acute space radiation hazards pose one of the most serious risks to future human and robotic exploration. Large Solar Energetic Particle events (*SEP events***,** including ions; also called Solar Particle Events, SPEs**)** are dangerous to astronauts and equipment. To mitigate the hazard they pose, we must develop the ability to predict when and where they will occur, and we must provide adequate shielding against them.

C-SWEPA combines two successful LWS strategic capabilities to produce a synthesis with transformational potential on many fronts. C-SWEPA integrates the Earth-Moon-Mars Radiation Environment Modules [EMMREM, Schwadron et al., 2010], describing energetic particles and their effects, with the Next Generation Model for the Corona and Solar Wind developed by the Predictive Science, Inc. (PSI) group. Our goal is to develop a coupled model that describes the conditions of the corona, solar wind, CMEs and associated shocks, particle acceleration and propagation via physics-based modules.

Assessing the threat of SPEs is a difficult problem. The largest SPEs typically arise in conjunction with X-class flares and very fast (>1000 km/s) coronal mass ejections (CMEs). These events are usually associated with complex sunspot groups (also known as active regions) that harbor strong, stressed magnetic fields. Highly energetic protons generated in these events travel near the speed of light and can arrive at Earth minutes after the eruptive event. The generation of these particles is, in turn, believed to be primarily associated with **the shock wave formed very low in the corona by the passage of the CME** (injection of particles from the flare site may also play a role). Whether these particles actually reach Earth (or any other point) is governed by whether the shock is magnetically connected to the location of interest, which depends on the structure of the magnetic field and local shock properties.

Practical threat assessment faces many challenges. The fast arrival time of the most dangerous particles means that a useful prediction must be carried out prior to the actual flare/CME event. Many fast CMEs do not produce significant radiation storms either because few energetic particles are generated or because they miss Earth. To predict energetic particle generation by a CME and associated shock, a detailed description of ambient conditions (e.g., Alfvén speed) is necessary, and the shock propagation from the low corona must be modeled. An acceleration and propagation model for the energetic particles is necessary to estimate particle fluxes. Finally, a radiation transport model is required to estimate radiation dose-related quantities.

C-SWEPA's central objective is to develop and validate a numerical framework of physics-based modules to couple the low corona, CMEs, shocks, solar wind, and energetic particle acceleration. Using pre-existing EMMREM modules, we characterize time-dependent radiation exposure in interplanetary space environments. Simulated observers provide synthetic probes of the space environment specifying solar wind conditions, energetic particle fluxes and MHD fluctuations. Model results are used in validation studies through comparisons with observations from widely distributed spacecraft.

C-SWEPA as originally proposed had a budget almost three times the budget that was granted. Efficiencies were found by focusing on the key elements central to the proposal. These elements define the core goals of the project:

Goal 1: Scientifically explore the seed populations and acceleration of energetic particles in the low corona, through interplanetary space, and over broad longitudinal regions

Goal 2: Couple the energetic particle acceleration model (EPREM, the energetic particle radiation environment model) with MHD models that describe the propagation of coronal mass ejections from the low coronal plasma environment through the interplanetary medium.

Goal 3: Validate results the coupled EPREM and EMMREM models with observations at distributed observers near 1 AU and out beyond Mars. Validation extends across our understanding of radiation induced hazards from solar energetic particles and galactic cosmic rays at Earth down to atmospheric levels, out into deep space and to Mars and beyond.

Goal 4: Extend key data sets useful for the project: shock parameters at 1 AU, CME propagation data, and radiation environment data through the inner heliosphere.

Deliverables to the CCMC include the EPREM model available for coupling with MHD models such as ENLIL, the PREDICCS (Predictions of radiation from REleASE, EMMREM, and Data Incorporating CRaTER, COSTEP, and other SEP measurements - is an on-line system to predict and forecast the radiation environment through interplanetary space) on-line radiation environment models, and a cone-model version of EPREM for rapid predictions of SEP events.

C-SWEPA's role in national and international teams. The C-SWEPA project lies at the cross-roads between a number of important national and international efforts, which we list here and refer to throughout the report:

- *The Cosmic Ray Telescope the for the Effect of Radiation (CRaTER) team (http://crater.unh.edu)* CRaTER is a cosmic ray telescope on the Lunar Reconnaissance Orbiter [Spence et al.., 2010; Schwadron et al., 2012]. CRaTER measures and characterizes the deep space radiation environment in terms of linear energy transer spectra of galactic cosmic rays and solar energetic particle. Through comparison between CRaTER measurements and radiation models developed as a part of the EMMREM and C-SWEPA projects, we investigate the effects of shielding and test models of radiation effects.
- *The Dynamic Response of the Environments at Asteroids, the Moon, and the Moons of Mars (DREAM and DREAM2 Projects, http://ssed.gsfc.nasa.gov/dream/).* Airless bodies like the Moon, the moons of Mars, or near earth asteroids (NEAs), are exposed to an energetic particle radiation environment that can significantly affect their surfaces. This environment comprises slowly varying, yet highly energetic galactic cosmic rays (GCRs) and sporadic, lower energy solar energetic particles (SEPs). Significant progress on C-SWEPA with energetic particle and cosmic ray modeling provides essential input for the DREAM2 team.
- *The Sun-2-Ice team (http://sun-2-ice.sr.unh.edu).* The NSF "Sun-to-Ice" project goals are to understand the chain linking solar energy and particle acceleration on the Sun, with the impact on Earth's atmosphere, chemistry, precipitation and ice chemistry. The project investigates signals frozen in polar ice, or other proxies, to discover the history of the extreme solar events that have affected the planet. The Sun-to-Ice project is happening at

an opportune moment, with the unusual Solar Maximum in 2012 and 2013. The benefits it provides include ultimately increasing the predictability of extreme energy from the Sun reaching Earth's atmosphere, and the effects of that energy on Earth, from affecting power grids to creating the aurora borealis and australis. The Sun-2-Ice project has benefitted significantly from SEP event modeling via C-SWEPA. Identification of the acceleration regions deep in the solar corona of prompt solar particle events has allowed critical insights into the source of the high energy SEP fluxes [Schwadron et al., 2015] that directly affect atmospheric chemistry. This topic exemplifies the chain of events of energetic coupling between the Sun and the Earth during explosive solar events. The Sun-2-Ice project has now reached substantial closure on affirming and strengthening one of the links in the chain. These results are central to the interdisciplinary project.

- *The Solar Probe Plus team (http://solarprobe.jhuapl.edu)* Solar Probe Plus is humanities first mission to directly probe the environment near the Sun. Insights from C-SWEPA into particle acceleration low in the corona will be essential for providing testable predictions for the Solar Probe Plus investigation. The tools developed by C-SWEPA will be essential for developing a global context in which to understand and investigate the origins of solar energetic particles.
- *The International Team on Radiation Interactions. (http://www.issibern.ch/teams/interactplanetbody/)* Recent measurements of galactic cosmic radiation and solar energetic particle radiation at planetary bodies including the Moon, Mars and the potentially new measurements at other planetary objects (e.g., the moons of Mars) raise new fundamental questions about how radiation interacts at planetary bodies and what its long term impacts are. The ISSI team advances the study of radiation interactions and enables development of a truly cross-disciplinary effort that facilitates a unified approach to the problem involving international cooperation across different participating teams and those in formation. The project relies in part on accurate modeling of energetic particles and the input via C-SWEPA provides critical enabling input to the team.

II. C-SWEPA Accomplishments:

II.1 C-SWEPA Progress in Understanding of Protracted Minimum of Cycle 23/24 and the Mini Maximum Cycle 24

The deep solar minimum between cycles 23 and 24 and the activity in cycle 24 differed significantly from those of the prior cycle (Schwadron et al., 2011; McComas et al., 2013). In the solar minimum, the fast wind was slightly slower, was significantly less dense and cooler, had lower mass and momentum fluxes (McComas et al., 2008), and weaker heliospheric magnetic fields (Smith et al., 2008). During the rise of activity in cycle 24 the mass flux of solar wind remained low, (McComas et al., 2013b) and the magnetic flux of the heliosphere remained at significantly lower levels than observed at previous solar maxima in the space age (Smith et al., 2013). (McComas et al.,, 2013b) showed that the current "mini" solar maximum of cycle 24 has shown only a small recovery in particle and magnetic fluxes. Therefore, the cycle 24 mini solar maximum continues to display the same trends as observed in the cycle 23-24 minimum. In fact, conditions during the cycle 23-24 minimum appear to be similar to conditions at the beginning of the 1800's at the start of the Dalton Minimum (Goelzer et al., 2013). Taken together, these recent changes suggest that the next solar minimum may continue to show declining sunspot numbers,

associated with declining values of magnetic flux and further reductions in solar wind particle flux.

Using the model from Schwadron et al. (2010) and monthly average sunspot numbers, Goelzer et al. (2013) were able to compute a monthly average HMF intensity from 1749 to the present. For comparison, Goelzer et al (2013) looked at the work of McCracken (2007), who modeled the HMF intensity from the levels of paleogenic nucleotide ^{10}Be and the Omni2 data, which is available back to 1963. These three estimations of flux as well as sunspot number are shown in Figure II.1.1, with a strong correlation and a clear hysteresis.

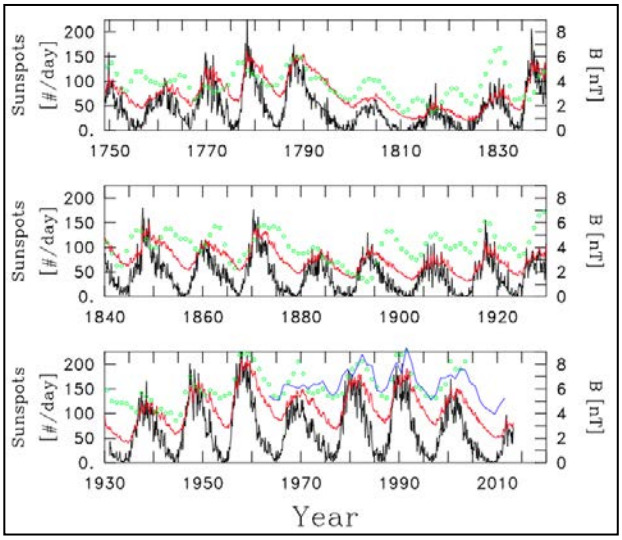

Figure II.1.1: *(black) Monthly ave SSN. (red) Predicted Parker comp. of the HMF intensity. (green) Yearly ave HMF intensity derived from ^{10}Be data. (blue) Measured yearly aves of HMF intensity (Smith et al. [2013]) from the Omni2 data.*

The anomalously weak heliospheric magnetic field and low solar wind flux during the last solar minimum have resulted in galactic cosmic rays (GCRs) achieving the highest flux levels observed in the space age (Mewaldt et al., 2010), and fluxes continue to be unusually elevated through the cycle 24 maximum. It is unknown if the recent anomalous deep solar minimum hints at larger changes in the near future, or if the unusual changes in GCR fluxes and conditions on the Sun have an impact on Earth's atmosphere. Given the fact that GCR radiation can damage living tissue, causing cellular mutagenesis, the changing state of the Sun may have long-term implications for life on the planet. Figure 2 illustrates the critical growing record of dose rate throughout the LRO mission that quantifies the changing conditions and radiation hazards posed by GCRs and SEPs. Pronounced discrete SEP events punctuate the underlying trend of diminishing long-term GCR doses.

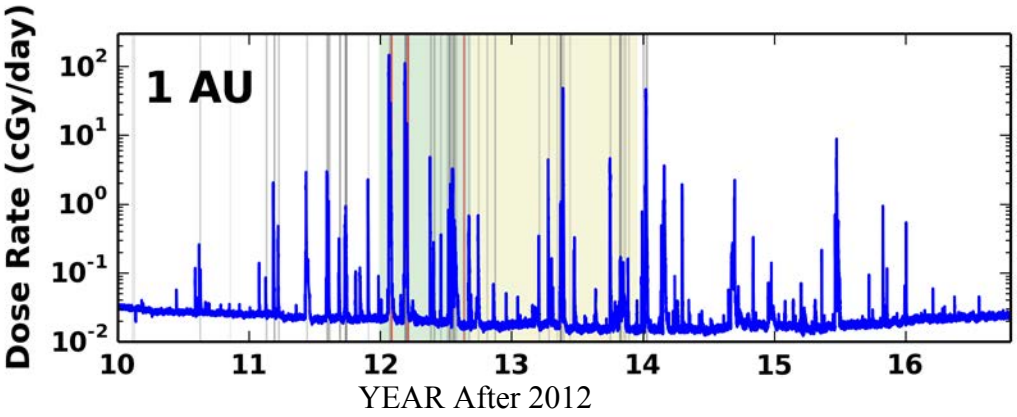

Figure II.1.2. *Dose Rates over time through the quantify radiation hazards that damage tissue, materials, and chemically change materials such as lunar regolith. The green region shows the 2012 period of most intense activity, the yellow region shows the second increase in activity of cycle 24. Grey lines indicate flux ropes and have a shading level corresponding to the peak speed of flux ropes. Red lines indicate a number of prominent flux ropes studied intensely.*

Figure II.1.2 reveals SEP events consistent with a double-peaked solar cycle. We further observe that the underlying GCR dose rate is now on the rise and has been rising since July, 2014. It would appear that the solar cycle 24 maximum is complete and the heliospheric modulation of GCRs is diminishing as we move toward the cycle 24-25 solar minimum.

The extremely high energies of GCRs make them both relevant to biology on the Earth, and also one of the greatest hazards for long-term space exploration. In deep interplanetary space and away from the shielding of Earth's atmosphere and magnetic field, these high energy particles are difficult to shield against, as some particles surpass a billion electron volts of kinetic energy. The effects of GCRs on the Earth system, including the biosphere, remain poorly understood and are oftentimes highly controversial (Shaviv and Veizer, 2003); this is because GCRs not only present a hazard to life through the breakdown of DNA, but also may help to stimulate evolution by increasing the rate of cell mutation (Todd, 1994). For example, a recent study of global diversity from paleontological data suggests there is a significant cycle of approximately 62 million years over which biodiversity rises and then falls; this cycle as of yet has no agreed upon cause but may be driven by extraplanetary processes (Rohde and Muller, 2005).

Schwadron et al. (2014a) used results of CRaTER, C-SWEPA, PREDICCS and EMMREM to understand implications of the changing space environment for human exploration. Several key results are shown in Figures II.1.3 and II.1.4. Figure II.1.3 shows the evolution of GCR dose over time based on C-SWEPA and EMMREM modeling and data from CRaTER and ACE. The implication of the weakening interstellar magnetic field is that the observed dose rates at successive solar minima and successive solar maxima have been increasing with time. It remains to be seen whether these changing conditions will persist. The latest trends demonstrate that the space environment is becoming increasingly hazardous and present a limiting factor for human exploration beyond LEO.

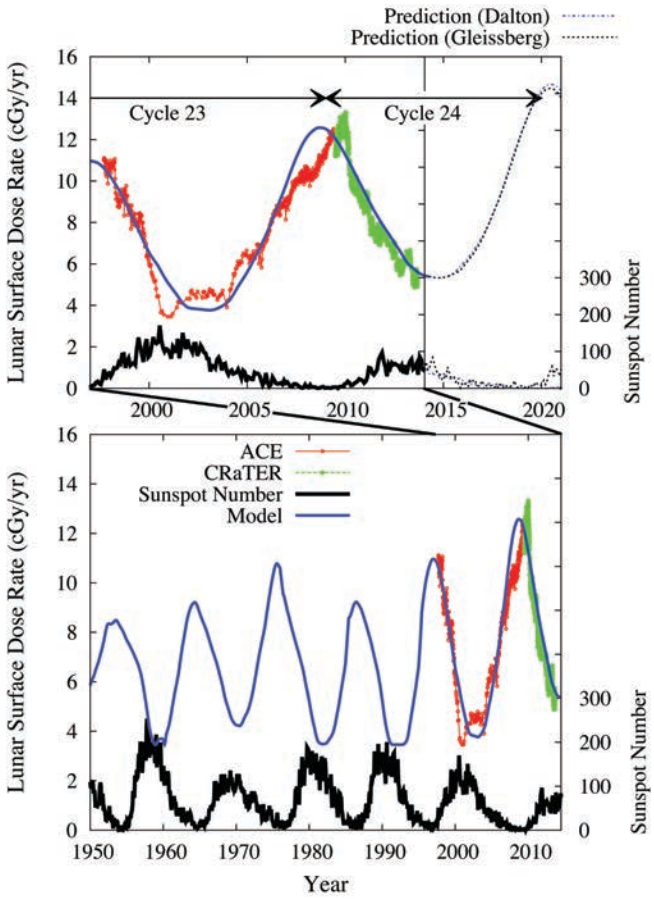

Figure II.1.3. *Evolving and increasingly hazardous radiation levels in space. (top) ACE dose rates (red) are based on fits to CRIS spectra; CRaTER measurements (green) from the zenith-facing D1/D2 detectors are used as proxies for lens dose rates behind 0.3 g/cm2 Al shielding. The sunspot number predictions (the lower black and blue dashed lines) show two cases based on a Gleissberg-like and a Dalton-like minimum, the results of which are similar. The dose predictions (solid blue line and the upper black and blue dashed lines) are from a sunspot-based model of the heliospheric magnetic field and the correlated variation in modulation of GCRs. The ACE data, CRaTER data, and model results are projected to the lunar surface. (bottom) Same as top panel but for a longer time span.*

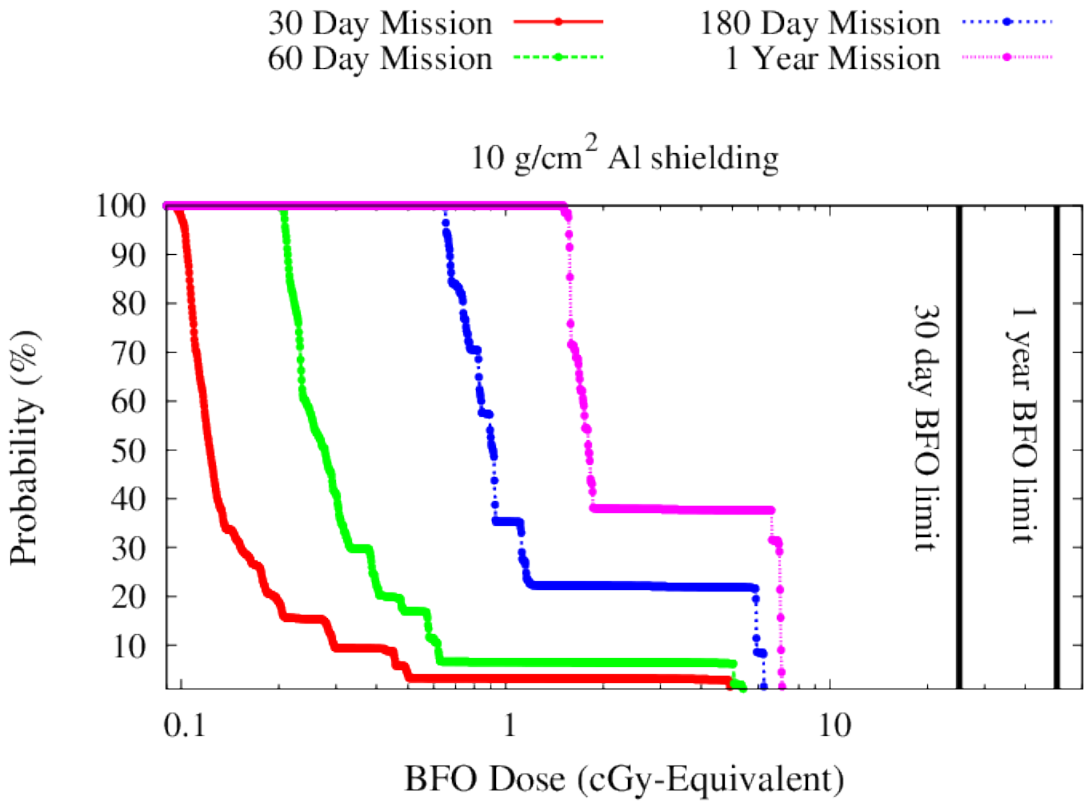

Figure II.1.4. *Probability (%) versus integrated BFO dose for 30 day to 1 year missions. We use the PREDICCS database (http://prediccs.sr.unh.edu) to build up statistics for the probability of SEP events of varying integrated dose behind spacecraft shielding (10 g/cm^2). The database currently provides doses for the period from July 2011 through April 2014. The PREDICCS doses are derived from proton spectra and use dose in 10 g/cm^2 water as a proxy for the blood forming organ (BFO) dose.*

Recently, *Rahmanifard et al*. (2017) extended previous studies of solar conditions including the prolonged solar minimum (2005-2009) and a solar maximum that has not fully recovered in terms of the Heliospheric Magnetic Field (HMF) strength when compared to the previous maximum values. These anomalies may indicate that we are entering an era of lower solar activity than observed at other times during the space age. *Rahmanifard et al*. (2017) studied past solar grand minima, especially the Maunder period (1645-1715) to gain further insight into grand minima. *Rahmanifard et al*. (2017) find the timescale parameters associated with three processes (Figure II.1.5) attributed to the magnetic flux balance in the heliosphere using chi-square analysis. In addition, *Rahmanifard et al*. (2017) find inversions in the heliospheric magnetic field (Figure II.1.6) also play an important role in the evolution of the magnetic field. *Rahmanifard et al*. (2017) use HMF time series reconstructed based on geomagnetic data and near-Earth spacecraft measurements (OMNI) data to find the fundamental timescales that influence heliospheric field evolution through conversion or opening of magnetic flux from coronal mass ejections (CMEs) into the ambient heliospheric field, removal or loss of the ambient heliospheric field through magnetic reconnection, and interchange reconnection between CME magnetic flux and ambient heliospheric magnetic flux. The observed correlation between coronal mass ejection rates and sunspot number (Figure II.1.7) allows for direct reconstruction of the heliospheric magnetic field. *Rahmanifard et al*. (2017) also investigate the existence of a floor in the heliospheric magnetic flux, in the absence of CMEs, and show that it is not required to describe the HMF evolution. The

minimum value for the HMF at 1 AU in the model predicted historic record is 3.13 $\pm$ 0.40 nT. The model results (Figure II.1.8) favorably reproduce paleocosmic data and near-Earth spacecraft measurements data and show how the heliospheric magnetic field may evolve through periods of extremely low activity. The improved understanding in the evolution of the heliospheric magnetic field provides an essential framework on which we base estimates of the evolving radiation environment.

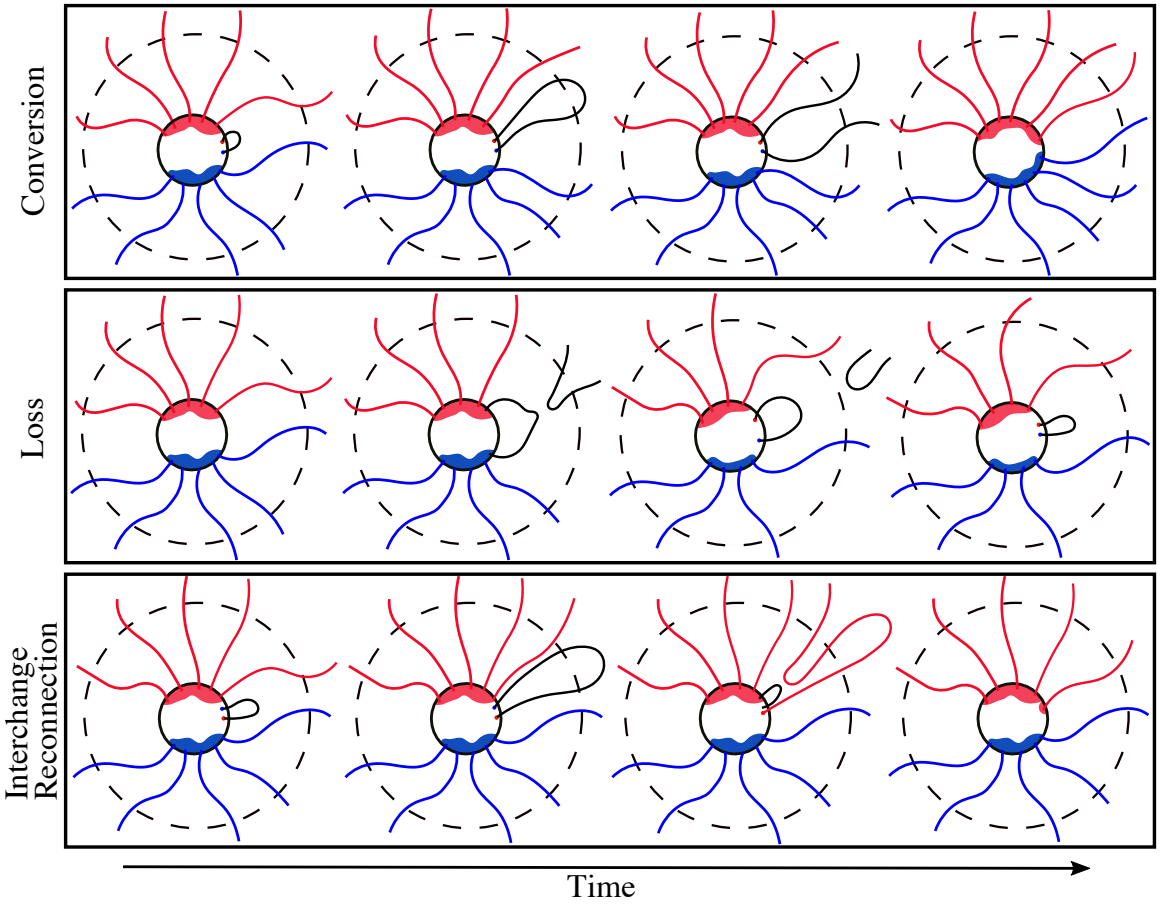

Figure II.1.5. Three processes responsible for transformation of CMEs, conversion (top), loss (middle) and interchange reconnection (bottom). **The top panel** shows conversion of transient CME magnetic flux to ambient heliospheric magnetic flux. When the closed flux has the same polarity as the surrounding ambient flux, the magnetic loop is dragged out into the solar wind beyond the Alfvén surface (shown in dashed line), and eventually becomes a component of the ambient HMF. **The middle panel** shows loss of heliospheric and CME magnetic flux which closes heliospheric magnetic flux below the Alfvén surface and releases inverted U-shaped field structures. This process is responsible for removing excessive open flux and limits the growth of the HMF. **The bottom panel** shows interchange reconnection, which occurs when CME-associated magnetic flux undergoes magnetic reconnection with the ambient HMF and reconfigures the magnetic fields. This figure is adapted from *Schwadron et al*. [2010].

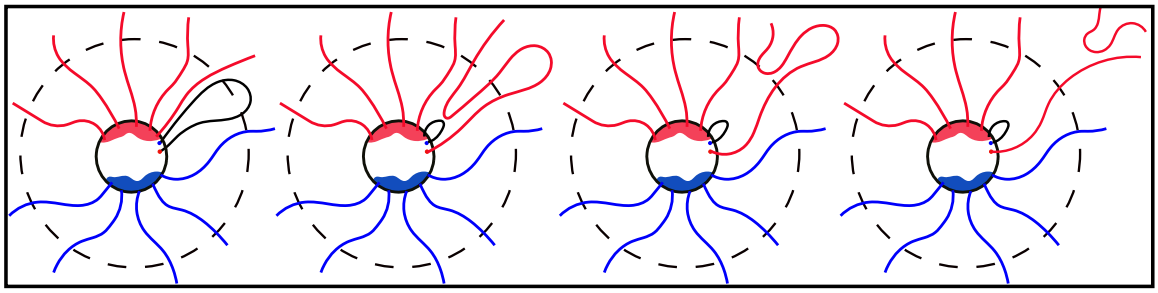

Figure II.1.6. HMF inversions can be created when the "switched-back" field segment is dragged out beyond the Alfvén surface by the solar wind after magnetic reconnection occurs between an open field line and a closed field line within a CME or a part of a flux rope [*Owens et al*., 2013].

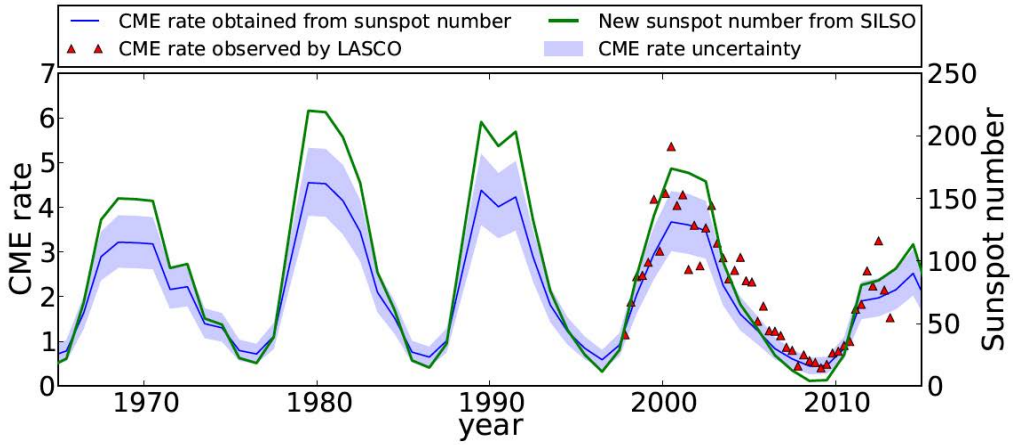

Figure II.1.7. CME rate derived from sunspot number (blue curve) using Equation 3 is compared to CME rates (red triangles) observed by LASCO. The shaded blue area shows the uncertainty caused by sunspot number uncertainty and the uncertainty of the linear relationship parameters obtained by chi-square method. The green line shows the new sunspot number released by SILSO.

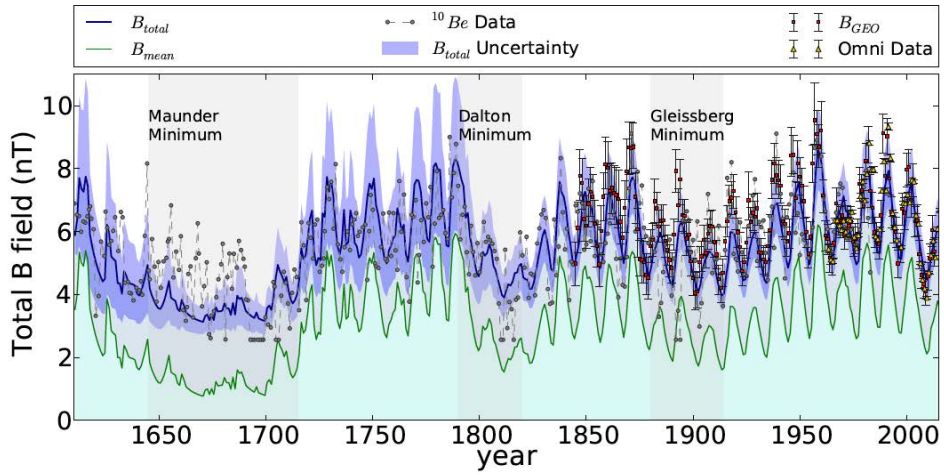

Figure II.1.8. The simulated heliospheric mean field is shown in green. The simulated HMF (B_{total}) is shown in dark blue with blue uncertainty region, found by adding 2.36 ± 0.08 nT to the mean magnetic field. The HMF estimates based on ^{10}Be data are shown with grey circles, the reconstructed HMF based on geomagnetic data is shown in red squares with error bars and OMNI data points are shown with yellow triangles. We use geomagnetic-based data and OMNI data as the data points in chi-square analysis.

Relevant Publications

- Goelzer, M. L., Smith, C. W., Schwadron, N. A., and McCracken, K. G., An analysis of heliospheric magnetic field flux based on sunspot number from 1749 to today and prediction for the coming solar minimum, Journal of Geophysical Research (Space Physics), 118, 7525, 2013
- Schwadron, N. A., Smith, S., and Spence, H. E., The CRaTER Special Issue of Space Weather: Building the observational foundation to deduce biological effects of space radiation, Space Weather, 11, 47, 2013
- McComas, D. J., Angold, N., Elliott, H. A., Livadiotis, G., Schwadron, N. A., Skoug, R. M., and Smith, C. W., Weakest Solar Wind of the Space Age and the Current "Mini" Solar Maximum, The Astrophysical Journal, 779, 2, 2013
- Smith, C. W., Schwadron, N. A., and DeForest, C. E., Decline and Recovery of the Interplanetary Magnetic Field during the Protracted Solar Minimum, The Astrophysical Journal, 775, 59, 2013
- Joyce, C. J., Schwadron, N. A., Wilson, J. K., Spence, H. E., Kasper, J. C., Golightly, M., Blake, J. B., Townsend, L. W., Case, A. W., Semones, E., Smith, S., and Zeitlin, C. J., Radiation modeling in the Earth and Mars atmospheres using LRO/CRaTER with the EMMREM Module, Space Weather, 12, 112, 2014
- Schwadron, N. A., Blake, J. B., Case, A. W., Joyce, C. J., Kasper, J., Mazur, J., Petro, N., Quinn, M., Porter, J. A., Smith, C. W., Smith, S., Spence, H. E., Townsend, L. W., Turner, R., Wilson, J. K., and Zeitlin, C., Does the worsening galactic cosmic radiation

environment observed by CRaTER preclude future manned deep space exploration?, Space Weather, 12, 622, 2014a

- Smith, C. W., McCracken, K. G., Schwadron, N. A., and Goelzer, M. L., The heliospheric magnetic flux, solar wind proton flux, and cosmic ray intensity during the coming solar minimum, Space Weather, 12, 499, 2014
- Schwadron, N. A., Goelzer, M. L., Smith, C. W., Kasper, J. C., Korreck, K., Leamon, R. J., Lepri, S. T., Maruca, B. A., McComas, D., and Steven, M. L., Coronal electron temperature in the protracted solar minimum, the cycle 24 mini maximum, and over centuries, Journal of Geophysical Research (Space Physics), 119, 1486, 2014b
- Zeitlin, C., Case, A. W., Schwadron, N. A., Spence, H. E., Mazur, J. E., Joyce, C. J., Looper, M. D., Jordan, A., Rios, R. R., Townsend, L. W., Kasper, J. C., Blake, J. B., Smith, S., Wilson, J., and Iwata, Y., Solar modulation of the deep space galactic cosmic ray lineal energy spectrum measured by CRaTER, 2009-2014, Space Weather, 14, 247, 2016
- Rahmanifard, F., Schwadron, N. A., Smith, C. W., McCracken, K. G., Duderstadt, K. A., Lugaz, N., and Goelzer, M. L., Inferring the Heliospheric Magnetic Field Back through Maunder Minimum, The Astrophysical Journal, 837, 165, 2017
-

Relevant Presentations

- Schwadron, N. A., Earth Moon Mars Radiation Environment Module, LWS Workshop, Princeton, NJ, Sept 18-20, 2013
- Schwadron, N., Spence, H., and Wilson, J., Lunar radiation environment, 40th COSPAR Scientific Assembly. Held 2-10 August 2014, in Moscow, Russia, Abstract B0.1-4-14., 40, 2014
- Schwadron, N. A. , Implications of the Worsening GCR Radiation Environment, Space Radiation Environment, Space Weather Week, Boulder CO, April, 2014
- Schwadron, N. A., Implications of the Worsening Space Radiation Panelist International Space Medicine Summit, July, 2014
- Schwadron, N. A., Lunar Radiation Environment, B0.1-0004-14, COSPAR, Moscow, July, 2014
- Schwadron, N. A., Panelist on Radiation Effects, International Space Medicine Summit, Rice, Houston, TX June, 2014
- Schwadron, N. A., Increasing Biological Hazards from Solar Energetic Particles and Cosmic Rays, Space Weather Workshop, Boulder, CO, April 7-11, 2014
- Schwadron, N. A., Particle radiation sources, propagation and interactions in deep space, at Earth, the Moon, Mars, and beyond: Examples of Radiation Interactions and Effects, The Scientific Foundation of Space Weather, ISSI Workshop, June 27 – July 1, (http://www.issibern.ch/workshops/foundationspaceweather/), 2016
-

II.2. C-SWEPA Progress in SEP Radiation Event Modeling

Accurate radiation modeling of SEP events is essential for future risk assessment efforts in the planning of missions. By modeling the transport of energetic particles through the inner heliosphere, the EMMREM module facilitates access to radiation environments beyond the reach of in-situ radiation measurements. Joyce et al. 2015 provides an example of this capability, by using EMMREM to compute dose rates for the massive ICME encountered by STEREO on 23 July 2012, an event which has drawn many comparisons to the historic Carrington event. Using STEREO A energetic proton flux measurements as input, EMMREM was used to compute dose rates at STEREO A for skin/eye as well as blood forming organs (BFO, essentially bone marrow) for levels of shielding corresponding to spacesuit, heavy spacesuit, spacecraft and heavy protective shielding (Figure II.2.1). This analysis shows that while the peak dose rate for the event (1970 cGy-Eq/day) is much higher than for previous large events, the total accumulated dose is less extreme than expected, falling below the Halloween storms of 2003 and above the January and March events measured by CRaTER in 2012 (Joyce et al., 2013). With the benefit of heavy protective shielding, astronauts aboard a spacecraft encountering the event would not have been exposed to levels of shielding above NASA's 30 day limits for skin, eye or BFO.

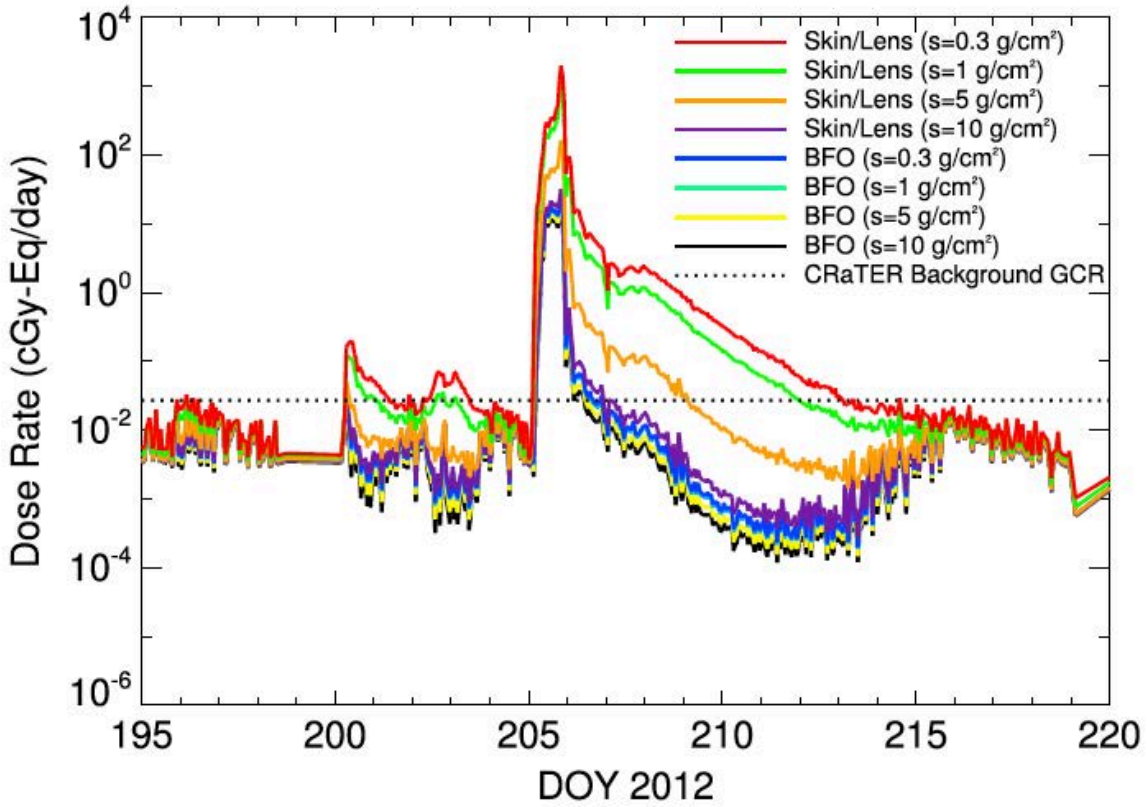

Figure II.2.1. *Radiation levels for the 23 July 2012 ICME as modeled by EMMREM using STEREO A proton flux data as input. The dose rate is shown for skin/eye and BFO for four levels of shielding corresponding to spacesuit, heavy spacesuit, spacecraft, and heavy protective shielding.*

EMMREM is also useful for studying how the radiation seen during an event varies with the position of the observer relative to the ICME. Figure II.2.2 shows the dose rates for the 23 July 2012 event computed at STEREO A and STEREO B using EMMREM and measured by

CRaTER at LRO. Output from the WSA-ENLIL+Cone model generated by the CCMC is used to show the position of each observer relative to the ICME as well as the magnetic fields connecting them to the Sun. The resulting profiles are in good agreement with the findings of Reames (1999), who studied how energetic particle fluxes varied due to position relative to ICMEs.

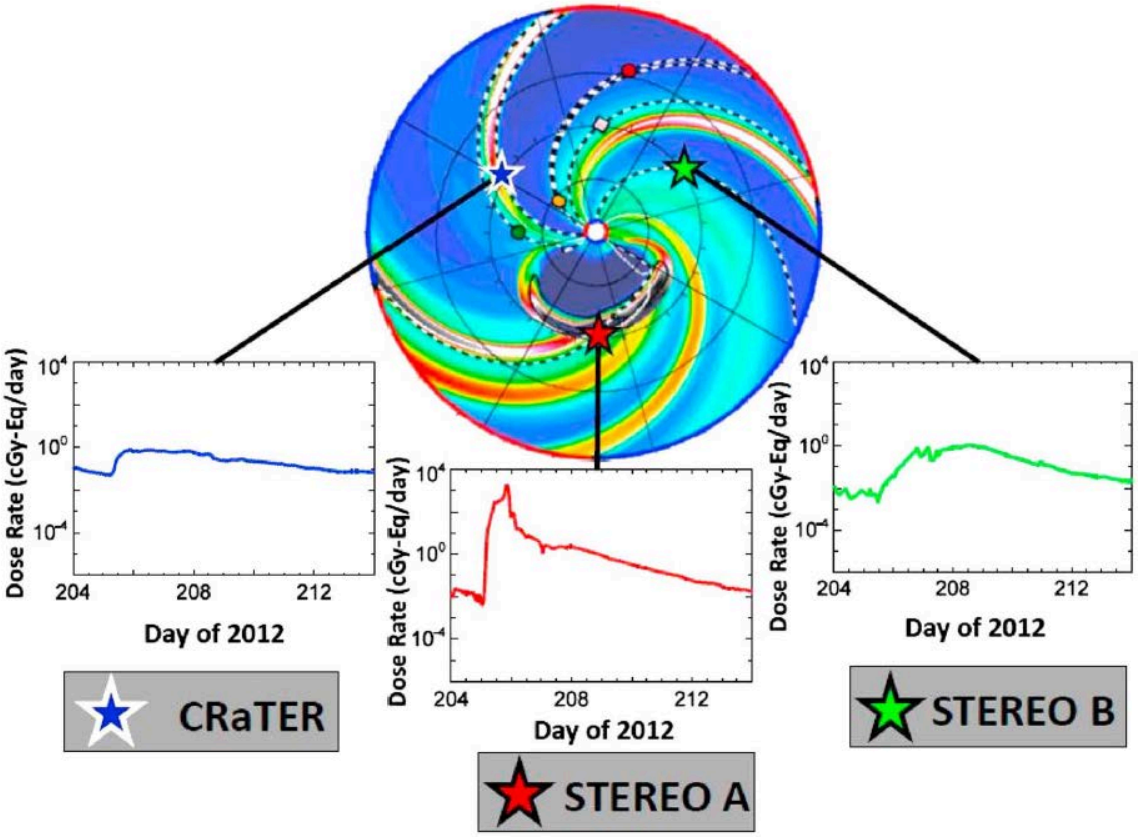

Figure II.2.2. *Dose rates at STEREO A, STEREO B and LRO/CRaTER during the 23 July 2012 event. Output from the WSA-ENLIL+Cone model provided by the CCMC is used to show the position of the observers relative to the ICME. The observed profiles are in keeping with those shown by Reames (1999).*

Relevant Publications

- Joyce, C. J., Schwadron, N. A., Wilson, J. K., Spence, H. E., Kasper, J. C., Golightly, M., Blake, J. B., Mazur, J., Townsend, L. W., Case, A. W., Semones, E., Smith, S., and Zeitlin, C. J., Validation of PREDICCS using LRO/CRaTER observations during three major solar events in 2012, Space Weather, 11, 350, 2013
- Schwadron, N. A., Townsend, L., Kozarev, K., Dayeh, M. A., Cucinotta, F., Desai, M. Golightly, M., Hassler, D., Hatcher, R., Kim, M. Y., Posner, A., PourArsalan, M., Spence, H. E., and Squier, R. K., Earth-Moon-Mars radiation environment module framework, Space Weather, 8, 2010
- Schwadron, N. A., Baker, T., Blake, B., Case, A. W., Cooper, J. F., Golightly, M., Jordan, A., Joyce, C. J., Kasper, J., Kozarev, K., Mislinski, J., Mazur, J., Posner, A., Rother, O., Smith, S., Spence, H. E., Townsend, L. W., Wilson, J., and Zeitlin, C., Lunar radiation environment and space weathering from the Cosmic Ray Telescope for the Effects of Radiation (CRaTER), J. Geophys. Res., 117, 2012

- Clements, E. B., Carlton, A. K., Joyce, C. J., Schwadron, N. A., Spence, H. E., Sun, X., and Cahoy, K., Interplanetary space weather effects on Lunar Reconnaissance Orbiter avalanche photodiode performance, Space Weather, 14, 343, 2016

Relevant Presentations

- Joyce, C. J., et al., Analysis of the potential radiation hazard of the 23 July 2012 SEP event observed by STEREO A using the EMMREM model and LRO/CRaTER, SHINE, Stowe, VT, July 2015

II.3. C-SWEPA Progress in Radiation Modeling Through Atmospheres

Evaluating atmospheric radiation levels is a critical step in the planning future manned missions to Mars and is also an important concern for airline passengers, who are exposed to radiation from energetic particles penetrating the Earth's atmosphere and magnetosphere. The C-SWEPA project utilizes CRaTER measurements together with modeling provided by the EMMREM module to compute GCR radiation levels for various altitudes in the Earth and Mars atmospheres.

Joyce et al. (2013) demonstrated a method for computing the modulation potential, the amount of energy lost by GCRs in transit through the heliosphere, at the Moon using CRaTER GCR dose rate data together with EMMREM-generated lookup tables. Figure II.3.1 shows the evolution of this computed modulation potential over the course of the LRO mission, spanning from the protracted solar minimum of solar cycle 23 to the weak maximum of cycle 24.

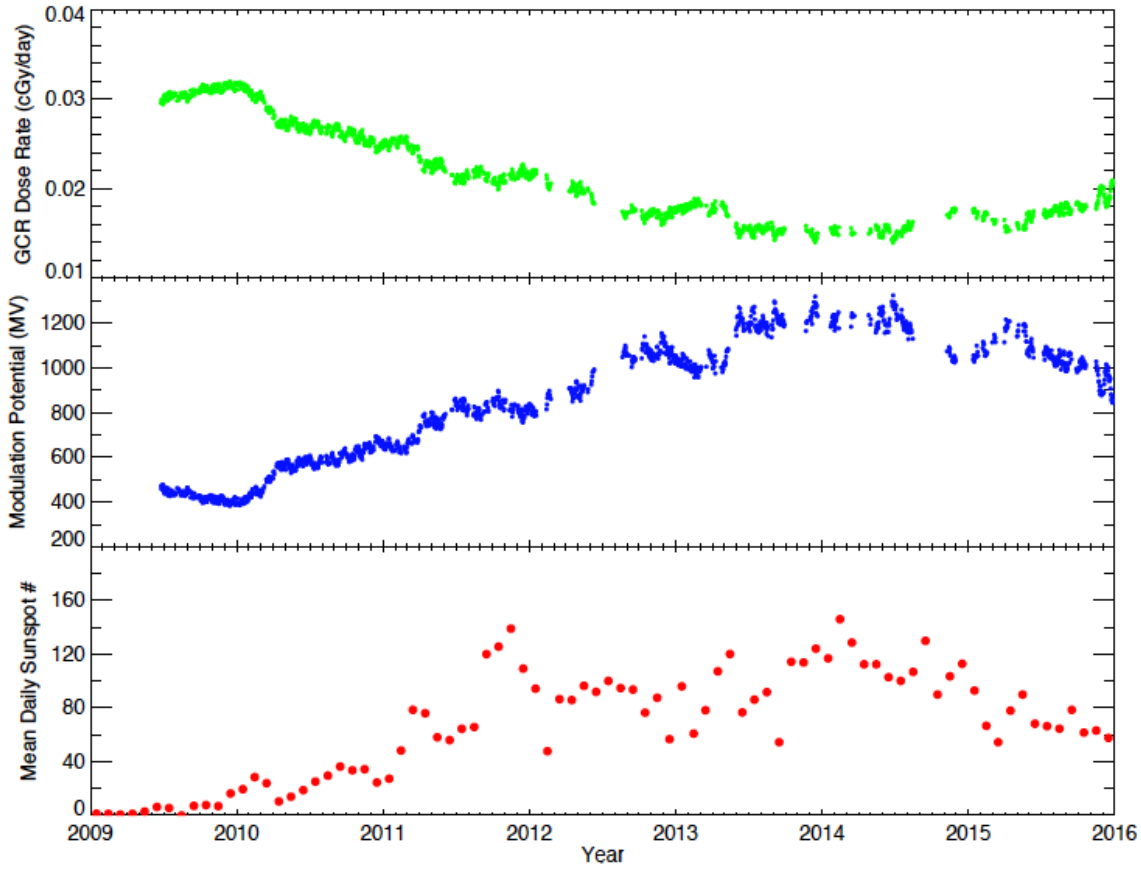

Figure II.3.1. *Computed modulation potential over the course of the LRO mission, computed from GCR dose rates (also plotted) using EMMREM-generated lookup tables. The plot extends from the protracted solar minimum of solar cycle 23 to the weak maximum of cycle 24. The average daily sunspot number is provided by the Solar Influences Data Analysis Center is plotted to provide context within the solar cycle.*

Joyce et al. 2014 used the computed modulation potential plotted in Figure II.3.2 as input to a program based on the formalism of O'Neil (2006) to generate flux spectra of the GCRs incident on the Earth. Then using these fluxes together with similar EMMREM-generated dose tables, computed GCR dose rates in Earth's atmosphere for altitudes extending down to airline levels. A new study in preparation updates this method using improved dose lookup tables as well as a method for computing geomagnetic cutoff rigidities (Nymmik et al., 2009) that enables the model to account for location-dependent effects of the magnetosphere on radiation levels. Additionally, this new study uses measurements from instruments aboard high-altitude balloons and commercial airlines as a means of evaluating the accuracy of the model. Figure II.3.2 shows the comparison between measured and modeled radiation levels for two simultaneous balloon launches in California and New Hampshire, demonstrating the accuracy of the model and its ability to account for magnetospheric effects on radiation levels.

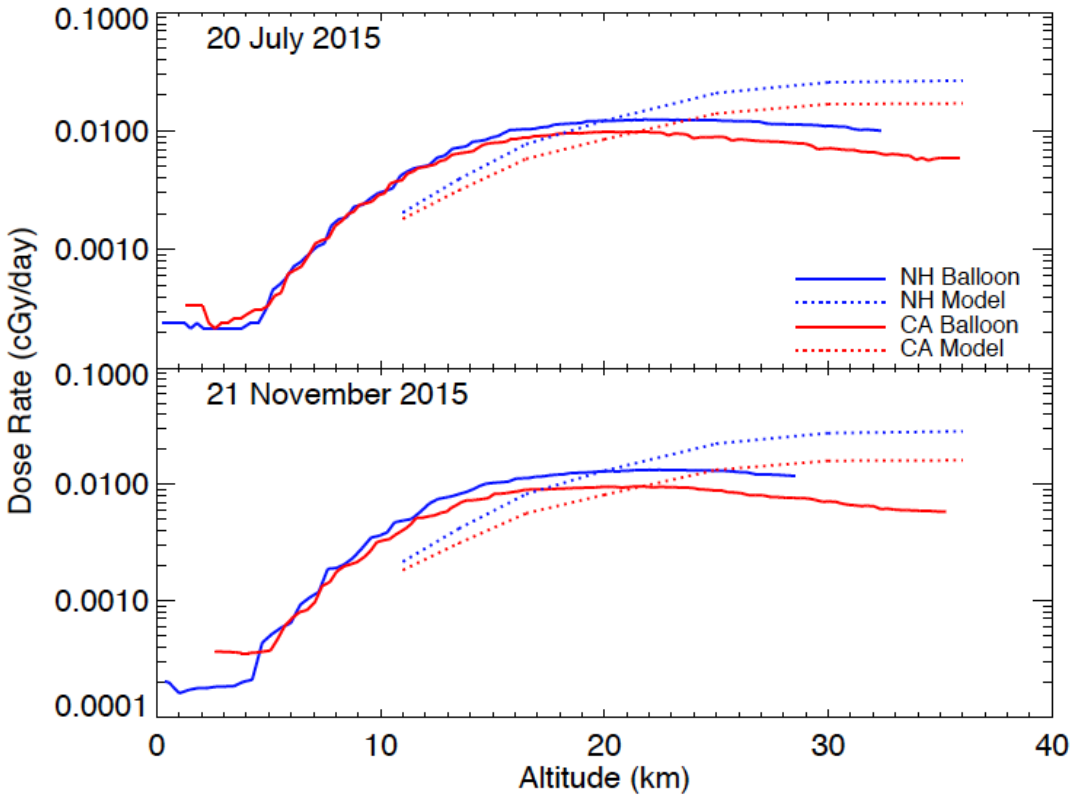

Figure II.3.2. *Radiation levels measured for two simultaneous balloon launches in 2015 and the corresponding modeled dose rates. We see good overall agreement between measurements and model with discrepancies being at least partially due to the balloon instruments measuring gamma rays and X-rays rather than the GCRs and secondary particles used in the model. Since gamma rays and X-rays are produced as secondaries from interactions between the GCRs and the atmosphere, we would expect relatively low levels at high altitudes where the atmospheric density is low and relatively high levels at low altitudes.*

The ARMAS project presents an additional means of comparison by providing radiation measurements from low-cost dosimeters aboard commercial aircraft. Figure II.3.3 shows the comparison between the model and measurements taken from 69 flights spanning from mid 2013 to early 2016. We see good agreement with the modeled dose rates being about 25% greater than the measurements. This discrepancy may partially be due to the dosimeters measuring only protons, electrons and gamma rays and not the heavy ions and neutrons included in the modeling. Latitude, longitude and cutoff rigidity are plotted for each flight to show that variations in the measured dose rates are due to location-dependent variations in the cutoff rigidity.

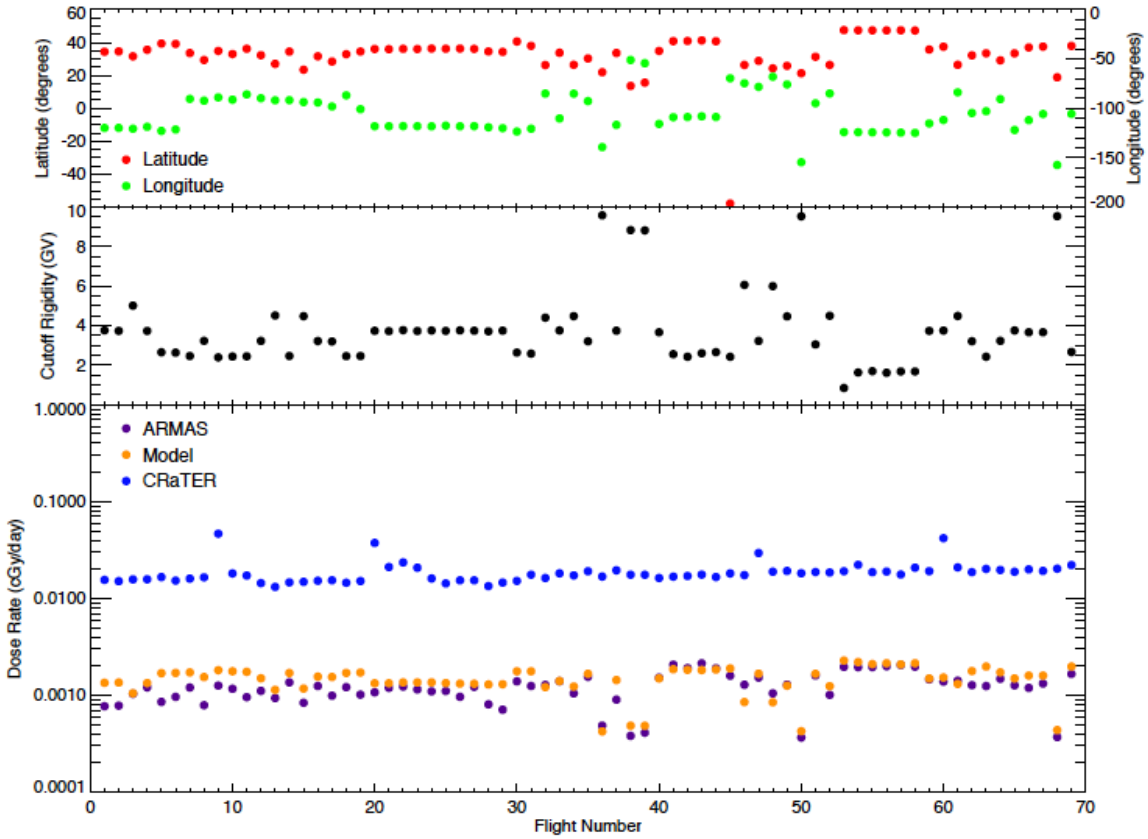

Figure II.3.3. *Radiation measurements made aboard commercial airlines as part of the ARMAS project and the corresponding modeled dose rates for 69 flights spanning from mid 2013 to early 2016. The model overestimates the dose rates by 25% on average. Average latitude, longitude and cutoff rigidity are plotted for each flight to show how geographic position affects the cutoff and resulting radiation, explaining variations seen in the dose rate. The dose rate measured by CRaTER at the time of each flight is also plotted for reference.*

The computed modulation potential shown in Figure II.3.1 can be scaled out to Mars using a simple equation (Schwadron et al. 2010) and used to compute GCR dose rates in the Martian atmosphere using the same EMMREM dose tables used to compute the modulation. Figure II.3.3 shows the results of this analysis. Zeitlin et al. (2013) showed that the Mars Science Laboratory measured an average GCR dose rate of 0.048 cGy/day in transit to Mars from 6 December 2011 to 14 July 2012. Converting from a free space measurement to one in which half the sky is blocked by Mars yields a dose rate of 0.024 cGy/day, somewhat smaller than the 0.03 cGy/day modeled at the highest altitude over this period, which makes sense because the GCR dose rate decreases with proximity to the Sun, thus lending credibility to the model.

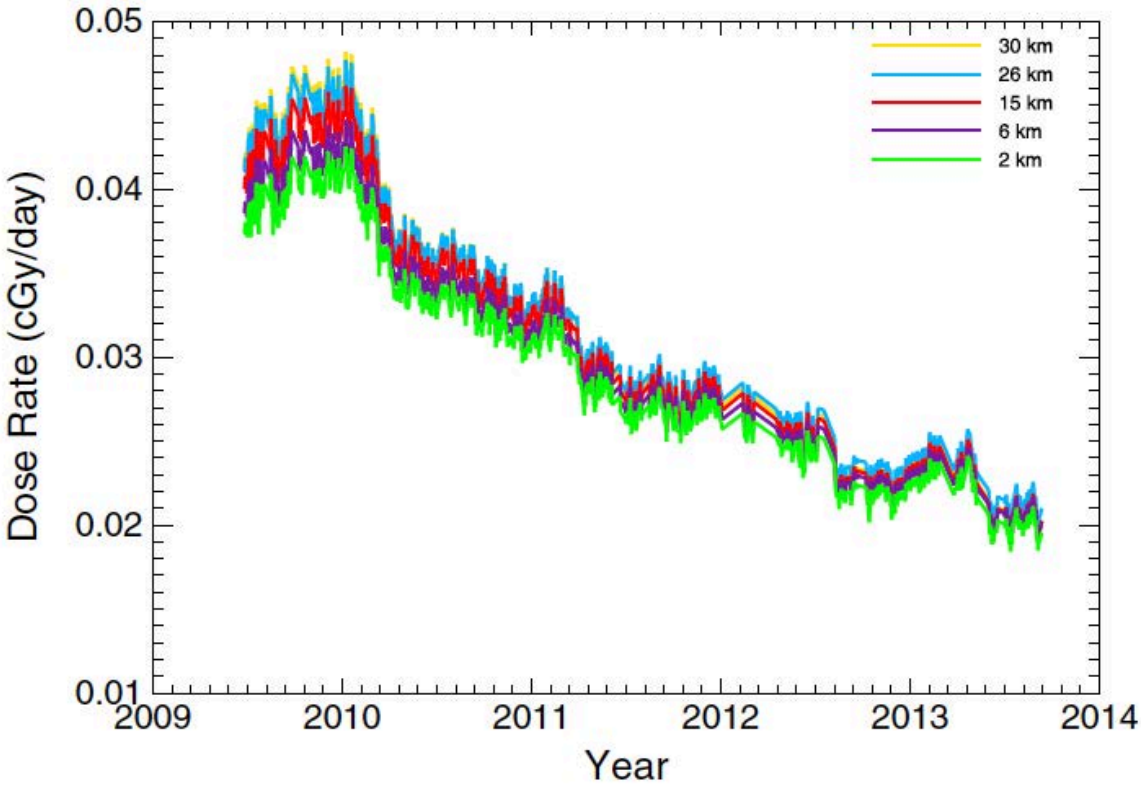

Figure II.3.4. *Modeled GCR dose rates in the Martian atmosphere, computed using EMMREM-generated dose lookup tables and the modulation potential scaled out to Mars. We see that the atmospheric effect on radiation levels at Mars decreases from solar minimum to solar maximum.*

Relevant Publications

- Joyce, C. J., Schwadron, N. A., Wilson, J. K., Spence, H. E., Kasper, J. C., Golightly, M., Blake, J. B., Townsend, L. W., Case, A. W., Semones, E., Smith, S., and Zeitlin, C. J., Radiation modeling in the Earth and Mars atmospheres using LRO/CRaTER with the EMMREM Module, Space Weather, 12, 112, 2014
- Joyce, C. J., et al., Atmospheric radiation modeling of galactic cosmic rays using LRO/CRaTER and the EMMREM model with comparisons to balloon and airline based measurements, (in preparation), 2016
- Schwadron, N. A., Townsend, L., Kozarev, K., Dayeh, M. A., Cucinotta, F., Desai, M. Golightly, M., Hassler, D., Hatcher, R., Kim, M. Y., Posner, A., PourArsalan, M., Spence, H. E., and Squier, R. K., Earth-Moon-Mars radiation environment module framework, Space Weather, 8, 2010
- Joyce, C. J., Schwadron, N. A., Townsend, L. W., deWet, W. C., Wilson, J. K., Spence, H. E., Tobiska, W. K., Shelton-Mur, K., Yarborough, A., Harvey, J., Herbst, A., Koske-Phillips, A., Molina, F., Omondi, S., Reid, C., Reid, D., Shultz, J., Stephenson, B., McDevitt, M., and Phillips, T., Atmospheric radiation modeling of galactic cosmic rays using LRO/CRaTER and the EMMREM model with comparisons to balloon and airline based measurements, Space Weather, 14, 659, 2016
-

Relevant Presentations

- Joyce, C. J., et al., Characterization of the Earth-Moon-Mars Radiation Environment during the LRO Mission using CRaTER and PREDICCS, SHINE, Telluride, CO, June 2014

II.4 C-SWEPA Progress on Modeling Pickup Ions and Seed Populations

Pickup ion observations in the region of the focusing cone are used as an indicator of the interstellar wind flow direction. However, these observations have consistently indicated a longitude slightly higher than the neutral atom observations of the Interstellar Boundary Explorer (IBEX). Quinn et al. 2016 compared the recent IBEX observations of Schwadron et al. 2015 and STEREO/PLASTIC observations of Drews et al. 2012 and showed by using EPREM that the transport of pickup ions in the region of the focusing cone carries fundamental information about the scattering of pickup ions inside 1 AU. First, by modeling the transport of pickup ions for a mean free path range of 0.1 AU to 1 AU (see Figure II.4.1), a mean free path of 0.19 + 0.29(-0.19) AU is derived based off the longitudinal difference between pickup ion and neutral atom observations. Second, the velocity distribution inside 1 AU was found to be anisotropic with an average azimuthal velocity reaching ~8% of the solar wind speed (see Figure II.4.2). Lastly, using the ability to turn select transport effects on or off within EPREM, Quinn et al. 2016 showed that pitch-angle scattering, adiabatic focusing, perpendicular diffusion, and particle drift contribute to shifting the focusing cone 20.00%, 69.43%, 10.56%, and <0.01%, respectively (see Figure II.4.3).

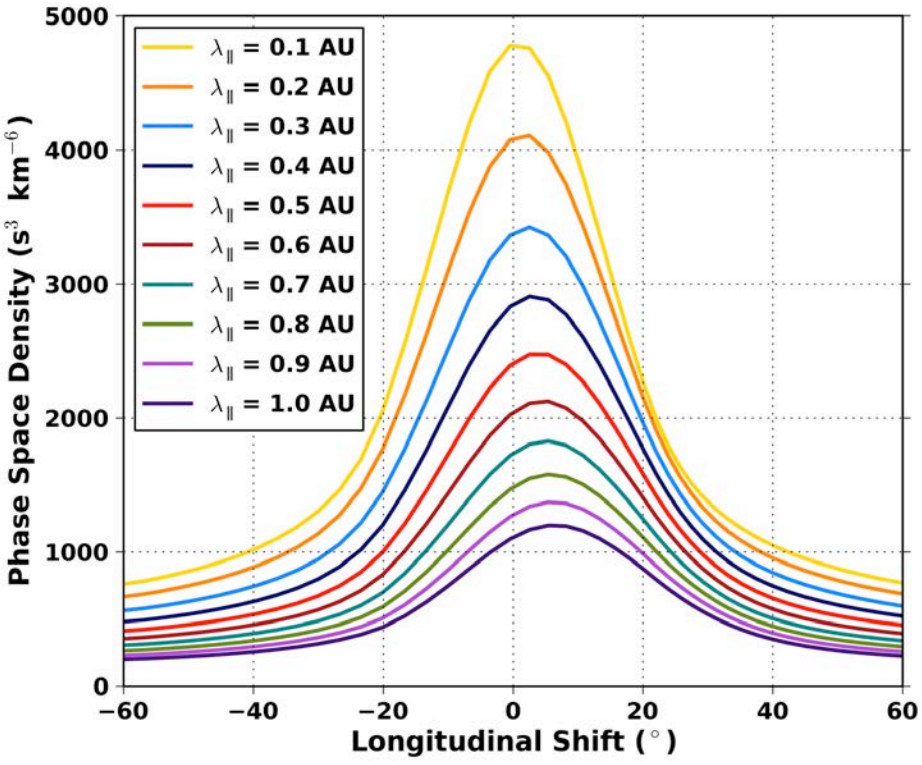

Figure II.4.1. *Simulated phase space density of helium pickup ions in the reference frame of STEREO/PLASTIC with limitations by the instrument's acceptance angles and averaged over the*

energy range of 1.5<w<2.0, where w is the ion speed to solar wind speed ratio. The longitudinal shift for parallel scattering mean free paths of 0.1 AU to 1 AU are shown.

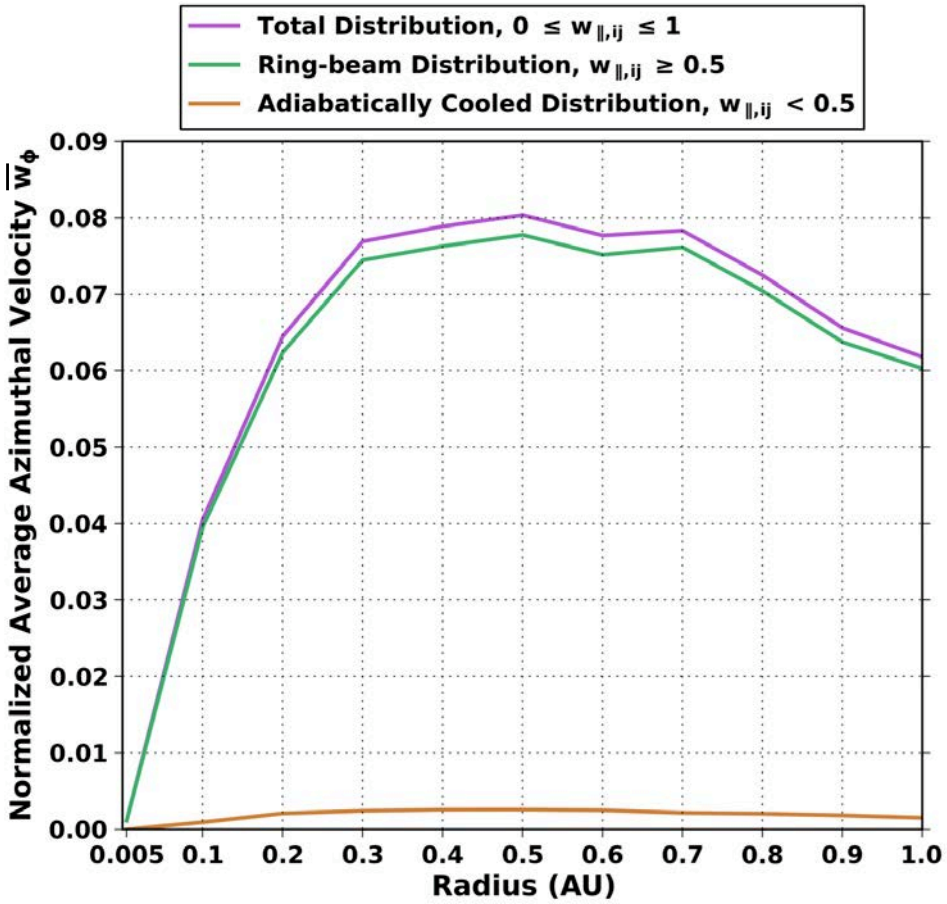

Figure II.4.2. *Normalized average azimuthal velocity of helium pickup ions as a function of heliocentric radius in the solar wind reference frame.*

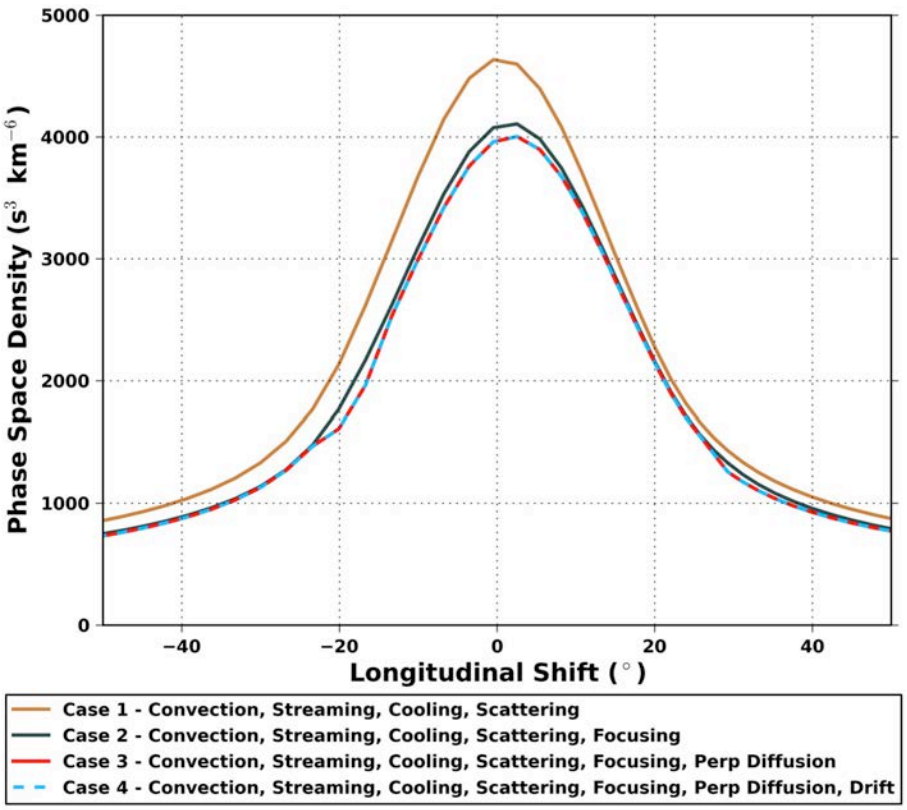

Figure II.4.3. *Longitudinal shift of the pickup helium focusing cone in the reference frame of STEREO/PLASTIC, limited to the instrument's acceptance angles, and averaged over the energy range of 1.5<w<2.0 where w is the ratio of ion speed to solar wind speed. The simulation was run for the derived mean free path of 0.19 AU. For each case, and new transport effect in EPREM is turned on. The amount of shift due to the new transport effect is found by differencing the peak longitude from the previous case.*

Chen et al. 2015 coupled EPREM with an MHD model (Giacalone et al. 2002) for CIR structures where the forward and reverse shocks have not yet formed. EPREM's modeled pickup ion velocity distribution within the compression region was found to have a high-energy tail with -5 power law index (see Figure II.4.4). This tail is comparable to pickup observations by STEREO/PLASTIC (see Figure II.4.5). The tail is also sensitive to the velocity gradient associated with the CIR formation causing the power law index to range from -3 to above -10 (see Figure II.4.6), but also suggests that the velocity gradient can efficiently create a seed population of pickup ions before a shock forms and without stochastic acceleration.

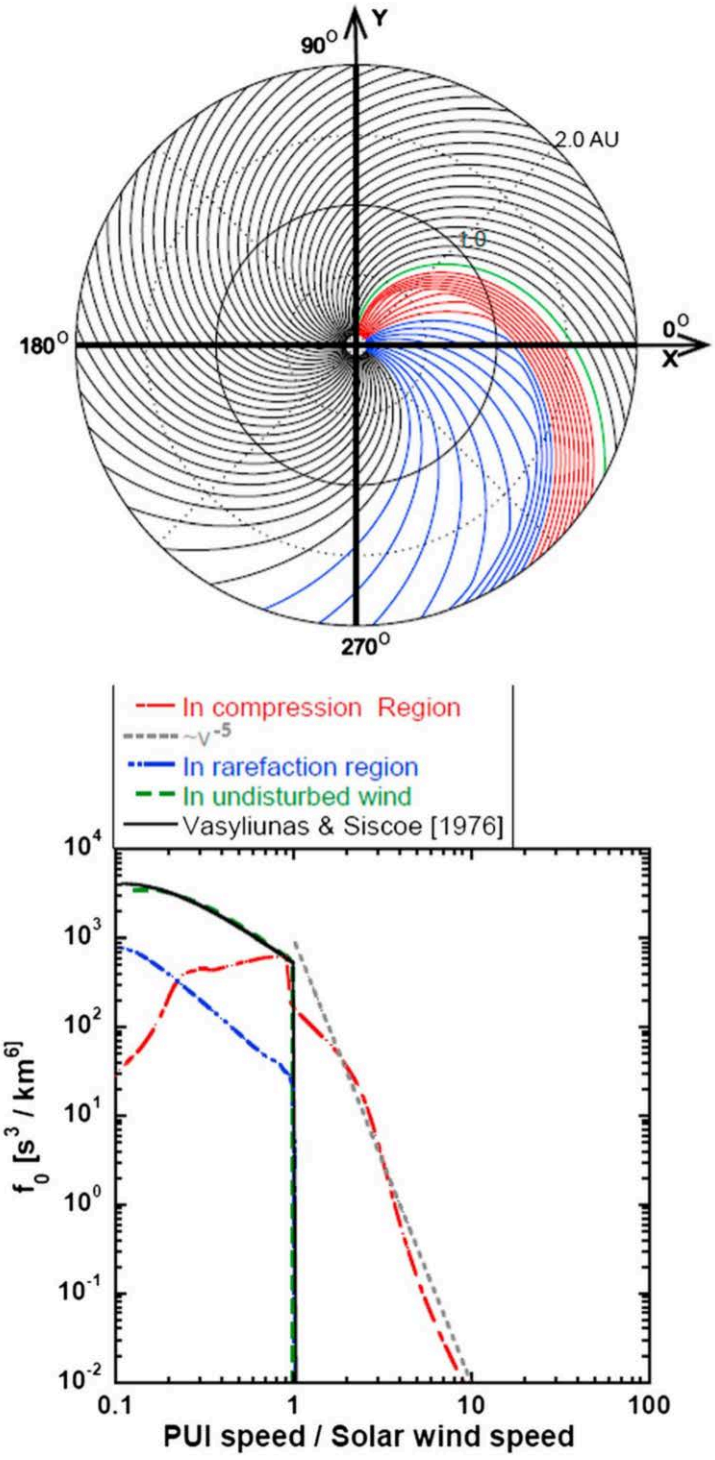

Figure II.4.4. *(Top) Simulated interplanetary magnetic field lines, with the regions colored according to the spectrum shown above. (Bottom) PUI distributions for the compression region (red) and rarefaction region (blue) of a CIR, as simulated by EPREM. A distribution in the undisturbed solar wind is also shown (green) in comparison with the analytic solution of Vasyliunas and Siscoe [1976] (black). A distribution that falls off as* -5 power law *is shown for comparison in grey.*

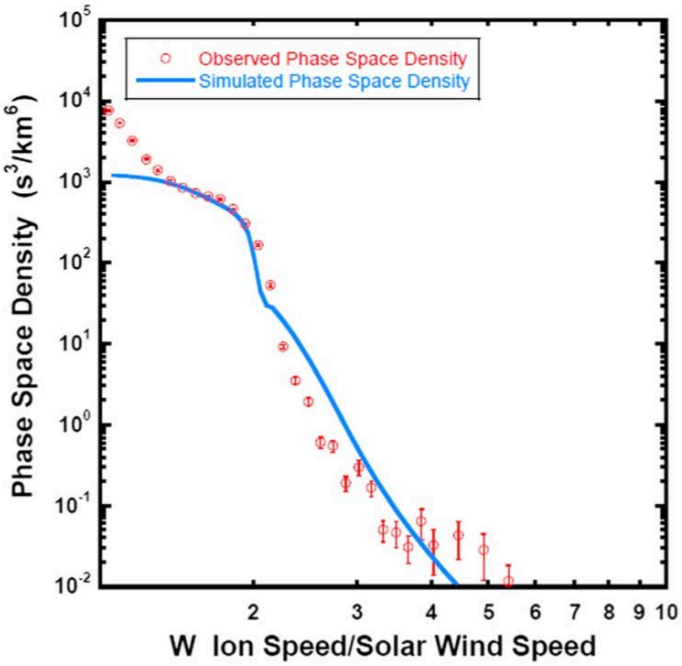

Figure II.4.5. *Comparison of predicted phase space density with observations plotted as a function of ion speed in the spacecraft frame divided by the solar wind speed. The predicted phase space density is obtained by integrating the simulation PUI velocity distribution averaged in the CIR over the PLASTIC field-of-view and energy channels.*

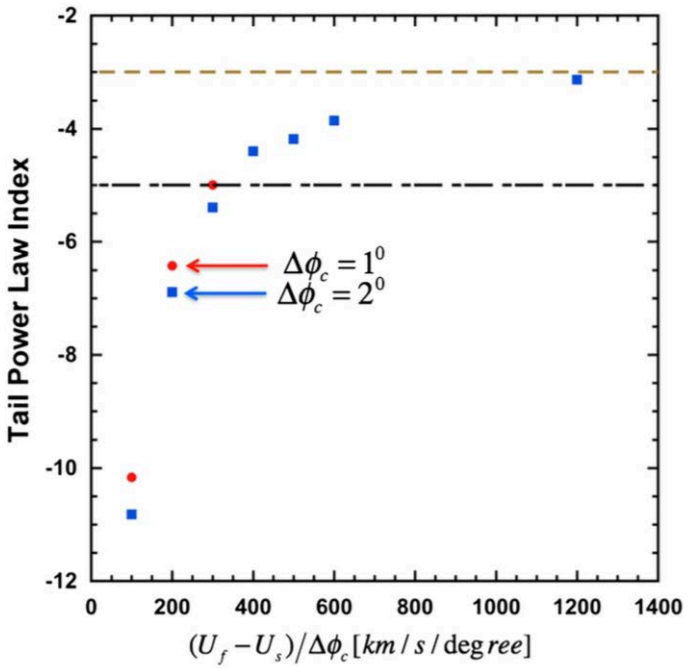

Figure II.4.6. *Power law index of the tail distribution, as simulated for various differences in the solar wind speed across the CIR. Two widths of the solar wind speed transition are shown. The green and black dashed lines indicate -3 and -5 power law indices, respectively.*

Relevant Publications:

- Quinn, P. R., Schwadron, N. A., and Mobius, E., Transport of Helium Pickup Ions within the Focusing Cone: Reconciling STEREO Observations with IBEX, The Astrophysical Journal, 824, 142, 2016
- Chen et al., "Modeling Interstellar Pickup Ion Distributions in Corotating Interaction Regions Inside 1 AU", J. Geophys. Res. Space Physics, 120, 2015.

II.5 C-SWEPA Progress in Modeling Solar Energetic particles

Solar energetic particles (SEPs) present significant acute hazards to human and robotic missions. The C-SWEPA project provides a unique coupling between MHD models and the energetic particle models, allowing fundamental capabilities to now-cast and predict the SEP events.

Significant progress has been made with PREDICCS (Predictions of Radiation from REleASE, EMMREM, and Data Incorporating the CRaTER, COSTEP and other SEP measurements, http://prediccs.sr.unh.edu), which is an online system that utilizes data from various satellites in conjunction with numerical models (C-SWEPA) to produce a near-real-time characterization of the radiation environment of the inner heliosphere. PREDICCS offers the community a valuable tool in forecasting events and improving risk assessment models for future space missions, providing up to date predictions for dose rate, dose equivalent rates and particle flux data at Earth, Moon and Mars. Joyce et al. [2013b] presented a comparison between lunar dose rates and accumulated doses predicted by the PREDICCS system with those measured by the Cosmic Ray Telescope for the Effects of Radiation (CRaTER) instrument aboard the Lunar Reconnaissance Orbiter (LRO) spacecraft during three major solar events in 2012 (Figure II.5.1). We also plot the dose rate measured by the microdosimeter aboard LRO for comparison, as well as additional PREDICCS dose rates for different levels of shielding, which demonstrate how advanced knowledge of events may be used to reduce radiation exposure to astronauts. Joyce et al. [2013b] find that the dose rates and accumulated doses predicted by PREDICCS and measured by CRaTER during the three solar events are in good agreement and differ by at most 40 percent. From this, we conclude that PREDICCS offers a credible characterization of the lunar radiation environment. The Joyce et al. [2013b] study offers the first long-term validation of C-SWEPA radiation models using in-situ measurements and demonstrates how valuable PREDICCS should become in future efforts in risk assessment and in the study of radiation in the inner heliosphere. This study also demonstrates typical dose rates and accumulated doses associated with large solar events.

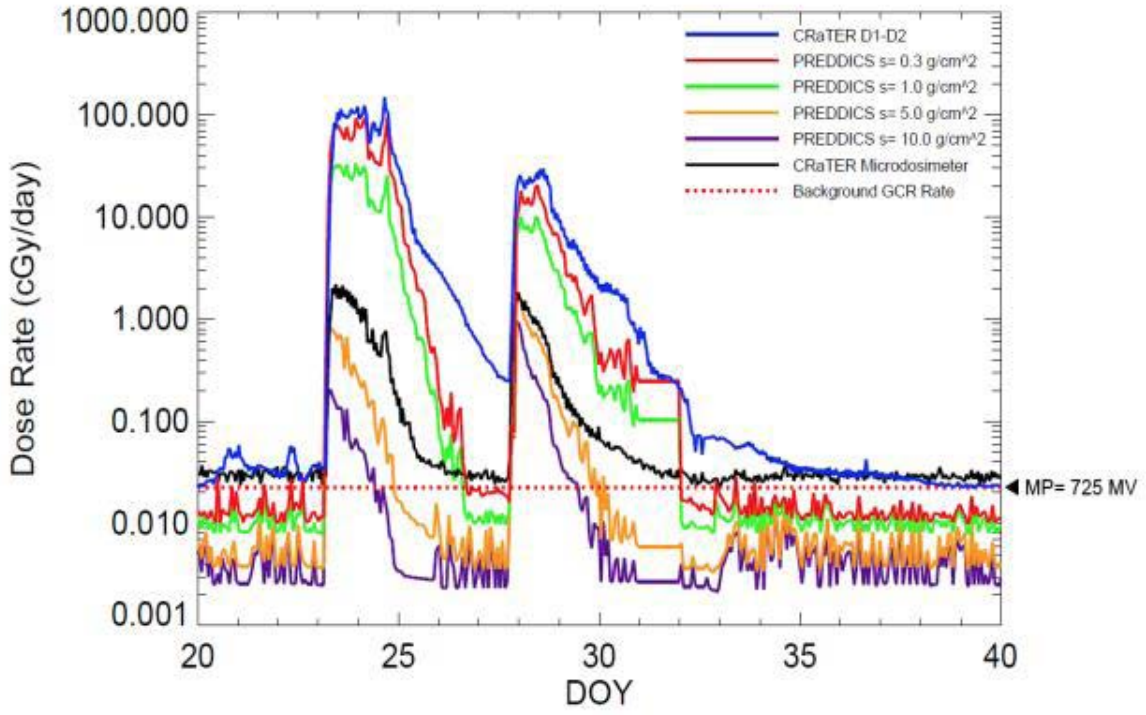

Figure II.5.1. *Dose rates measured by CRaTER (blue) vs. those predicted by PREDICCS for various levels of shielding during the January 2012 solar event. The 0.3 g/cm2 shielded PREDICCS dose rate (red) offers the closest comparison to the level of shielding seen by CRaTER. Figure taken from Joyce et al., [2013b].*

Kozarev et al. (2013) coupled results from a detailed global three-dimensional MHD time-dependent CME simulation to a global proton acceleration and transport model, in order to study time-dependent effects of SEP acceleration between 1.8 and 8 solar radii in the 2005 May 13 CME. Kozarev et al. (2013) find that the source population is accelerated to at least 100 MeV, with distributions enhanced up to six orders of magnitude. Acceleration efficiency varies strongly along field lines probing different regions of the dynamically evolving CME, whose dynamics is influenced by the large-scale coronal magnetic field structure. We observe strong acceleration in sheath regions immediately behind the shock. Results from the Kozarev et al. (2013) study are shown in Figures II.5.1-II.5.3.

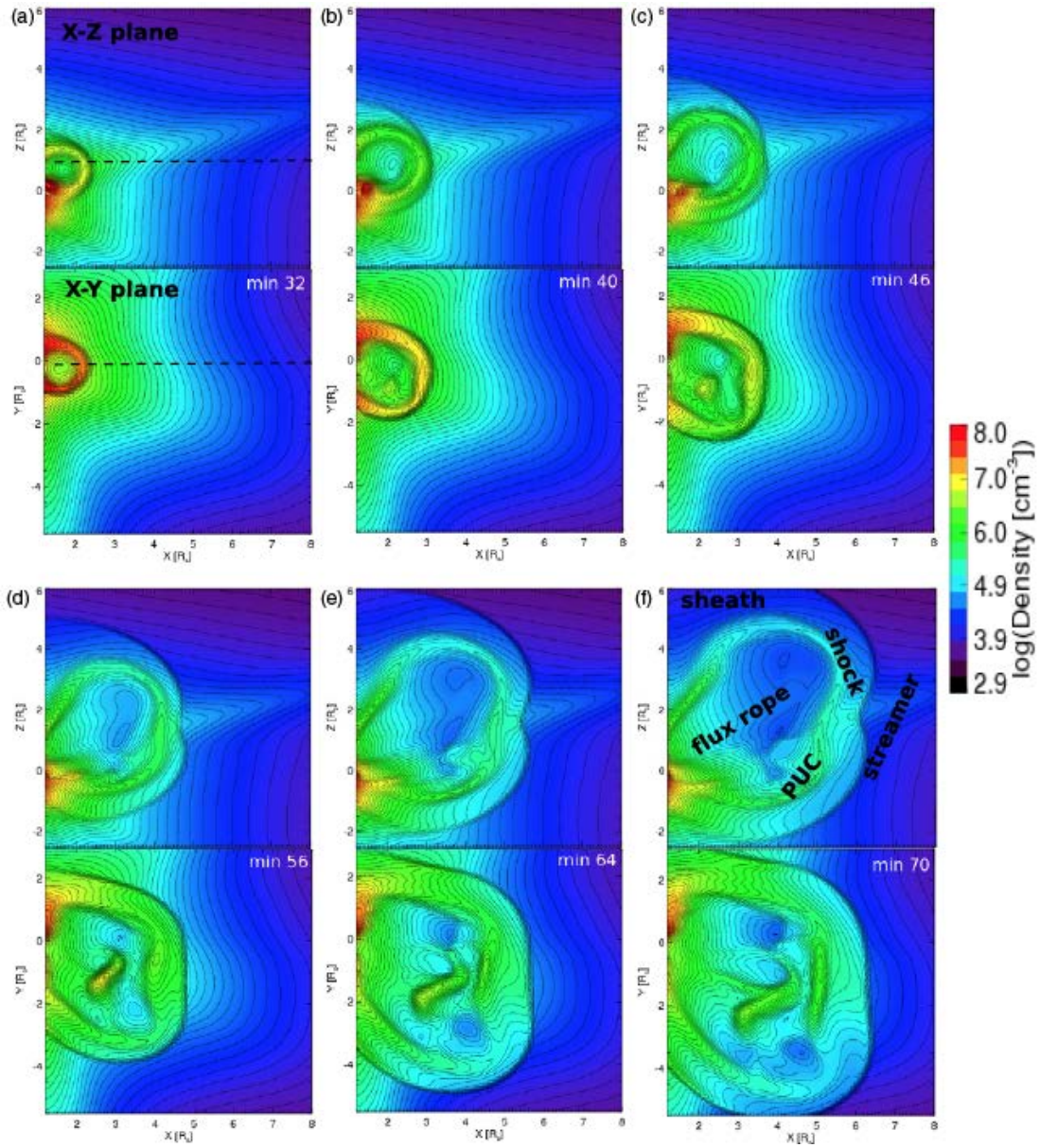

Figure II.5.2. *X–Z and X–Y slices showing color and line contours of proton density for six snapshots of the CME simulation used in Kozarev et al. [2013]. The snapshots span about 38 minutes of simulation time. The larger structure is a coronal streamer.*

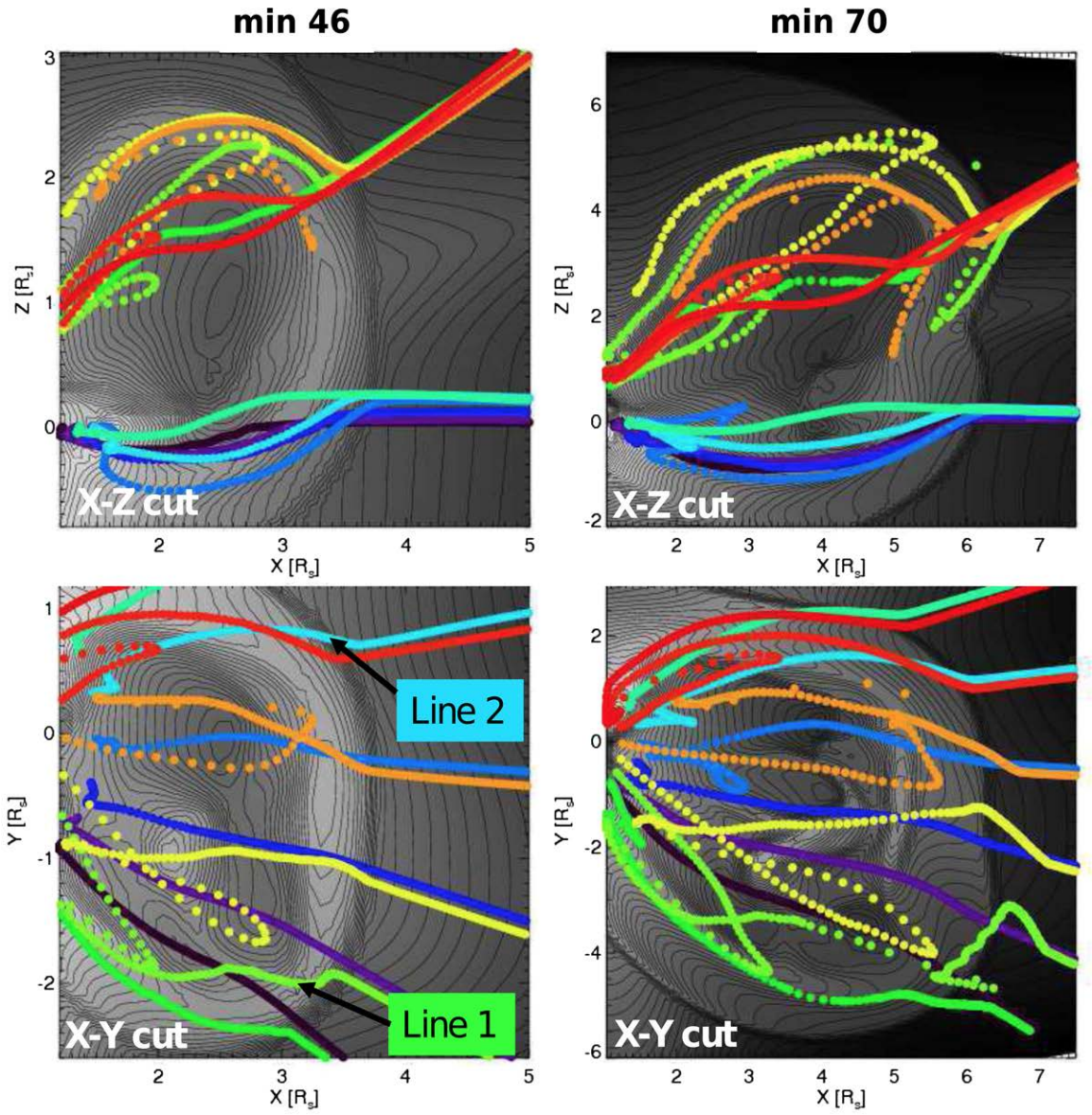

Figure II.5.3. *Evolving CME distorts the C-SWEPA grid lines, as can be seen in these panels. The solar wind density is shown as grayscale density contours. Overlaid, color dots represent the grid node positions along individual field lines. The top and bottom panels show the X–Z and X–Y cuts for two times, similar to previous figures. The two lines marked "Line 1" and "Line 2" point to the two lines discussed later in this section. Figure taken from Kozarev et al., 2013.*

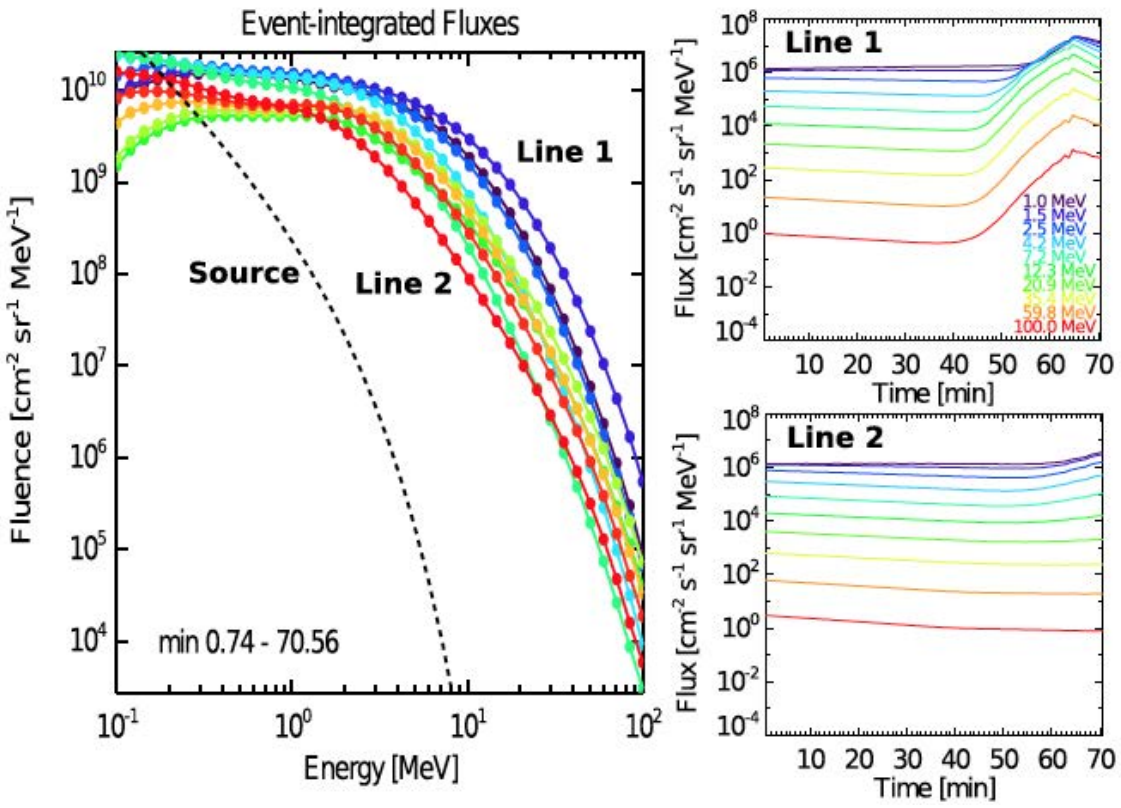

Figure II.5.4. *Panel (a): event-integrated fluences for the 10 lines shown in Figure II.5.3. Proton energy is on the X-axis; fluence is on the Y-axis. The dashed line represents the fluence at the model inner boundary (source). Panels (b) and (c): simulated flux, "measured" over time at a constant distance of ~8 RS on the two lines denoted in the bottom left panel of Figure II.5.3 as Line 1 and Line 2, respectively. Time is on the X-axis; proton flux is on the Y-axis. Figure taken from Kozarev et al. [2013].*

The C-SWEPA team has (1) completed an analysis of the July 23, 2012 extreme CME event, including the acceleration of energetic particles; (2) completed a thermodynamic MHD relaxation run for the Bastille Day event; and (3) began preliminary simulations with an embedded spheromak field within our cone-model generator.

A suite of model solutions for the July 23, 2012 CME explored a variety of input parameters, including the shape, duration, amplitude, and speed of the main CME as well as whether or not a precursor CME was first launched. One promising candidate was chosen to provide the background plasma and magnetic field parameters to accelerate protons using the C-SWEPA code. The results suggest that the included particle acceleration mechanisms can more than adequately produce distributions like those observed.

A thermodynamic MHD relaxation run was completed of the Bastille Day event corona with improved spatial resolution and inserted a pre-relaxed flux rope into the solution. The test, which was successful, was to assess whether the rope would remain coherent or transform into a sheared arcade. While a significant amount of magnetic energy was still released as the system adjusted to the inserted, strong-field flux rope, the rope now retains its coherence much better. Moreover, the improved resolution greatly improves the quality of synthetic satellite images in the sense that spurious oscillations and disturbances that we had previously seen in the images are now almost

completely absent within the active region. In more recent simulations, we now include the full eruption in our thermodynamic MHD code (up to 20 solar radii) and then followed the CME evolution with our heliospheric code to 1 AU [Linker et al., 2016, Figures II.5.5 and II.5.6].

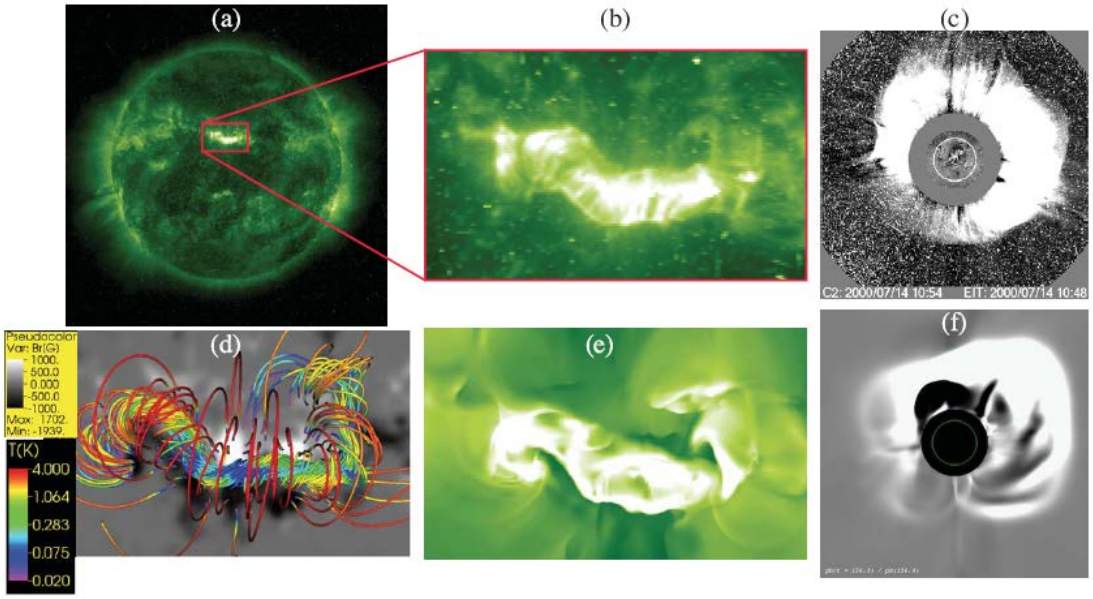

Figure II.5.5. [*From Linker et al., 2016*] *Comparison of observations from the Bastille Day Event (July 14, 2000) with an MHD simulation using TDm flux ropes to initiate a CME. (a) SOHO EIT 195Å observations of the X-class flare. (b) Closeup of EIT 195Å showing post flare loops in eruption. (c) Halo CME from SOHO LASCO C2 differenced white light images. (d) The resulting equilibrium flux rope after a chain of seven pre-relaxed TDm flux ropes is introduced into the thermodynamic MHD simulation. The field lines are colored by log(T) in* 10^6 *K; cold (prominence-like) plasma condenses on the flux rope. The gray scale image shows* B_r *at the boundary in Gauss. (e) Post-flare loops in 195Å from the simulated eruption. (f) White-light halo (from running ratio of polarization brightness) from the simulated CME.*

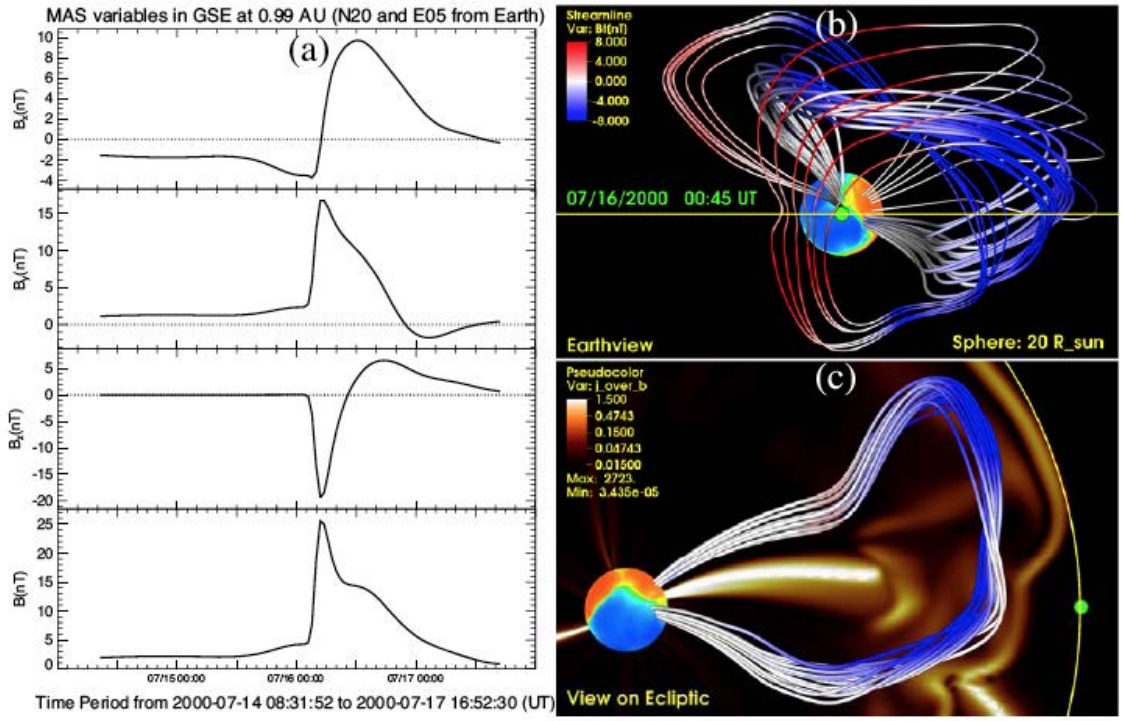

Figure II.5.6. [*From Linker et al., 2016*] *(a) Magnetic field signature of the simulated ICME at 1 AU. (b) Selected magnetic lines in the ICME as viewed from Earth. (c) Magnetic field lines in the ICME as viewed from above the ecliptic plane. The colored sphere is at the position of the inner boundary of the heliospheric calculation. The small green sphere shows the approximate Earth position.*

The C-SWEPA team further developed an analytic description of the modified Titov-Demoullin (TDm) model. We were able to eliminate the current concentrations surrounding the symmetry axis of the TDm current ring, allowing us to study tilted (with respect to the vertical direction) flux rope configurations without introducing unphysical currents into the domain. We are currently running simulations of this updated version.

To address the limitation that current cone model simulations cannot capture any of the magnetic structure within ICMEs, we developed a simple prescription of a spheromak magnetic field that can be inserted within a cone model ejecta. Although the dynamics of the eruption are still primarily controlled by the plasma properties of the ejecta (speed and density primarily), initial tests suggest that even a modest magnetic field modifies the profiles of the disturbance at 1 AU. We are in the process of investigating these results in more detail, and, in particular, assessng the effects of different field strengths within the ejecta.

Figures II.5.7 – II.5.13 further exemplify results of recent model runs that explore the effects of CMEs on solar energetic particles. These results have been incorporated in one published paper [Schwadron et al., 2014c] and in three draft manuscripts in preparation.

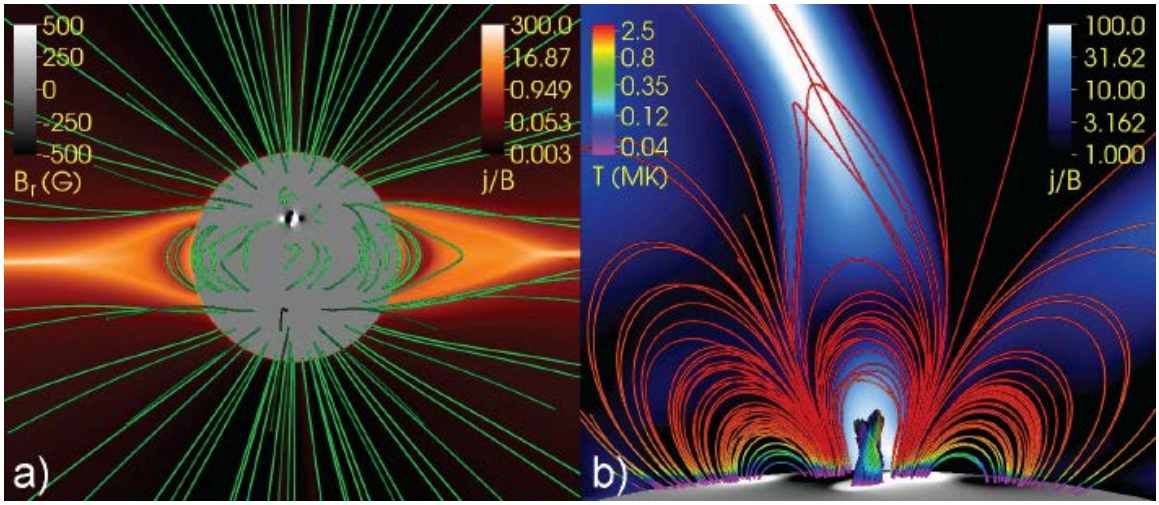

Figure II.5.7. *[Titov et al., 2013] Magnetic field configuration after flux rope insertion and subsequent relaxation. active region located in the northern hemisphere. b): View on the active region. Field lines are colored by temperature. Cold (and dense) flux rope core is visible in the center. The streamer is seen overlying the active region.*

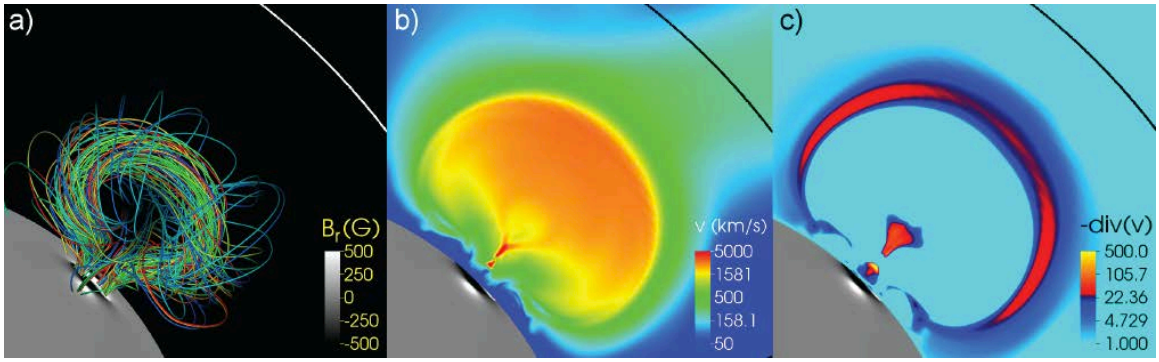

Figure II.5.8. *Modified version of the flux rope model by Titov & Demoulin (1999) above the central polarity inversion line of an active region. Active region and flux rope total unsigned flux of 7.5 x 10^{22} Mx. Maximum radial-field strength of 1070 G at the photospheric level. [from Gorby et al., 2013]*

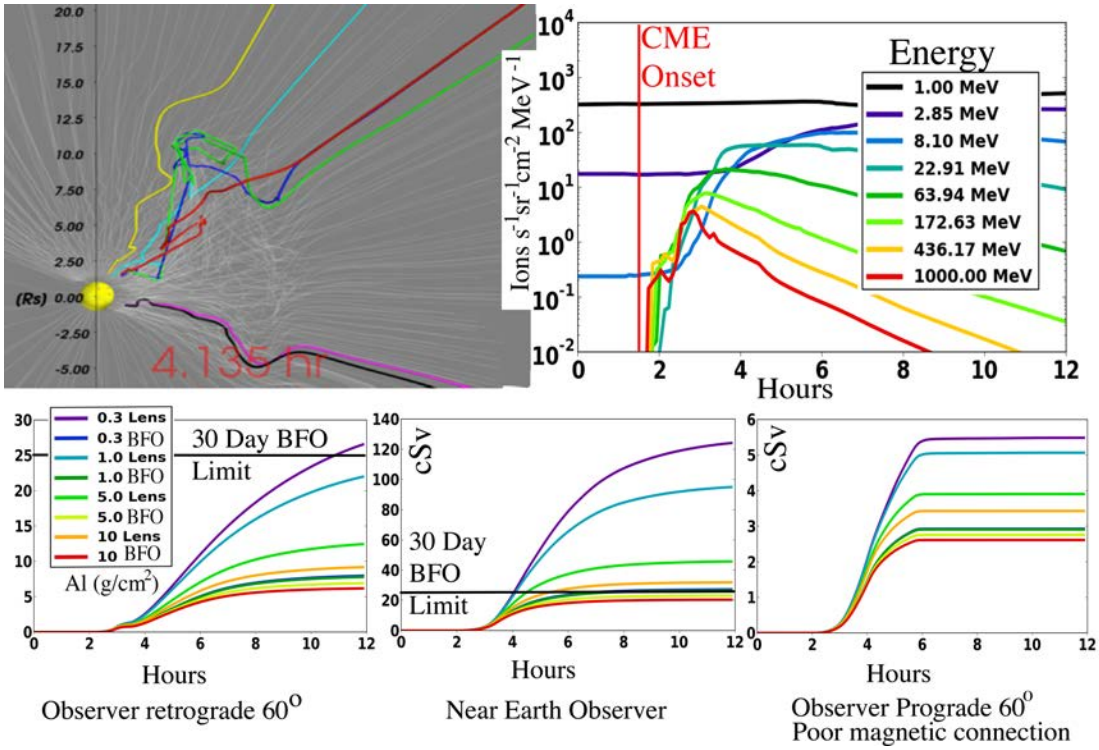

Figure II.5.9. *Energetic particles are accelerated over a broad latitudinal and longitudinal spread from the CME released following destabilization. The colored magnetic field lines show strong distortions by the plasma flow. [from Schwadron et al., 2014c]*

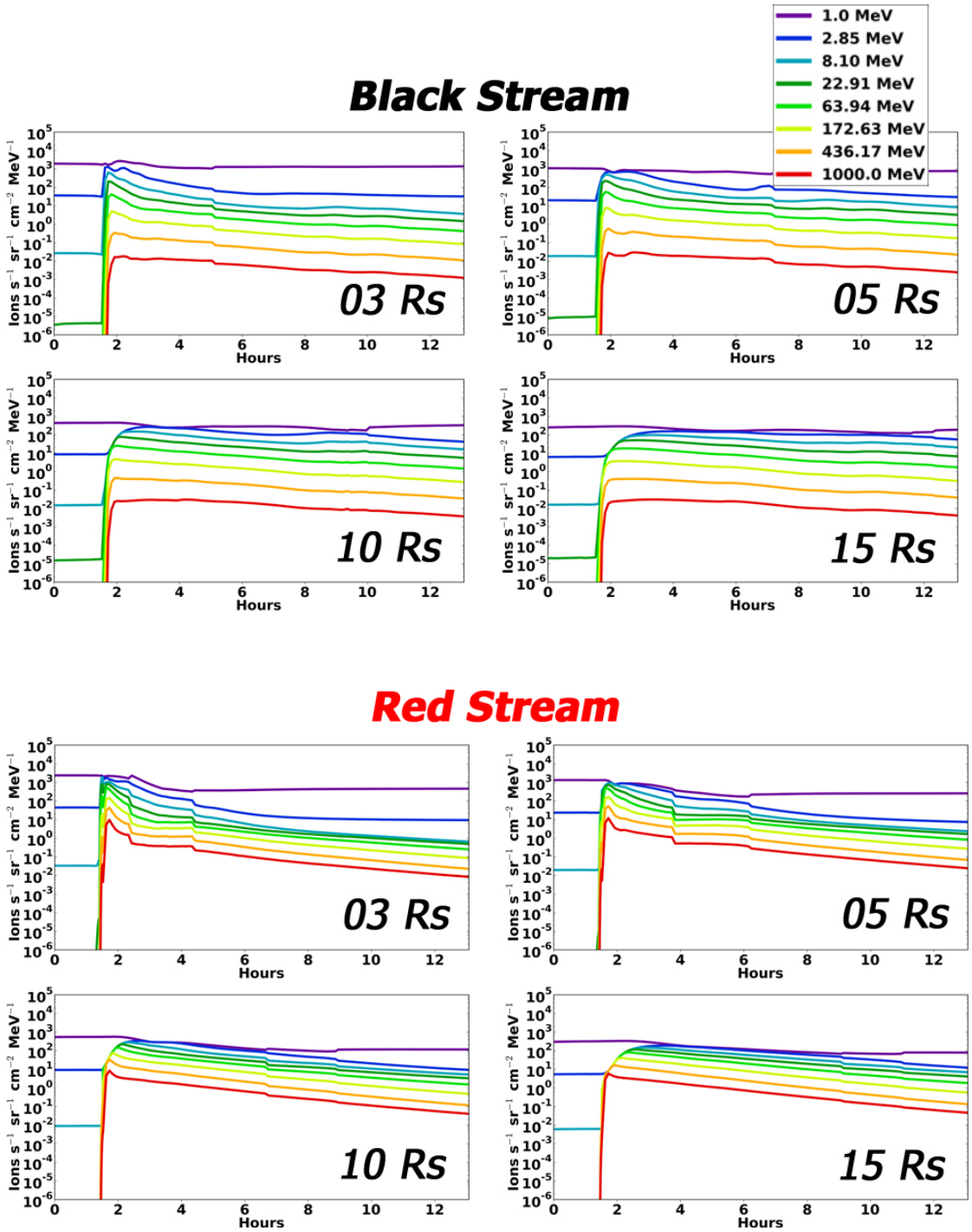

Figure II.5.10. *The CME causes particle acceleration up to GeV energies. Shown here are the time-dependent histories of energetic particles at 3, 5, 10 and 15 solar radii along the Black and Red Streamlines shown in Figure II.5.9 [from Gorby et al., 2013].*

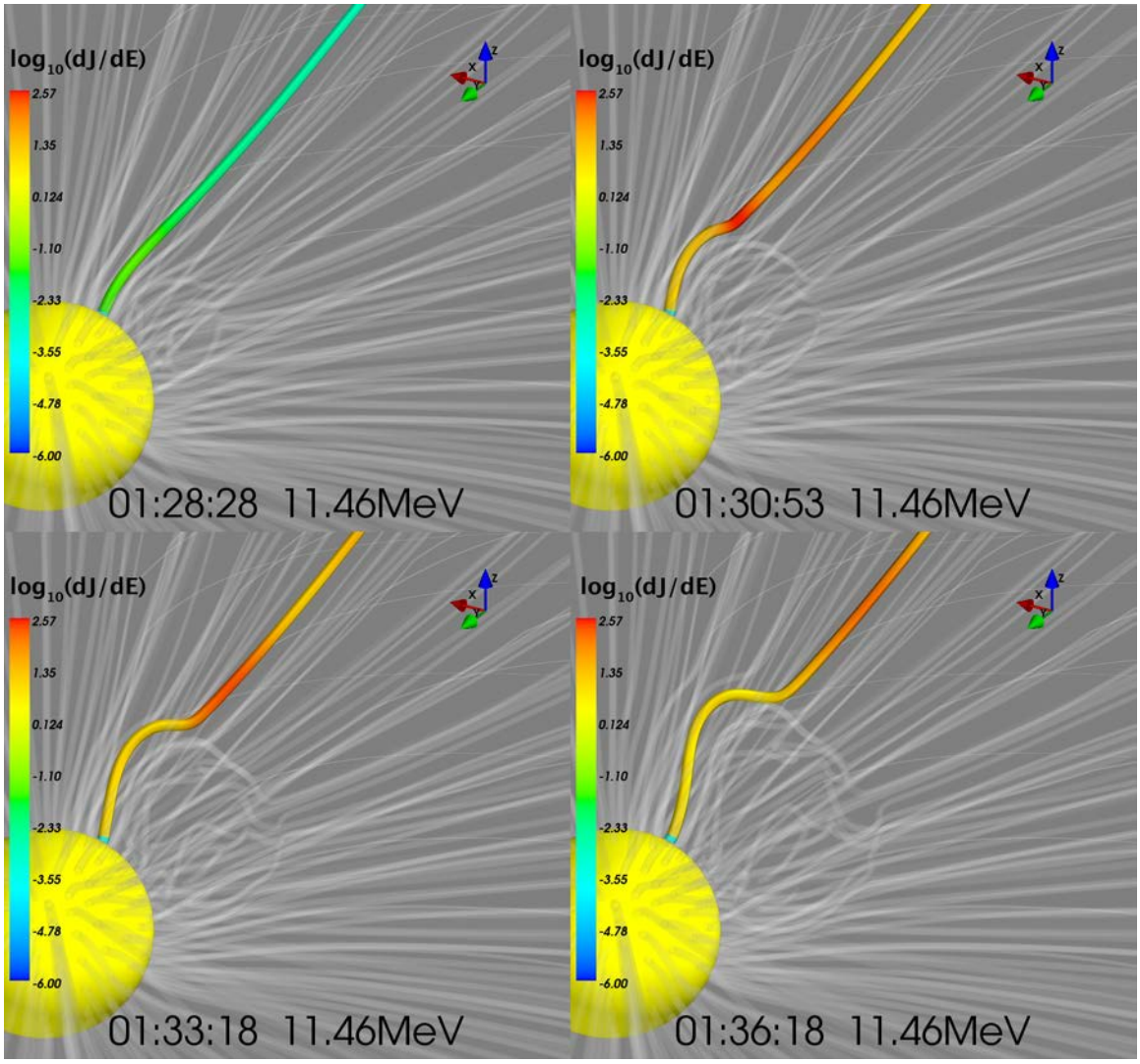

Figure II.5.11. *Domain with the stream associated with the plots on the left colored by log10 of the differential energy flux at 11.46 MeV [From Gorby 2014].*

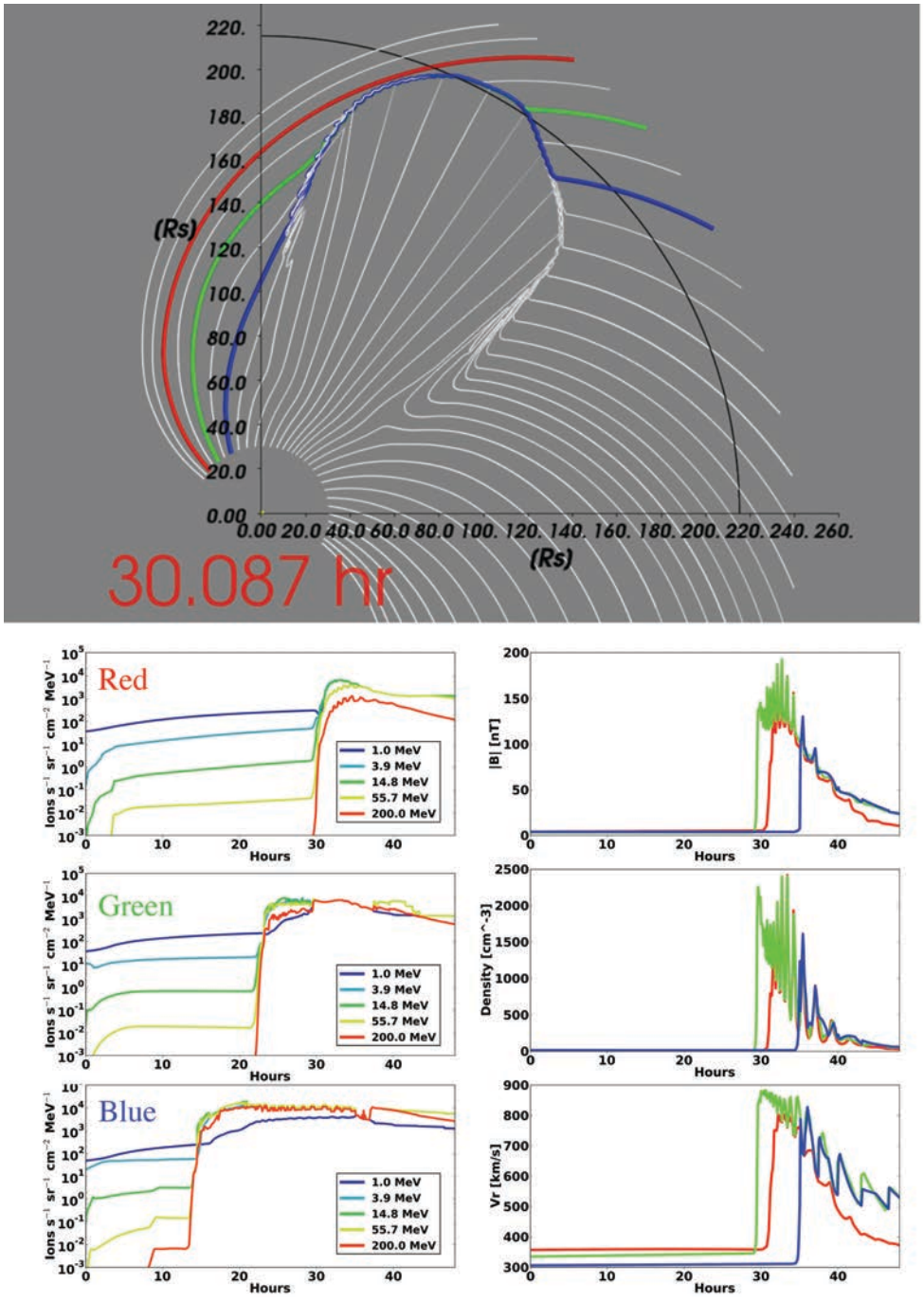

Figure II.5.12. *C-SWEPA models solve for the energetic charged particle distributions along and across magnetic field lines, from KeV to GeV energies. The code produces time histories of the particle distribution functions at various pitch angles, energies, and locations within the heliosphere. The red/green/blue traces shown here represent fluxes associated with the west/center/east of the ICME, that is, two at the flanks and one near the nose [From Riley et al., 2013].*

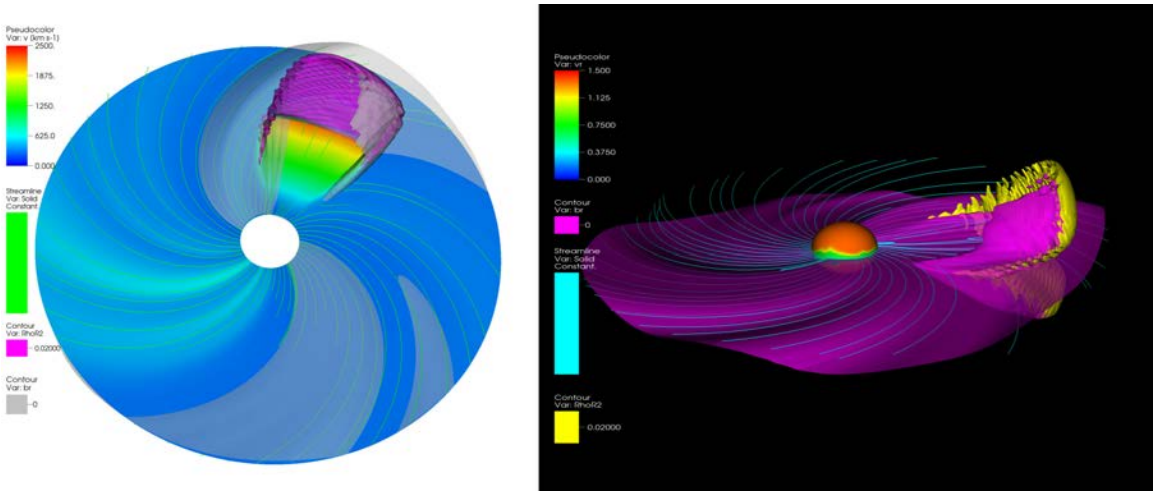

Figure II.5.13. *Two 3-D views of ICME (simulation 15) as it approaches 1 AU. The legends to the left of each panel indicate what parameters are being displayed. A selection of interplanetary magnetic field lines are also shown [From Riley et al., 2013].*

Schwadron et al. (2014a) also examined the probabilities of SEP events in the cycle 24 maximum [Figure II.5.14]. Because of the weak activity, the probability of large SEP events was greatly diminished. Again, this has major implications for human exploration. Specifically, this suggests that solar maximum may be a good time to send humans into deep space provided that solar activity remains suppressed in coming maxima.

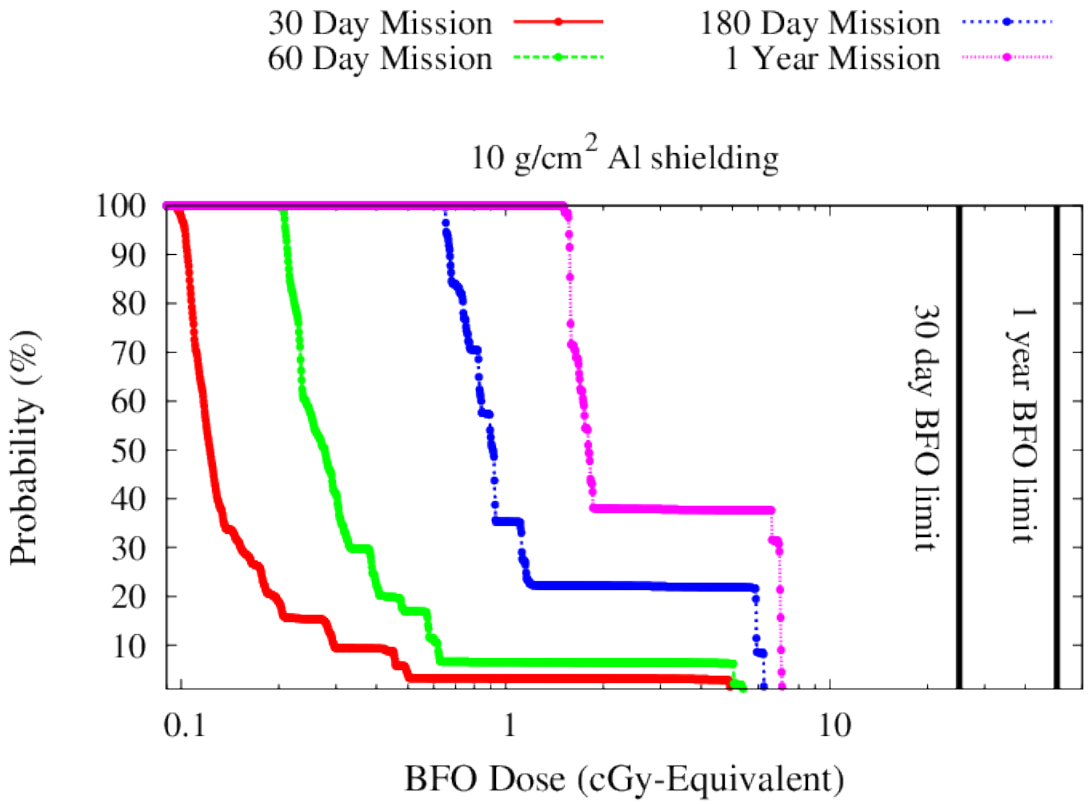

Figure II.5.14. *Probability (%) versus integrated BFO dose for 30 day to 1 year missions. We use the PREDICCS database (http://prediccs.sr.unh.edu) to build up statistics for the probability of SEP events of varying integrated dose behind spacecraft shielding (10 g/cm^2). The database currently provides doses for the period from July 2011 through April 2014. The PREDICCS doses are derived from proton spectra and use dose in 10 g/cm^2 water as a proxy for the blood forming organ (BFO) dose.*

Schwadron et al. [2015] studied particle acceleration in the low corona associated with the expansion and acceleration of CMEs. Because CME expansion regions low in the corona are effective accelerators over a finite spatial region, we showed that there is a rigidity regime where particles effectively diffuse away and escape from the acceleration sites using analytic solutions to the Parker transport equation. This leads to the formation of broken power-law distributions. Based on our solutions, we found a natural ordering of the break energy and second power-law slope (above the break energy) as a function of the scattering characteristics. These relations provide testable predictions for the particle acceleration from low in the corona. Our initial analysis of solar energetic particle observations suggests a range of shock compression ratios and rigidity dependencies that give rise to the solar energetic particle (SEP) events studied. The wide range of characteristics inferred suggests competing mechanisms at work in SEP acceleration. Thus, the study concluded that CME expansion and acceleration in the low corona may naturally give rise to rapid particle acceleration and broken power-law distributions in large SEP events.

Figures II.5.15 and II.5.16 show key results from the Schwadron et al. [2015] study indicating a sweet spot for particle acceleration near 2-3 solar radii. The simulations of large CMEs have shown just how ideal the low corona is for very rapid particle acceleration in the fronts and flanks of CMEs. These conditions lead to the acceleration of particles in ground level events [Figure II.5.17].

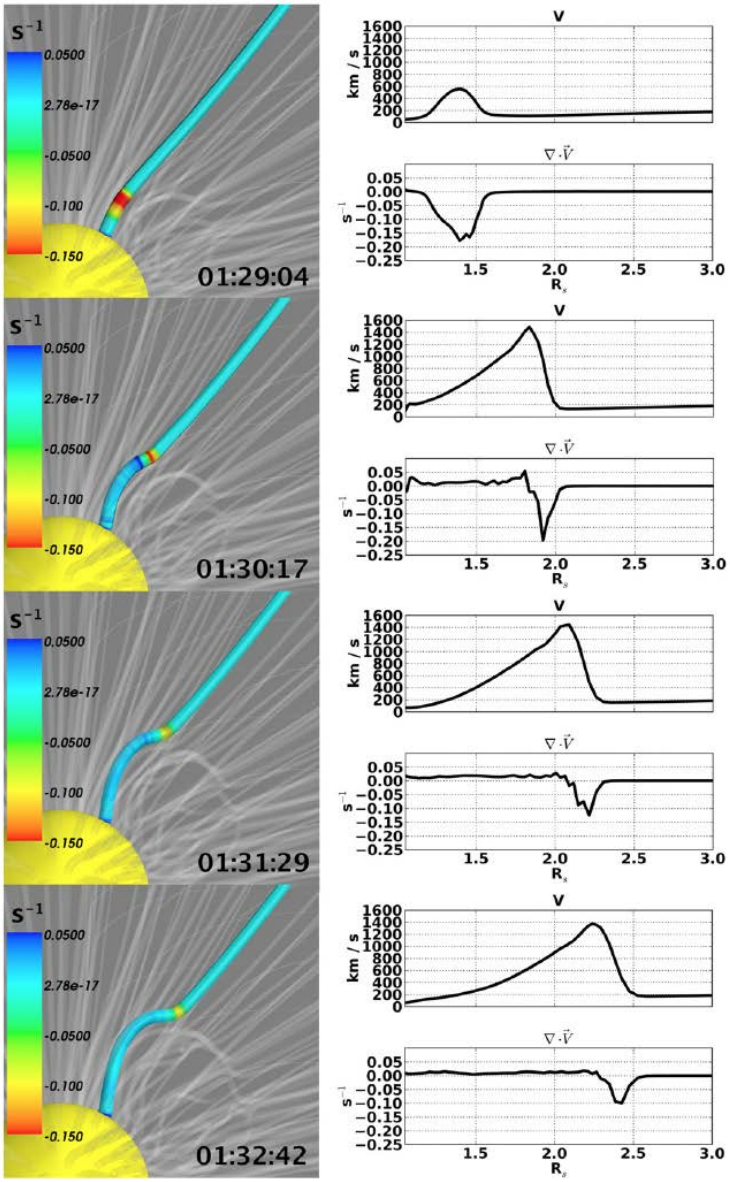

Figure II.5.15. *We show the development of a compression region on a bundle of field lines. The curves on the right show flow speed and divergence of the flow along the field line bundle as the CME expansion acts in the low corona at four different instances within the simulation. The configuration on the left shows the open magnetic field bundle (depicted as a tube) that is deformed by the expansion of the CME. The color-coding on this field line bundle indicates the relative flux of energetic particles. Times are in hh:mm:ss, where time zero corresponds to the point where the CME first started to form. Note that the simulation shows the formation of a coronal compression region low in the corona, causing the flow divergence magnitude to increase. After the initial expansion, the flow divergence magnitude forms a maximum and then falls at later times as the CME pushes the compressed sheath into the inner heliosphere.*

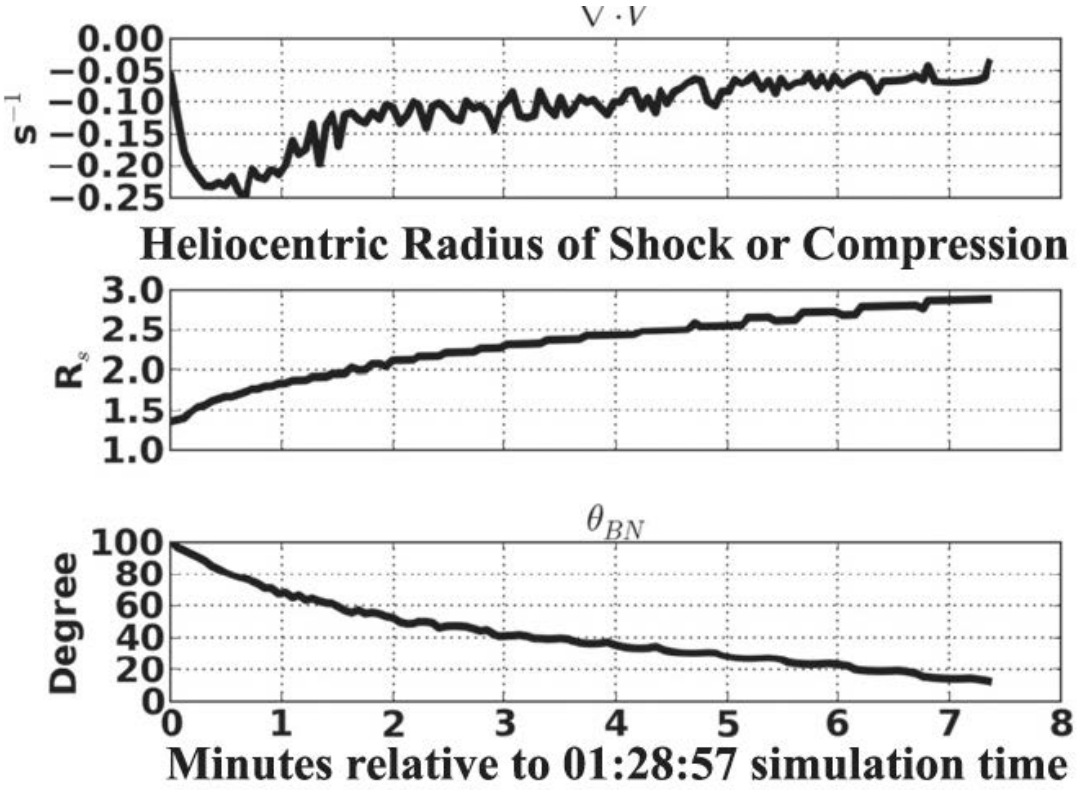

Figure II.5.16. *Utilizing the flux bundle tracked in Figure II.5.20, we find the velocity divergence (top panel), shock or compression radius (middle panel), and shock angle (magnetic field angle with respect to the shock normal). The time axis is relative to 01:28:57 in the simulation time.*

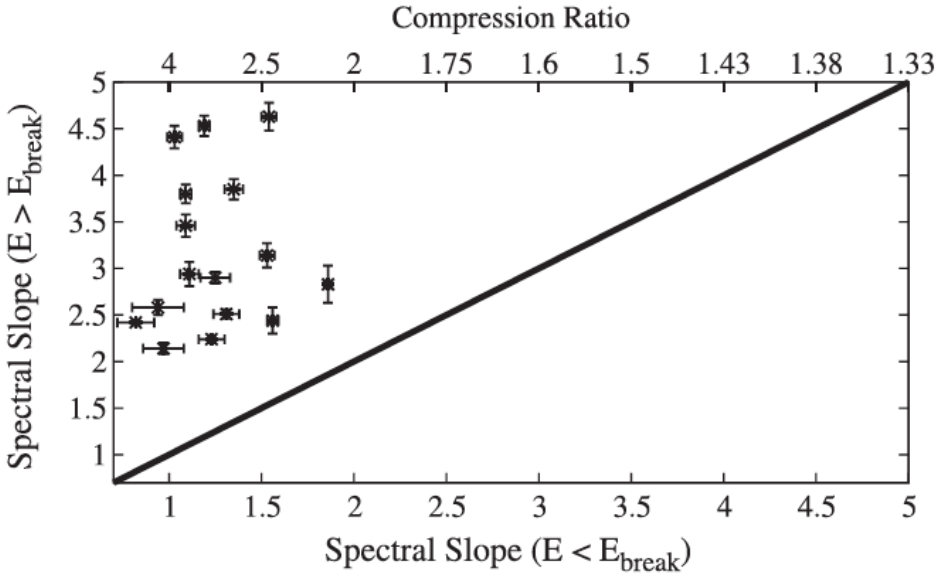

Figure II.5.17. *Observed spectral slopes associated with ground-level events from Mewaldt et al. (2012). The upper x-axis shows the compression ratio associated with shocks that produce a given value of the lower-energy spectral slope.*

Kozarev and Schwadron (2016) have recently studied the development of an eruptive filament-driven, large-scale off-limb coronal bright front (OCBF) in the low solar corona, using remote observations from the Solar Dynamics Observatory's Advanced Imaging Assembly EUV telescopes. In that study, we obtained high-temporal resolution estimates of the OCBF parameters regulating the efficiency of charged particle acceleration within the theoretical framework of diffusive shock acceleration (DSA). These parameters include the time-dependent front size, speed, and strength, as well as the upstream coronal magnetic field orientations with respect to the front's surface normal direction. We create an analytical particle acceleration model, specifically developed to incorporate the coronal shock/compressive front properties described above, derived from remote observations. We verified the model's performance through a grid of idealized case runs using input parameters typical for large-scale coronal shocks, and demonstrate that the results approach the expected DSA steady-state behavior. We then applied the model to the event of 2011 May 11 using the OCBF time-dependent parameters derived by Kozarev et al. We find that the compressive front likely produced energetic particles as low as 1.3 solar radii in the corona. Comparing the modeled and observed fluences near Earth, we found that the bulk of the acceleration during this event must have occurred above 1.5 solar radii. *Kozarev and Schwadron (2016)* we have taken a first step in using direct observations of shocks and compressions in the innermost corona to predict the onsets and intensities of solar energetic particle events.

Relevant Publications:

- Valori et al., "Initiation of Coronal Mass Ejections by Sunspot Rotation", Proceedings IAU Symposium No. 300, 2013.
- Torok et al., "The Evolution of Writhe in Kink-Unstable Flux Ropes and Erupting Filaments", Plasma Physics and Controlled Fusion (PPCF) 56, 064012 (2014)
- Torok et al., "Distribution of Electric Currents in Solar Active Regions", ApJL 782, L10 (2014)
- Lionello et al., "Magnetohydrodynamic Simulations of Interplanetary Coronal Mass Ejections", ApJ 777, 76 (2013).
- Leake et al., "Simulations of Emerging Magnetic Flux. I: The Formation of Stable Coronal Flux Ropes", ApJ 778, 99 (2013).
- Lugaz, N., Farrugia, C. J., Manchester, W. B., IV, and Schwadron, N., The Interaction of Two Coronal Mass Ejections: Influence of Relative Orientation, The Astrophysical Journal, 778, 20, 2013
- Joyce, C. J., Schwadron, N. A., Wilson, J. K., Spence, H. E., Kasper, J. C., Golightly, M., Blake, J. B., Mazur, J., Townsend, L. W., Case, A. W., Semones, E., Smith, S., and Zeitlin, C. J., Validation of PREDICCS using LRO/CRaTER observations during three major solar events in 2012, Space Weather, 11, 350, 2013
- Kozarev, K. A., Evans, R. M., Schwadron, N. A., Dayeh, M. A., Opher, M., Korreck, K. E., and van der Holst, B., Global Numerical Modeling of Energetic Proton Acceleration in a Coronal Mass Ejection Traveling through the Solar Corona, The Astrophysical

Journal, 778, 43, 2013

- Schwadron, N. A., Gorby, M., Torok, T., Downs, C., Linker, J., Lionello, R., Mikic, Z., Riley, P., Giacalone, J., Chandran, B., Germaschewski, K., Isenberg, P. A., Lee, M. A., Lugaz, N., Smith, S., Spence, H. E., Desai, M., Kasper, J., Kozarev, K., Korreck, K., Stevens, M., Cooper, J., and MacNeice, P., Synthesis of 3-D Coronal-Solar Wind Energetic Particle Acceleration Modules, Space Weather, 12, 323, 2014c
- Titov, V. S., Torok, T., Mikic, Z., and Linker, J. A., A Method for Embedding Circular Force-free Flux Ropes in Potential Magnetic Fields, The Astrophysical Journal, 790, 163, 2014
- van Driel-Gesztelyi, L., et al.: ApJ 788, 85 (2014)
- Kliem, B., et al.: ApJ 789, 46 (2014)
- Kliem, B., et al.: ApJ 792, 107 (2014)
- Schwadron, N. A., Lee, M. A., Gorby, M., Lugaz, N., Spence, H. E., Desai, M., Torok, T., Downs, C., Linker, J., Lionello, R., Mikic, Z., Riley, P., Giacalone, J., Jokipii, J. R., Kota, J., and Kozarev, K., Broken Power-law Distributions from Low Coronal Compression Regions or Shocks, Journal of Physics Conference Series, 642, 012025, 2015

- Schwadron, N. A., Lee, M. A., Gorby, M., Lugaz, N., Spence, H. E., Desai, M., Torok, T., Downs, C., Linker, J., Lionello, R., Mikic;, Z., Riley, P., Giacalone, J., Jokipii, J. R., Kota, J., and Kozarev, K., Particle Acceleration at Low Coronal Compression Regions and Shocks, The Astrophysical Journal, 810, 97, 2015
- Linker, J., Torok, T., Downs, C., Lionello, R., Titov, V., Caplan, R. M., Mikic, Z., and Riley, P). MHD simulation of the Bastille day event. In American Institute of Physics Conference Series, vol. 1720 of American Institute of Physics Conference Series, pg 020002, 2016
- Kozarev, K. A. and Schwadron, N. A., A Data-driven Analytic Model for Proton Acceleration by Large-scale Solar Coronal Shocks, The Astrophysical Journal, 831, 120, 2016
-

Relevant Presentations

- M Gorby, N A Schwadron, M A Lee, A C Booth, H E Spence, T Torok, C Downs, R Lionello, J Linker, V S Titov, Z Mikic, P Riley, M I Desai, M A Dayeh, K A Kozarev, Particle Acceleration in the Low Corona Over Broad Longitudes:
  Coupling Between 3D Magnetohydrodynamic and Energetic Particle Models, Fall AGU, 2013
- P Riley, M Ben-Nun, R Lionello, C Downs, T Török, J Linker, Z Mikic, N Schwadron and M Gorby, Understanding the Evolution of the July 23, 2012 Extreme ICME: Global Modeling and Comparison with Observations, Fall AGU, 2013
- Joyce, C. J., Blake, J. B., Case, A. W., Golightly, M., Kasper, J. C., Mazur, J., Schwadron, N. A., Semones, E., Smith, S., Spence, H. E., Townsend, L. W., Wilson, J. K., and Zeitlin, C. J., Validation of PREDICCS Using LRO/CRaTER Observations During Three Major Solar Events in 2012, Lunar and Planetary Institute Science

Conference Abstracts, 44, 2707, 2013

- Lugaz, N., Farrugia, C. J., Schwadron, N., Lee, C. O., Davies, J. A., and Roussev, I. I., Coronal Mass Ejections and Associated Phenomena: Recent Observations and Numerical Simulations, EGU General Assembly Conference Abstracts, 15, 2079, 2013
- Linker, J., Mikic, Z., Schwadron, N., Riley, P., Gorby, M., Lionello, R., Downs, C., and Torok, T., Time-Dependent Coupled Coronal-Solar Wind-SEP Modeling, 40th COSPAR Scientific Assembly. Held 2-10 August 2014, in Moscow, Russia, Abstract D2.5-31-14., 40, 1840, 2014
- Gorby, M., N. A. Schwadron, N., J. A Linker, T. Rorok, C. Downs, P. Riley, R. Lionello, M. Desai, M. Dayeh, C-SWEPA: Particle Acceleration Low in the Corona, Fall AGU, SH21B-4127
- Lugaz, N., Farrugia, C., and Schwadron, N., The interaction of successive coronal mass ejections: recent observations and numerical modeling, 40th COSPAR Scientific Assembly. Held 2-10 August 2014, in Moscow, Russia, Abstract D2.5-55-14., 40, 2014
- Jon Linker presented a seminar at the Observatoire de Paris in Meudon entitled "Modeling CMEs: Eventual Space Weather Applications?" on 9/25. The seminar described our approaches to modeling CME events, with examples from an idealized extreme event and initial results from simulations of the Bastille Day event. The talk also described the coupling of MAS CME simulations to EPREM solutions of the focused transport equation, and showed the resulting generation of high intensity SEPs in the idealized extreme event simulations.
- Jon Linker and Tibor Torok attended the FESD/C-SWEPA team meeting at the University of New Hampshire October 15-16, and presented talks describing the field line evolution and associated MHD quantities in the idealized CME simulation. Discussions led to a recognition that we need to unambiguously identify which features of the MHD solution are producing the SEP acceleration.
- Jon Linker presented a colloquium at the University of Sydney Department of Physics on 10/27 in which he described the use of the new TDm flux rope model in simulations of the Bastille Day event.
- Slava Titov presented the invited talk "Global Magnetic Topology and Large-Scale Dynamics of the Solar Corona" in session E2.1, Coronal Magnetism, at the COSPAR meeting in Moscow, August 3-9
- Titov, V., Torok, T., Mikic, Z., and Linker, J. A., A Method for Embedding Circular Force-Free Flux Ropes in Potential Magnetic Fields, American Astronomical Society Meeting Abstracts #224, 224, #212.04, 2014
- T. Torok, seminar at St. Andrews University in Scotland, UK, on April 24, the thermodynamic MHD CME simulations done at PSI, 2016
- T. Torok, progress on the Bastille Day event simulations at the EGU General Assembly, Vienna, Austria, 04/27-05/02, 2016
- T. Torok, (oral presentation), Distribution of electric currents in source regions of solar eruptions, AAS/SPD meeting held in Boston, MA, June 1-5, 2014.
- T Torok, Progress on the Bastille Day event simulations, Extreme Space Weather Events (ESWE) workshop in Boulder, CO, June 9-11, 2016.

- T. Torok, (invited talk), What Can We Learn from MHD Simulations and Observations about the Initial Phase of Solar Eruptions?, LWS Science workshop held in Portland, OR, Nov. 2-6, 2014.
- T. Torok, Sympathetic Eruptions in Quadrupolar Magnetic Configurations, AGU fall meeting, San Francisco, CA, December 15-19, 2014.
- T. Torok (contributed talk) Thermodynamic MHD Simulation of the 2000 July 14 'Bastille Day' Eruption", EGU General Assembly 2015, April 12-17 in Vienna, Austria.
- T. Torok (oral talk), numerical modeling of CMEs, IAU XXIX General Assembly in Honolulu, HI, 3-14 August 2015
- T. Torok (invited presentation), Numerical modeling of dynamic phenomena in the solar corona (detailed presentation of the Bastille Day eruption simulations), CSPM meeting, Coimbra, Portugal, 5-9 October 2015.
- T. Torok (seminar), Numerical modeling of dynamic phenomena in the solar corona (detailed presentation of the Bastille Day eruption simulations), solar physics seminar of the Paris Observatory, Sept, 2015
- T. Torok (poster), Coupling MHD Simulations of CMEs to SEP Models (review of coupling of MAS CME simulations to EPREM), AGU Fall Meeting, San Francisco, CA, December 14-18, 2016
- J. Linker, N. Schwadron, D. Falconer, C. Downs, R. Lionello, Z. Mikic, P. Riley, T. Torok, and M. Gorby, Towards a Predictive Model for SEPs, European Space Weather Week, 2013
- J. Linker, N. Schwadron, T. Torok, M. Gorby, C. Downs, R. Lionello, Z. Mikic, and P. Riley, Modeling Radiation Impacts with Coupled CME-SEP Simulations, European Space Weather Week, 2014
- J. Linker, T. Torok, R. Lionello, C. Downs, Z. Mikic, V. Titov, and P. Riley, MHD Simulation of the Bastille Day Event, Solar Wind 14, 2015
- J. Linker, T. Torok, C. Downs, V. Titov, R. Lionello, P. Riley, and Z. Mikic, How Much Energy Can Be Stored in Active Region Magnetic Fields? SHINE Workshop, 2015
- J. Linker, T. Torok, C. Downs, V. Titov, R. Lionello, R. Caplan, P. Riley, and Z. Mikic, How Much Energy Can Be Stored in Solar Active Region Magnetic Fields? Fall AGU, 2015
- Mays, M. L., Odstrcil, D., Luhmann, J., Bain, H., Li, Y., Schwadron, N., Gorby, M., Thompson, B., Jian, L., Möstl, C., Rouillard, A., Davies, J., Temmer, M., Rastaetter, L., Taktakishvili, A., MacNeice, P., and Kuznetsova, M., ENLIL Global Heliospheric Modeling as a Context For Multipoint Observations, EGU General Assembly Conference Abstracts, 18, 11638, 2016
- Kozarev, K. and Schwadron, N., A Data-Driven Analytical Model for Proton Acceleration at Remotely Observed Low Coronal Shocks, EGU General Assembly Conference Abstracts, 18, 1022, 2016
- Mays, M. L., Luhmann, J. G., Odstrcil, D., Lee, C., Bain, H. M., Li, Y., Schwadron, N., Gorby, M., Baker, D. N., Dewey, R. M., Larson, D. E., Halekas, J. S., Connerney, J. E. P., von Rosenvinge, T. T., Galvin, A. B., and McComas, D. J., SEP modeling based on the ENLIL global heliospheric model, AGU Fall Meeting Abstracts, 2015

II.6 Survey of Spectral Properties of SEP events from solar cycles 23 and 24

II.6.a Properties of Fe and O spectra in large SEP events

We have surveyed ~0.1-100 MeV nucleon^{-1} O and Fe fluence spectra during 46 isolated, large gradual SEP events observed at ACE during solar cycles 23 and 24. Most SEP spectra are well represented by the four-parameter Band function with normalization constant, low-energy spectral slope, high-energy spectral slope, and break energy. The O and Fe spectral slopes are similar and most spectra steepen above the break energy probably due to common acceleration and transport processes affecting different ion species. SEP spectra above the break energies depend on the origin of the seed population; larger contributions of suprathermal flare material result in higher Fe/O ratios and flatter spectra at higher energies. SEP events with steeper O spectra at low energies and higher break energies are associated with slower CMEs, while those associated with fast (>2000 km s^{-1}) CMEs and GLEs have harder or flatter spectra at low and high energies, and O break energies between ~1-10 MeV nucleon^{-1}. The latter events are enriched in ^{3}He and higher-energy Fe, and have Fe spectra that rollover at significantly lower energies compared with O, probably because Fe ions with smaller Q/M ratios can escape from the distant shock more easily than O ions with larger Q/M ratios. We conclude that SEP spectral properties result from many complex and competing effects, namely Q/M-dependent scattering, shock properties, and the origin of the seed populations, all of which must be taken into account to develop a comprehensive picture of CME-driven shock acceleration of large gradual SEP events.

These new results are summarized in Figure II.6.1, and are published in the Astrophysical Journal (see Desai et al., 2016a).

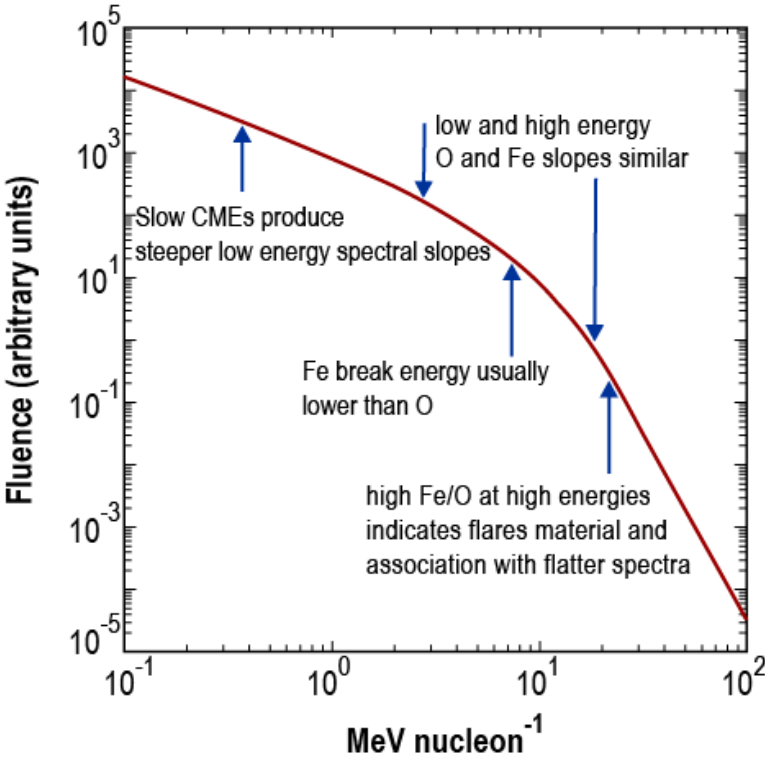

Figure II.6.1: *Arbitrary O spectrum summarizing key results in terms of the SEP Band-parameters and their relationships with CME speeds and Fe/O ratios, taken from Desai et al. (2015).*

II.6.b Q/M-dependence of heavy ion spectral breaks in large SEP events

In a follow-up paper (see Desai et al., 2016b), we fit the ~0.1-500 MeV nucleon^{-1} H-Fe spectra in 46 large SEP events surveyed by Desai et al. (2016a) with the double power-law Band function to obtain a normalization constant, low- and high-energy Band parameters γ_a and γ_b; and spectral break energy E_B. We also calculate the low-energy power-law spectral slope γ_1. Our results are: 1) γ_a, γ_1, and γ_b are species-independent and the spectra steepen with increasing energy; 2) the low-energy power-law spectral slopes γ_1 are consistent with diffusive acceleration at shocks with compression ratios between ~2–4 as predicted by Schwadron et al. (2015a;b); 3) the spectral breaks E_B's are well ordered by Q/M ratio, and decrease systematically with decreasing Q/M, scaling as $(Q/M)^{\alpha}$ with α in most events varying between ~0.2-2, as predicted by Li et al (2009; see Figure 6); 4) α is well correlated with Fe/O at ~0.16-0.23 MeV nucleon^{-1}, but not with the ~15-21 MeV nucleon^{-1} Fe/O and the ~0.5-2.0 MeV nucleon^{-1} ^{3}He/^{4}He ratios; 5) In most events: $\alpha<1.4$, the spectra steepen significantly at higher energy with $\gamma_b-\gamma_a>3$, and O E_B increases with $\gamma_b-\gamma_a$; and 6) Many extreme events (associated with faster CMEs and GLEs) are Fe-rich and ^{3}He-rich, have large $\alpha\geq1.4$, flatter spectra at low and high energies with $\gamma_b-\gamma_a<3$, and E_B that anti-correlates with $\gamma_b-\gamma_a$. In most events, the Q/M-dependence of E_B is consistent with the equal diffusion coefficient condition, while the event-to-event variations in α may be driven by differences in the near-shock wave intensity spectra, which are flatter than the Kolmogorov turbulence spectrum but weaker when compared to extreme events. We interpret these results as being due to weaker turbulence that allows the SEPs to easily escape, resulting in weaker Q/M-dependence of E_B, lower α values, and spectral steepening at higher energies. In contrast for extreme events, the stronger Q/M-dependence of E_B, larger α values, and harder spectra at high and low energy occur because enhanced wave power enables faster CME shocks to accelerate flare suprathermals more efficiently than ambient coronal ions.

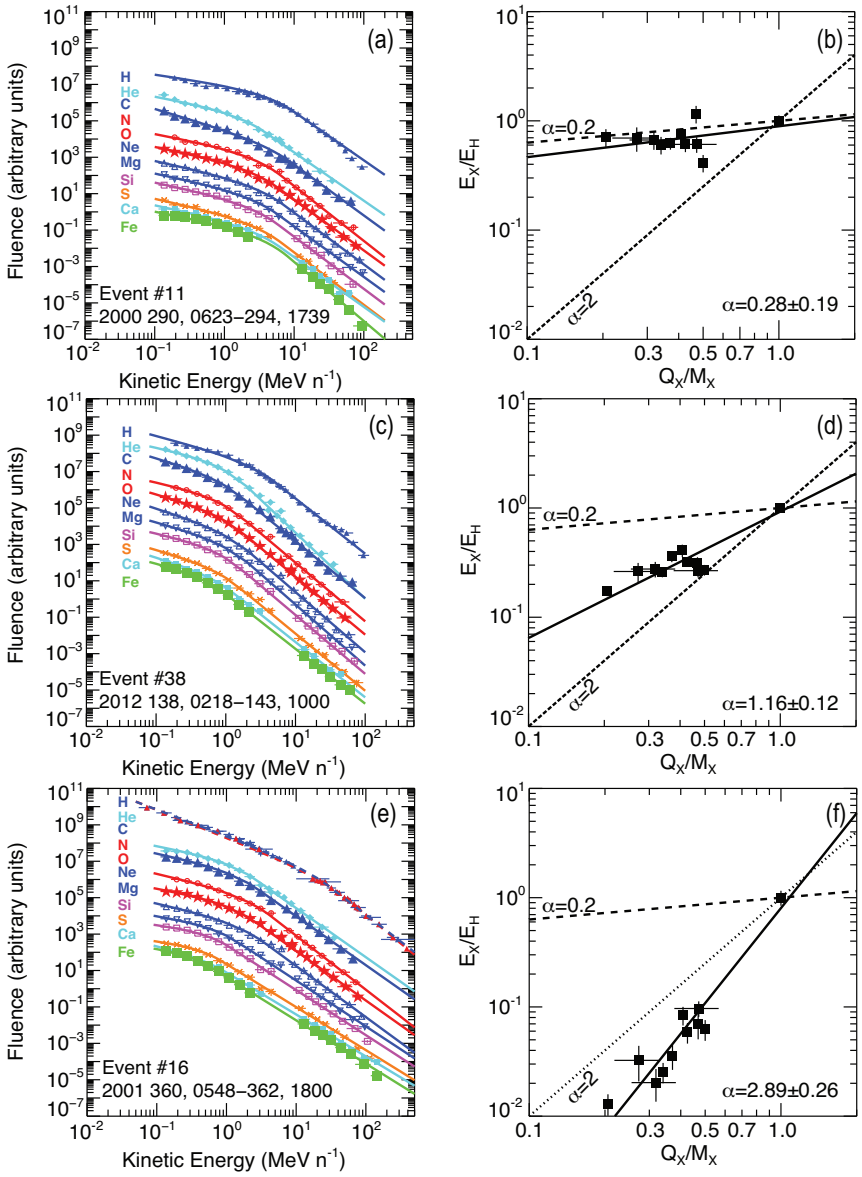

Figure II.6.2: *Three examples of Q/M dependence of the spectral breaks in SEP events.*

Three examples of the Q/M-dependence of the spectral breaks are shown in Figure II.6.2. This figure shows event-integrated differential fluences versus energy of ~0.1-500 MeV nucleon^{-1} H-Fe nuclei during three large SEP events. The energy spectra for different species are offset for clarity. Solid lines: fits to the spectra using the double-power law Band function (Band et al., 1993). Figure II.6.2e: red data points superposed on the blue symbols are proton data from EPAM/ ACE, EPS/GOES-8, and PET/SAMPEX; the dotted red-curve shows the corresponding band-function fit from Mewaldt et al. (2012) study. (b, d, f) Spectral break energy E_X of species X normalized to E_H -- break energy of H vs. the ion's charge-to-mass (Q/M) ratio. Solid line: fit to the data $\frac{E_X}{E_H} = n_0(Q/M)_X{}^{\propto}$; dashed line: same equation with $\propto = 2$; dotted line: same equation with $\propto = 0.2$; $\propto$ -- power-law dependence of E_X/E_H on Q_X/M_X. The ionic charge states, Q_X for

each species are taken as the mean Q-state observed in several large SEP events (Mobius et al., 2000; Klecker et al., 2007).

References

- Band, D., J. Matteson, L. Ford, et al. 1993, *Astrophys. J*, 413, 281–292
- Desai, M. I., M. A. Dayeh, R. W. Ebert, D. J. McComas, G. M. Mason, G. Li, C. M. S. Cohen, R. A. Mewaldt, N. A. Schwadron, and C. W. Smith, "Spectral Properties of Large Gradual Solar Energetic Particle Events – I – Fe, O and Seed material, *The Astrophysical Journal*, *816*(2), 68. doi:10.3847/0004-637X/816/2/68, 2016a
- Desai, M. I., M. A. Dayeh, R. W. Ebert, D. J. McComas, G. M. Mason, G. Li, C. M. S. Cohen, R. A. Mewaldt, N. A. Schwadron, and C. W. Smith, "Spectral Properties of Large Gradual Solar Energetic Particle Events – II – Systematic Q/M-dependence of Heavy Ion spectral Breaks, , 2016b

Klecker, B., E. Möbius & M. A Popecki, 2007, *Space Science Reviews,* 130, 273-282, doi: 10.1007/s11214-007-9207-1

Li G., Zank G. P., Verkhoglyadova, O, Mewaldt, R. A., Cohen C. M. S., Mason G. M., and Desai M. I., Shock Geometry and Spectral Breaks in Large SEP Events, Astrophysical Journal, 702, 2, 2009

Möbius, E., B. Klecker, M. A. Popecki, D. Morris, G. M. Mason et al., 2000, in Acceleration and Transport of Energetic Particles observed in the Heliosphere: ACE 2000 Symposium, eds. R. A. Mewaldt, M. Miller, J.R. Jokipii, M. A. Lee, T. H. Zurbuchen, and E. Mobius, AIP Conference Proceedings, 528, 131, doi: 10.1063/1.1324296

Schwadron N. A., M. A. Lee, M. Gorby, N. Lugaz, H. E. Spence, et al., 2015a, *J. Phys: Conf. Ser.* 642, 012025, doi:10.1088/1742-6596/642/1/012025

Schwadron N. A., M. A. Lee, M. Gorby, N. Lugaz, H. E. Spence, et al., 2015b, The *Astrophysical Journal, 810,* issue 2, artice id. 97, doi: 10.1088/0004-637X/810/2/97

Relevant Publications:

- Mason, G. M., M. I. Desai, R. A. Mewaldt, and C. M. S. Cohen, "Particle Acceleration in the Heliosphere," in American Institute of Physics Conference Proceedings, vol., 1516, pp 117-120, 2013
- Mason, G. M., G. Li, C. M. S. Cohen, M. I. Desai, D. K. Haggerty, R. A. Leske, R. A. Mewaldt, and G. P. Zank, "Fe Enhancements in SEP Onsets: Flare/CME Mixture or Transport Effect?" in Outstanding Problems in Heliophysics: From Coronal Heating to the Edge of the Heliosphere. Proceedings of a conference held 14-19 April 2013 at Myrtle Beach, South Carolina, USA. Edited by Qiang Hu and Gary P. Zank. Astronomical Society of the Pacific (ASP) Conference Series, Vol. 484, 2014, p.137
- Schwadron, N. A., M A Lee, M Gorby, N Lugaz, H E Spence, M. I Desai, T Török, C Downs, J Linker, R Lionello, Z Mikić, P Riley, J Giacalone, J R Jokipii, J Kota, and K Kozarev, "Broken Power-law Distributions from Low Coronal Compression Regions or Shocks," *Journal of Physics: Conference Series*, *642*(1), 012025. doi:10.1088/1742-6596/642/1/012025

- Desai, M. I., and J. Giacalone, "Large Gradual Solar Energetic Particle Events," in press in Living Reviews of Solar Physics
- Desai, M. I., M. A. Dayeh, R. W. Ebert, D. J. McComas, G. M. Mason, G. Li, C. M. S. Cohen, R. A. Mewaldt, N. A. Schwadron, and C. W. Smith, "Spectral Properties of Large Gradual Solar Energetic Particle Events – I – Fe, O and Seed material, *The Astrophysical Journal*, *The Astrophysical Journal*, *816*(2), 68. doi:10.3847/0004-637X/816/2/68
- Dayeh, M. A., "Coronal Mass Ejections, Solar Energetic Particles, and Space Weather", in the proceedings of the *Third Middle-East and Africa regional International Astronomical Union meeting, MEARIMIII*, Lebanese Science Journal, ISN 1561, 2015
- Zhao, L., G. Li, R. W. Ebert, M. I. Desai, M. A.Dayeh, G. M. Mason, Z. Wu, and Y. Chen, "Modeling Transport Of Energetic Particles In Corotating Interaction Regions -- A Case Study," Journal of Geophysical Research: Space Physics, doi: 10.1002/2015JA021762
- Desai, M. I., M. A. Dayeh, and R. W. Ebert, "Origin and Acceleration of Suprathermal Particles," in Solar Wind 14: Proceedings of the Fourteenth International Solar Wind Conference, eds., L. Wang, R. Bruno, E. Möbius, and G. P. Zank, AIP Conference Proceedings 1720: 060002 (2016); doi: 10.1063/1.4943837
- Dayeh, M. A., M. I. Desai, R. W. Ebert, and G. M. Mason, "Properties of the suprathermal heavy ion population near 1 AU during solar cycles 23 and 24," in Solar Wind 14: Proceedings of the Fourteenth International Solar Wind Conference, eds., L. Wang, R. Bruno, E. Möbius, and G. P. Zank, AIP Conference Proceedings 1720: 070001 (2016); doi: 10.1063/1.4943838
- Desai, M. I., M. A. Dayeh, R. W. Ebert, D. J. McComas, G. M. Mason, G. Li, C. M. S. Cohen, R. A. Mewaldt, N. A. Schwadron, and C. W. Smith, "Spectral Properties of Large Gradual Solar Energetic Particle Events – II – Systematic Q/M-dependence of Heavy Ion spectral Breaks, , *The Astrophysical Journal*, 828, 106, 2016b
- Desai, M. I., Mason, G. M., Dayeh, M. A., Ebert, R. W., McComas, D. J., Li, G., Cohen, C. M. S., Mewaldt, R. A., Schwadron, N. A., and Smith, C. W., Charge-to-mass dependence of heavy ion spectral breaks in large gradual solar energetic particle events, Journal of Physics Conference Series, 767, 012004, 2016

Relevant Presentations

- Desai, M. I., D. J. McComas, E. R. Christian, A. C. Cummings, J. Giacalone, M. E. Hill, S. M. Krimigis, S. A. Livi, R. L. McNutt, R. A. Mewaldt, D. G. Mitchell, W. H. Matthaeus, E. C. Roelof, T. T. von Rosenvinge, N. A. Schwadron, E. C. Stone, M. M. Velli, and M. E. Wiedenbeck, "Suprathermal and Solar Energetic Particles: Key Questions for Solar Probe Plus," *Invited Talk (30 minutes)*, presented at the 1st Solar Probe Plus Workshop, Pasadena, March 26-29, 2013
- Desai, M. I., "Space Weather and the UTSA/SwRI Graduate Program in Physics," (1 hr.) Invited Seminar: The Jose Miguel Cimadevilla Memorial Seminar, Presented at St. Mary's University, Feb. 21, 2014

- Desai, M. I., D. J. McComas, E. R. Christian, A. C. Cummings, J. Giacalone, M. E. Hill, S. M. Krimigis, S. A. Livi, R. L. McNutt, R. A. Mewaldt, D. G. Mitchell, W. H. Matthaeus, E. C. Roelof, T. T. von Rosenvinge, N. A. Schwadron, E. C. Stone, M. M. Velli, and M. E. Wiedenbeck, "Suprathermal and Solar Energetic Particles: Key Questions for Solar Probe Plus and Solar Orbiter," *Invited Talk (25 minutes)*, presented at the Huntsville Workshop

2014, Solar and Stellar Processes from the Chromosphere to the Outer Corona', Orlando, Florida, March 23-28, 2014

- Desai, M. I., "Space Physics Research at SwRI and UTSA in San Antonio," (25 min.) Keynote Talk, Witte Museum, San Antonio, May 5, 2014
- Desai, M. I., G. M. Mason, M. A. Dayeh, R. W. Ebert, D. J. McComas, G. Li, C. M. S. Cohen, R. A. Mewaldt, N. A. Schwadron, and C. W. Smith, "Systematic Behavior of Heavy Ion Spectra in Large Gradual Solar Energetic Particle Events," Invited Paper (25 mins.) Presented at the 14th Annual International Astrophysics Conference (AIAC) in Tampa Bay, Fl, April 20-24, 2015
- Desai, M. I., "Origin and Acceleration of Suprathermal Ions," Invited Paper (30 mins), Presented at the 14th Solar Wind Conference, Weihei, China, June 22-27, 2015
- Desai, M. I., "The Role of Suprathermal Ions in Particle Acceleration," Invited Paper (25mins), Presented at the From IMP-8 to Solar Orbiter: Glenn M. Mason Commemorative Conference, March 8, 2016, Johns Hopkins University/Applied Physics Laboratory, Laurel, MD, USA
- Desai, M. I., G. M. Mason, M. A. Dayeh, R. W. Ebert, D. J. McComas, G. Li, C. M. S. Cohen, R. A. Mewaldt, N. A. Schwadron, and C. W. Smith, "Systematic Behavior of Heavy Ion Spectra in Large Gradual Solar Energetic Particle Events," Invited Paper (25 mins.) Presented at the 15th Annual International Astrophysics Conference (AIAC) in Cape Coral, FL, April 20-24, 2016
- Gorby, M., N. A. Schwadron, M. A. Lee, A. C. Booth, H. E. Spence, T. Torok, C. Downs, R. Lionello, J. Linker, V. S. Titov, Z. Mikic, P. Riley, M. I. Desai, M. A. Dayeh, and K. A. Kozarev, Contributed paper (15 mins), "Particle Acceleration in the Low Corona Over Broad Longitudes: Coupling Between 3D Magnetohydrodynamic and Energetic Particle Models," Abstract SH32B-06, presented at 2013 Fall Meeting, AGU, San Francisco, Calif., 9-13 Dec., 2013.
- Vines, S. K., M. I. Desai, K. Ogasawara, K. Leera, S. G. Kanekal, S. A. Livi, and E. R. Christian, "Characterizing SEP electrons with the Compact Radiation Belt Explorer (CeREs)," Poster paper presented at the SHINE workshop in Telluride, Colorado, June 22-27, 2014
- Desai, M I.,M. A. Dayeh, R. W. Ebert, D. J. McComas, G. M. Mason, C. M. S. Cohen, Gang Li, R. A. Mewaldt & C. W. Smith, "Spectral Properties of Large Gradual SEP Events," Paper no. D1.2-0009-14, Contributed Talk (25 mins.) Presented at the 40th COSPAR Scientific Assembly, 2 -10 August 2014, Moscow, Russia
- Gorby, M., N. A. Schwadron, T. Torok, C. Downs, R. Lionello, J. Linker, V. Titov, Z. Mikic, P. Riley, M. I. Desai, and M. A. Dayeh, "Particle Acceleration in the Low Corona Over Broad Longitudes: Coupling MHD and 3D Particle Simulations," Abstract SH21B-4127, poster paper presented at 2014 Fall Meeting, AGU, San Francisco, Calif., 15-19 Dec., 2014
- Desai, M. I., D. J. McComas, E. R. Christian, R. A. Mewaldt, and N. A. Schwadron, "Suprathermal and Solar Energetic Particles – Key questions for the Interstellar Mapping and Acceleration Probe (IMAP)," Abstract SH23B-4157, Poster paper presented at 2014 Fall Meeting, AGU, San Francisco, Calif., 15-19 Dec., 2014
- Mason, G. M., M. I. Desai, M. A. Dayeh, R. W. Ebert, D. J. McComas, G. Li, C. M. S. Cohen, R. A. Mewaldt, and C. W. Smith, "Spectral Properties of Large Gradual Solar Energetic Particle Events," Abstract SH32A-04, Contributed Talk (13 mins) presented at 2014 Fall Meeting, AGU, San Francisco, Calif., 15-19 Dec., 2014
- Desai, M. I., G. M. Mason, M. A. Dayeh, R. W. Ebert, D. J. McComas, G. Li, C. M. S. Cohen, R. A. Mewaldt, N. A. Schwadron, and C. W. Smith, "Spectral Properties of Large

Gradual Solar Energetic Particle Events," Contributed Poster presented at the Solar, Heliospheric and Interplanetary (SHINE) Workshop, July 6 – 10, 2015, Stowe, Vermont.

- Desai, M. I., G. M. Mason, M. A. Dayeh, R. W. Ebert, D. J. McComas, G. Li, C. M. S. Cohen, R. A. Mewaldt, N. A. Schwadron, and C. W. Smith, "Systematic Behavior of Heavy Ion Spectra in Large Gradual Solar Energetic Particle Events," Contributed Talk (15 mins.), Presented at the 34th International Cosmic Ray Conference at The Hague, Netherlands, July 30 – August 6, 2015
- Desai, M. I., G. M. Mason, M. A. Dayeh, R. W. Ebert, D. J. McComas, G. Li, C. M. S. Cohen, R. A. Mewaldt, N. A. Schwadron, and C. W. Smith, "Systematic Behavior of Heavy Ion Spectra in Large Gradual Solar Eneregtic Particle Events," Contributed Poster, Presented at the Joint Solar Probe Plus Solar Orbiter Workshop in Artiminio, Italy, August 31 – September 4, 2015
- Ebert, R. W., M. A. Dayeh, M. I. Desai, G. Li, and G. M. Mason, "Multi-Spacecraft Analysis of Energetic Heavy Ions and Interplanetary Shock Properties in Energetic Storm Particle Events at 1 AU," Abstract SH33B-2469, poster paper presented at 2015 Fall Meeting, AGU, San Francisco, Calif., 14-18 Dec., 2015
- Desai, M., Mason, G., McComas, D., Cohen, C., Smith, C., Ebert, R., Schwadron, N., Li, G., Mewaldt, R., and Dayeh, M. A., Systematic Charge-to-Mass-Dependence of Heavy Ion Spectral Breaks in Large Gradual Solar Energetic Particle Events, 41st COSPAR Scientific Assembly, 41, 2016
- Desai, M., Mason, G., Ebert, R., Dayeh, M., McComas, D., Li, G., Mewaldt, R., Cohen, C., Schwadron, N., and Snith, C., Systematic Charge-to-Mass-Dependence of Heavy Ion Spectral Breaks in Large Gradual Solar Energetic Particle Events, EGU General Assembly Conference Abstracts, 18, 2199, 2016
- Desai, M., McComas, D., Dayeh, M., Funsten, H., Schwadron, N., Heerikhuisen, J., Fuselier, S., Pogorelov, N., Zank, G., and Allegrini, F., Latitude, Energy, and Time Variations of Energetic Neutral Atom Spectral indices Measured by IBEX, EGU General Assembly Conference Abstracts, 18, 2196, 2016

II.7 C-SWEPA Progress Deliverable Models

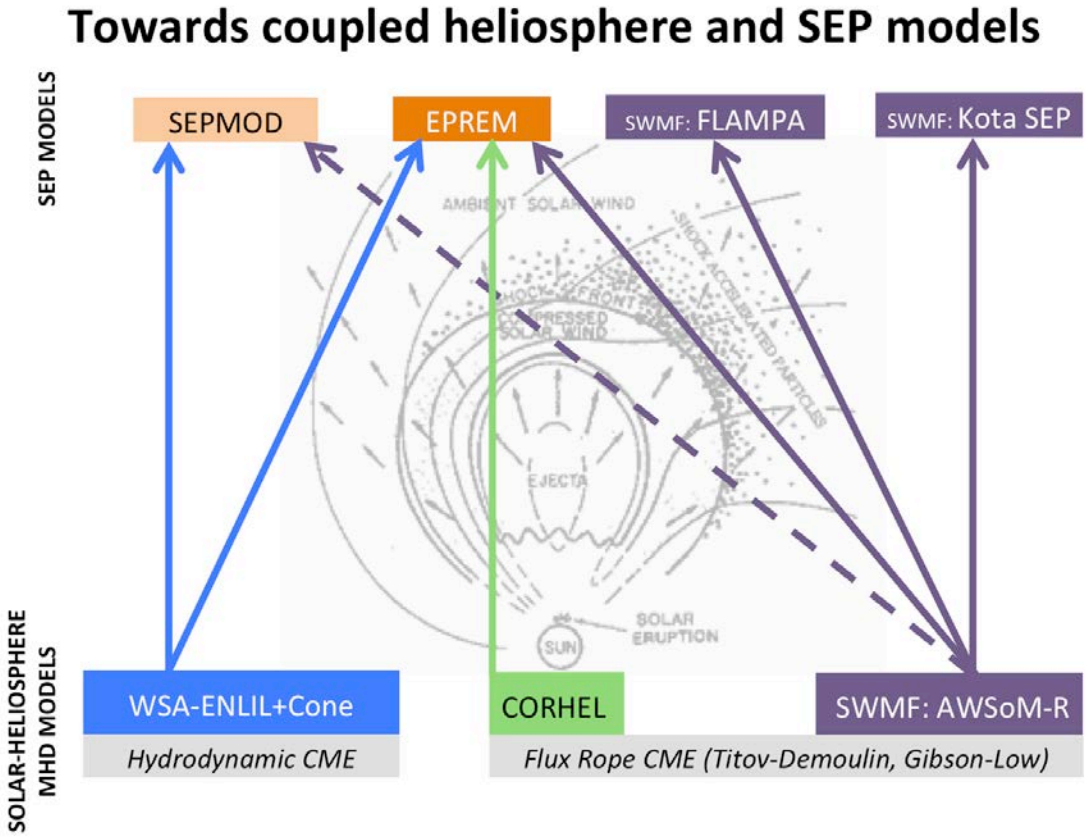

Figure II.7.1: *Diagram of SEP models at the CCMC and the MHD simulations they couple to.*

Coupled Models:

EPREM has already been coupled to the main MHD codes working at the CCMC (Figure II.7.1). The coupling between EPREM and both Enlil and MAS work in the same way, with the specific differences discussed below. After the MHD simulation is completed the output files containing the field values are used as inputs for the values on the EPREM nodes. No intermediate interpolation is necessary as EPREM handles it internally as the simulation is running. An appropriate spatial resolution is chosen to ensure the EPREM domain reaches to the end of the MHD simulation domain, which due to the Lagrangian grid is a mixture of the time-step and flow magnitude. The first MHD output file is treated as an equilibrium solution for the purpose of reaching an initial stable state for EPREM. An initial time-step can be specified manually or usually the time difference between the first two MHD files is used. The field values and the chosen time-step are used to propagate the EPREM nodes out until the streams (nodes spawned at the same footpoint) are static in space. A source distribution is then injected on the inner nodes and the simulation continues with the same time-step and field values until the solution along each stream is stable to within a tolerance. At that point the coupling is allowed to advance with

each new global time-step being a new input file from the MHD simulation. To ensure a tight coupling the nodes advance in space on a subdivided time-step and the field values are interpolated linearly in time. EPREM finishes when the final MHD output file has been used.

An EPREM run is initiated with an easy-to-edit configuration file that specifies the conditions for the simulation. Energy range, mean free path scaling, cross-field diffusion efficiency, source distribution scaling, inner boundary, and many other quantities can be specified at run-time. In addition, the different physics modules can be turned on/off: parallel diffusion, adiabatic focusing, adiabatic change, shock solver, particle drift, and perpendicular diffusion. The type of output and output cadence can be specified as well. There is a specific section on output and visualization below.

EPREM-Enlil Coupling:

The Enlil domain begins at 0.1AU and can extend out well past 5AU. Most simulations are run for actual events using time-dependent magnetograms as the source for the inner boundary. Comparison between EPREM output and actual observations are possible as Enlil provides .evo (observer evolution) files that specify the positions of the planets and satellites which are then used to create point observers within EPREM. The coupling between EPREM and Enlil can handle both the previous version of Enlil (v2.7) with the static magnetograms and the newest Enlil version (v2.8) which supports the time-dependent maps. This backward compatibility taps into the massive back-catalog of Enlil runs currently stored at the CCMC.

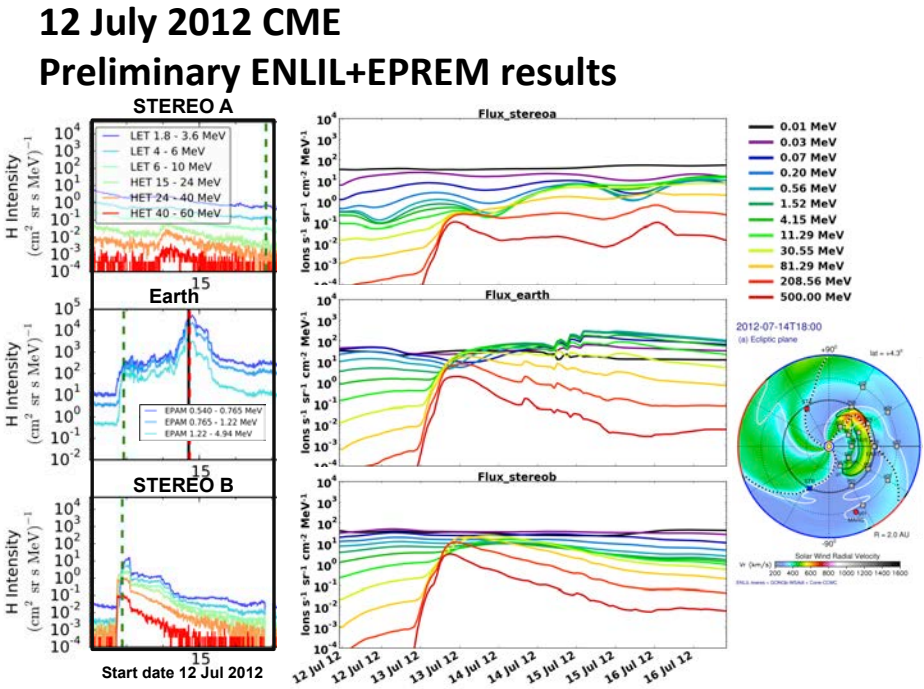

Figure II.7.2: *Initial results comparing the observed and simulated differential energy flux for the 12 July 2012 event at Stereo A, Stereo B, and Earth.*

EPREM-MAS Coupling:

The CMEs simulated by Predictive Science Inc's MAS code are extremely detailed and cover the low coronal environement. They are initiated with a modified Tetov-Demoulin flux rope, contain a complex internal magnetic structure, and output at a high cadence with the time-steps dropping to as low as 30 seconds during the eruption phase. The inner boundary is at the photosphere with an outer boundary of 20 solar radii. It is still possible to run the EPREM streams past the outer boundary to obtain results at 1AU. Whereas the Enlil coupled simulations are good for direct comparison to observations, the MAS simulations excel at examining the fine-detailed processes of particle acceleration in and around a prompt CME low in the corona.

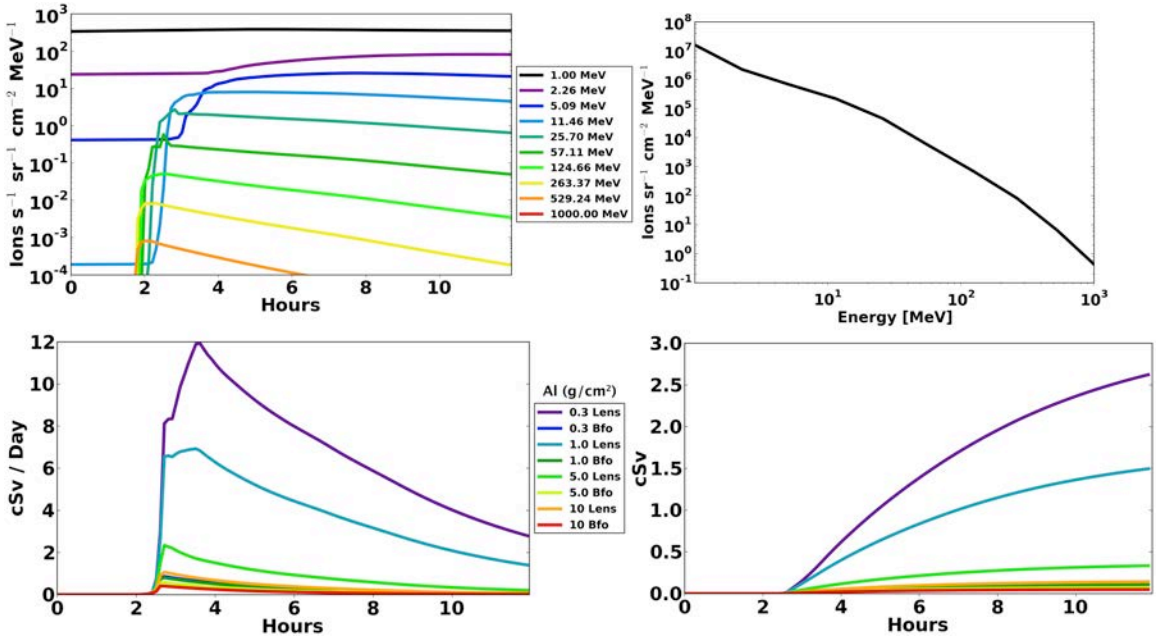

Figure II.7.3: *(Clock-wise from top left) Differential energy flux, event integrated spectrum, dose, and event integrated dose at 1AU for an EPREM-MAS coupled simulation of a prompt CME initiated at the photosphere and propagating out to 20 solar radii.*

Cone-CME:

Originally developed as a diagnostic tool for the newly implemented shock routine, the Cone-CME module has taken on a life of its own as a stand-alone EPREM product. Due to coupling to multiple MHD codes the dependencies for the full EPREM model have grown myriad. The stand-alone CME module strips away the dependency barriers and works as an easy-to-install, easy-to-use product for examining particle acceleration. It is still included in the EPREM-ENLIL coupled code as a module and can be used with the runs-on-request and eventually the runs-on-demand at the CCMC. The stand-alone product will be available for download through an FTP site at UNH and linked to through the model webpage at the CCMC.

As with the coupled models, a configuration file is passed to the simulation that specifies the inner boundary radius, energy range, output types, which physics to turn on/off, etc. In addition to the usual parameters the conditions for the shock are also specified. The shock jump magnitude, scale length, injection efficiency, shock speed, and time of shock arrival at the inner boundary are

all configuration parameters. The shock can be run as a spherically symmetric discontinuity which appears everywhere on the domain, or an angular spread can be specified which allows it to be run as a cone CME.

Dr. Kozarev will conduct future work on the Cone-CME module and include: the ability to specify a more complex field configuration; a proper rarefaction region; and the ability to specify a different distribution source.

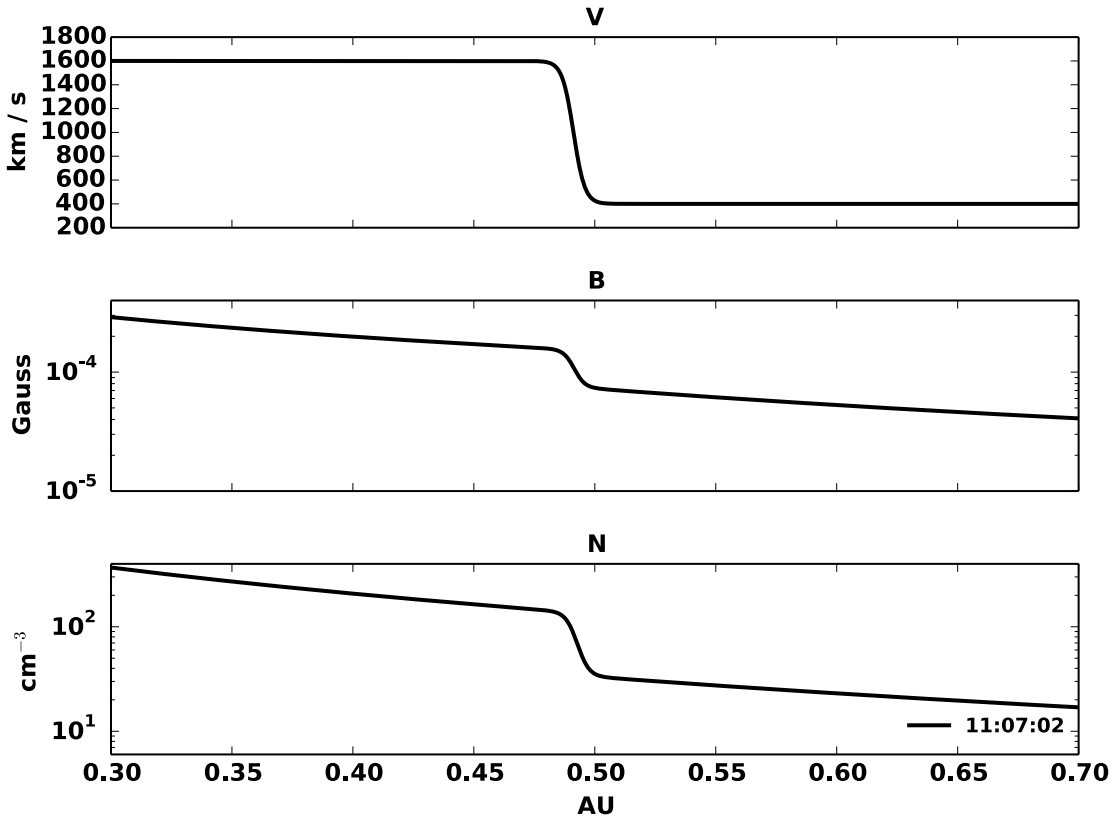

Figure II.7.4: *Velocity, magnetic field, and density magnitude profiles for a shock specified with a solar wind speed of 400 km/s, a jump of 4x, and a scale length of 0.01AU.*

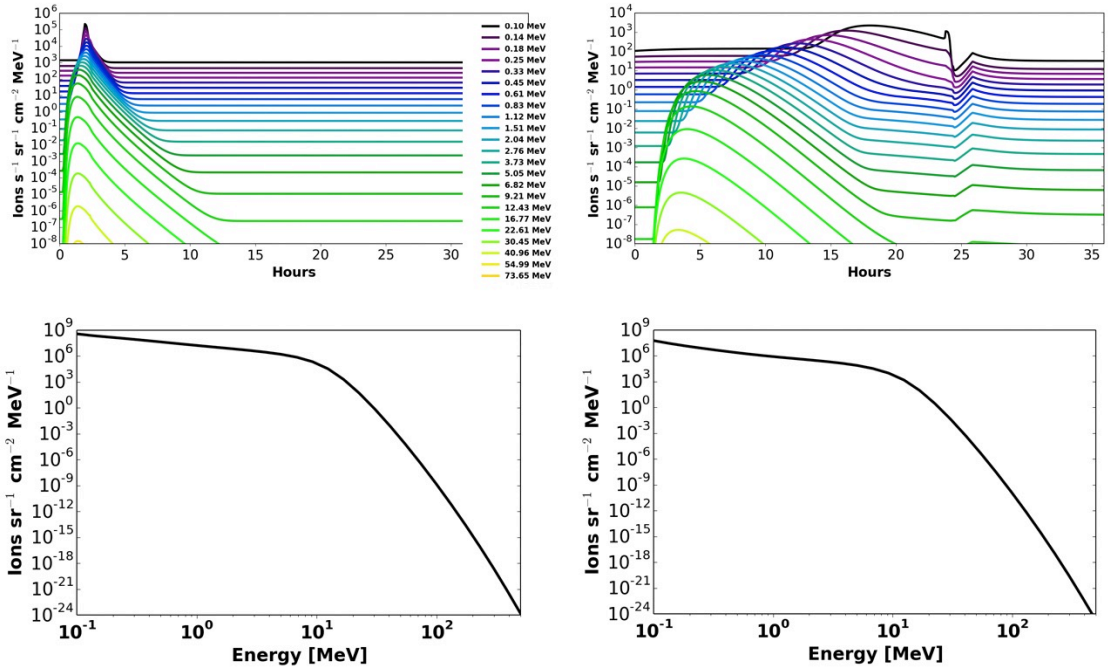

Figure II.7.5: *Results for the stand-alone cone CME module. The top two panels are the differential energy flux vs. time for a cut along a stream at 0.1AU and 1.0AU. The bottom two panels are the event integrated spectrum, also at 0.1 and 1.0AU.*

Output and visualization:

EPREM has three types of output file: domain, stream, and point observer. The domain output is a single netCDF file which contains the spatial position of each node along all the streams, for every output time-step. Stream output files contain not only spatial positions of each node along a stream but also field values and the distribution function at each output time-step. In addition to the time dependent information, all of the static data structures such as the energy and velocity bins, pitch angle bins, and mass and charge bins are stored in the output file. The point observer files have an identical structure to the stream output files, but are used when either a static or dynamic point observer is specified when the simulation runs, e.g. Earth, a satellite, Mars, etc.

The suite of visualization routines are all written using Python and are command-line configurable for ease of scripting or putting together animations. The output netCDF files can be used at any point during their creation to visualizing the progress of the simulation while it is still running is possible.

In addition to the domain file being used to visualize how the streams evolve over time, it can be combined with the individual stream output to overlay either field values or the distribution function. The differential energy flux, spectra, time integrated spectra, field values at a radial cut, field values along a stream, time and spatial derivatives, scattering mean free path, and many other derived quantities can be plotted either individually or on a grid of images in a single frame.

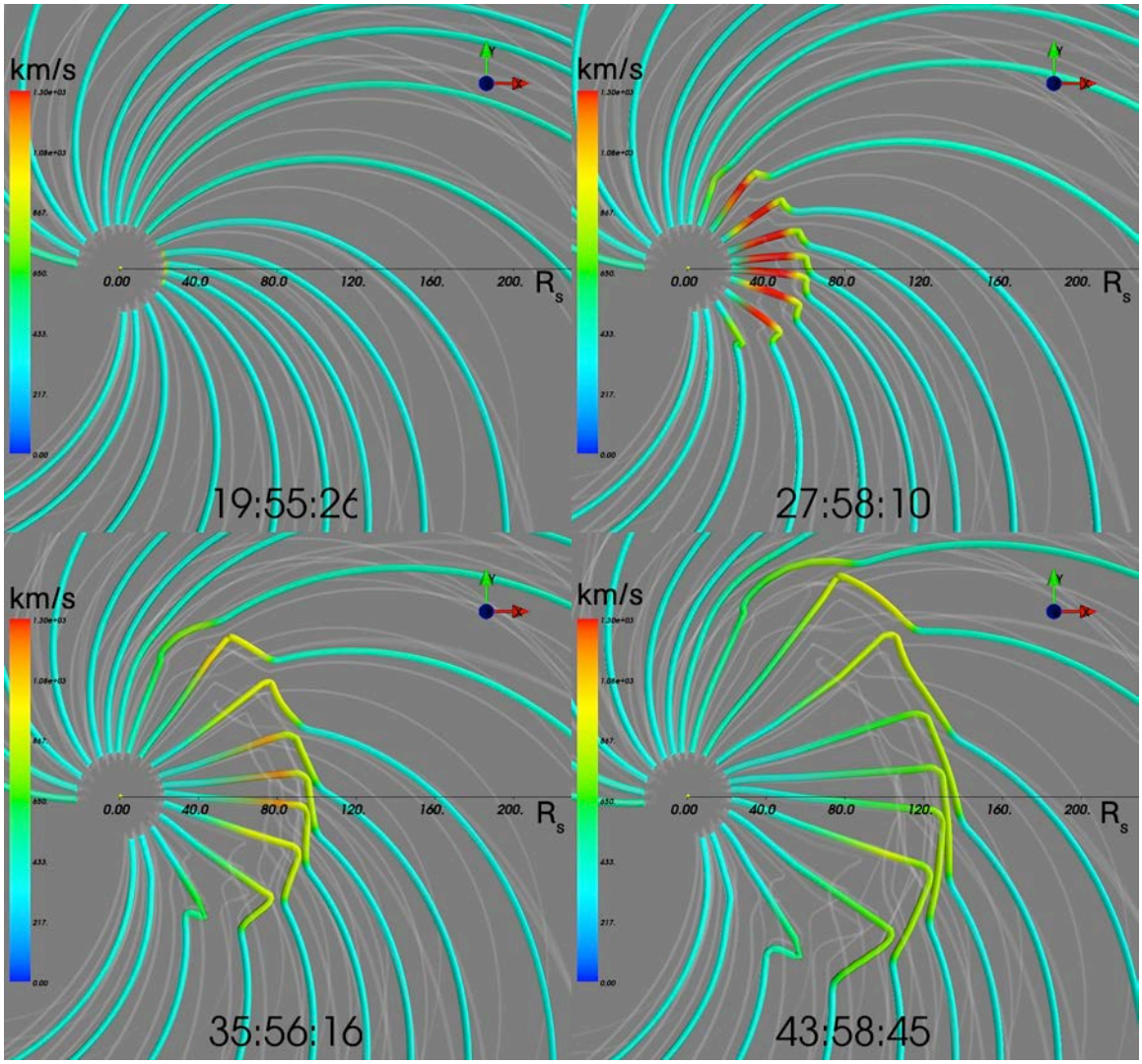

Figure II.7.5: EPREM domain plot at four snapshots during the evolution of an Enlil simulated CME. The bold streams are on the ecliptic plane and are colored by the velocity magnitude.

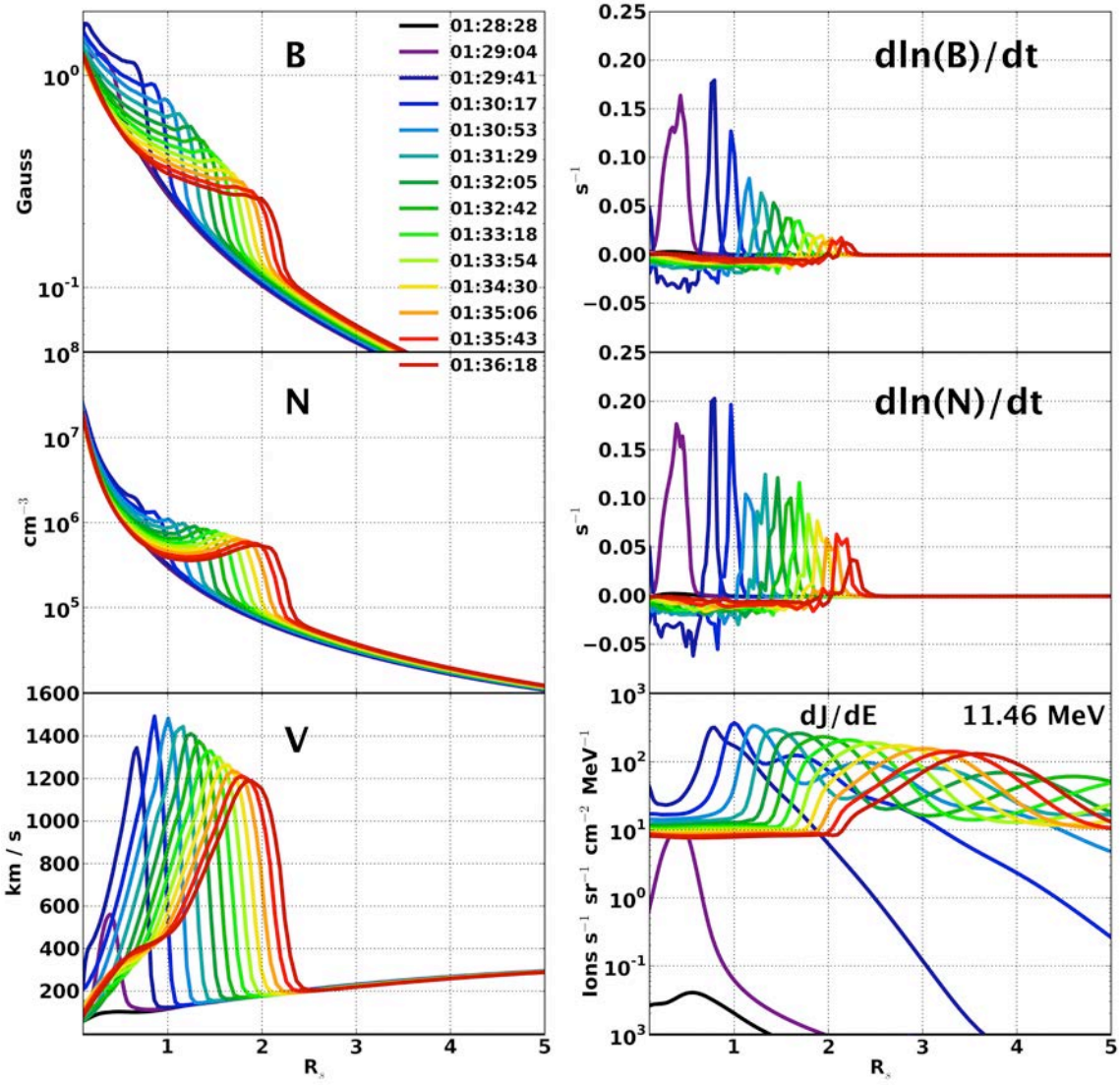

Figure II.7.6: *An example of a grid of different plots, all presented on the same frame. In this case, multiple time-steps are represented on the same plot to clearly show the evolution of the CME along a stream during an eruption. This plot was produced with a single call on the command-line.*

CONTINUED WORK ON DELIVERABLES:

The bulk of the development for the model deliverables is completed. The work to still complete includes: having the resolution adjust automatically based on the initial time-step and number of processors; initial particle equilibrium detected automatically vs. specifying an equilibrium time duration; complete the output pipeline through to calculating and visualizing the radiation doses behind various levels of shielding; get the web-form based runs-on-request system up online at the CCMC; and producing a robust set of documentation for both the coupled models and the Cone-CME.

Relevant Publications:

- Schwadron, N. A., Gorby, M., Torok, T., Downs, C., Linker, J., Lionello, R., Mikic, Z., Riley, P., Giacalone, J., Chandran, B., Germaschewski, K., Isenberg, P. A., Lee, M. A., Lugaz, N., Smith, S., Spence, H. E., Desai, M., Kasper, J., Kozarev, K., Korreck, K., Stevens, M., Cooper, J., and MacNeice, P., Synthesis of 3-D Coronal-Solar Wind Energetic Particle Acceleration Modules, Space Weather, 12, 323, 2014
- Schwadron, N. A., Lee, M. A., Gorby, M., Lugaz, N., Spence, H. E., Desai, M., Torok, T., Downs, C., Linker, J., Lionello, R., Mikic, Z., Riley, P., Giacalone, J., Jokipii, J. R., Kota, J., and Kozarev, K., Broken Power-law Distributions from Low Coronal Compression Regions or Shocks, Journal of Physics Conference Series, 642, 012025, 2015
- Schwadron, N. A., Lee, M. A., Gorby, M., Lugaz, N., Spence, H. E., Desai, M., Torok, T., Downs, C., Linker, J., Lionello, R., Mikic, Z., Riley, P., Giacalone, J., Jokipii, J. R., Kota, J., and Kozarev, K., Particle Acceleration at Low Coronal Compression Regions and Shocks, The Astrophysical Journal, 810, 97, 2015

Relevant Presentations

- Linker, J., Mikic, Z., Schwadron, N., Riley, P., Gorby, M., Lionello, R., Downs, C., and Torok, T., Time-Dependent Coupled Coronal-Solar Wind-SEP Modeling, 40th COSPAR Scientific Assembly, 40, 2014
- Gorby, M., Schwadron, N., Torok, T., Downs, C., Lionello, R., Linker, J., Titov, V. S., Mikic, Z., Riley, P., Desai, M. I., and Dayeh, M. A., Particle Acceleration in the Low Corona Over Broad Longitudes: Coupling MHD and 3D Particle Simulations, AGU Fall Meeting Abstracts, 2014
- Gorby, M., Schwadron, N., Lee, M. A., Booth, A. C., Spence, H., Torok, T., Downs, C., Lionello, R., Linker, J., Titov, V. S., Mikic, Z., Riley, P., Desai, M. I., Dayeh, M. A., and Kozarev, K. A., Particle Acceleration in the Low Corona Over Broad Longitudes: Coupling Between 3D Magnetohydrodynamic and Energetic Particle Models, AGU Fall Meeting Abstracts, 2013
- Riley, P., Ben-Nun, M., Lionello, R., Downs, C., Torok, T., Linker, J., Mikic, Z., Schwadron, N., and Gorby, M., Understanding the Evolution of the July 23, 2012 Extreme ICME: Global Modeling and Comparison with Observations, AGU Fall Meeting Abstracts, 2013
- Schwadron, N. A., Christian, E. R., Gorby, M. J., and McComas, D. J., Revealing the Acceleration and Propagation of SEPs with the Unprecedented and Coordinated Near-Sun Observations from Solar Probe and Solar Orbiter, AGU Spring Meeting Abstracts, 2013
- Gorby, M. J., Schwadron, N. A., Linker, J. A., Spence, H. E., Townsend, L. W., and Cucinotta, F. A., New Tools to Discover the Physical Links From CME Eruptions to Radiation Effects in Deep Space: a First in Heliospheric End-to-End Coupling, AGU Fall Meeting Abstracts, 2012
- Gorby, M. J., Schwadron, N. A., Linker, J. A., Spence, H. E., Townsend, L. W., Cucinotta,

F. A., and Wilson, J. K., From CMEs to Earth/Lunar Radiation Dosages: A First in Heliospheric End-to-End Coupling, Annual Meeting of the Lunar Exploration Analysis Group, 1685, 3043, 2012

- Spence, H. E., Schwadron, N. A., Gorby, M., Joyce, C., Quinn, M., LeVeille, M., Smith, S., Wilson, J., Townsend, L., and Cucinotta, F., PREDICCs: A Radiation Prediction Tool for Lunar, Planetary, and Deep Space Exploration, Annual Meeting of the Lunar Exploration Analysis Group, 1685, 3032, 2012
- Mays, M. L., Odstrcil, D., Luhmann, J., Bain, H., Li, Y., Schwadron, N., Gorby, M., Thompson, B., Jian, L., Möstl, C., Rouillard, A., Davies, J., Temmer, M., Rastaetter, L., Taktakishvili, A., MacNeice, P., and Kuznetsova, M., ENLIL Global Heliospheric Modeling as a Context For Multipoint Observations, EGU General Assembly Conference Abstracts, 18, 11638, 2016
- Mays, M. L., Luhmann, J. G., Odstrcil, D., Lee, C., Bain, H. M., Li, Y., Schwadron, N., Gorby, M., Baker, D. N., Dewey, R. M., Larson, D. E., Halekas, J. S., Connerney, J. E. P., von Rosenvinge, T. T., Galvin, A. B., and McComas, D. J., SEP modeling based on the ENLIL global heliospheric model, AGU Fall Meeting Abstracts, 2015
- Mays, M. L., Luhmann, J. G., Odstrcil, D., Schwadron, N., Gorby, M., Bain, H. M., Mewaldt, R. A., and Gold, R. E., Modeling SEPs and Their Variability in the Inner Heliosphere, AGU Fall Meeting Abstracts, 2015
- Torok, T., Gorby, M., Linker, J., and Schwadron, N., Coupling MHD Simulations of CMEs to SEP Models, AGU Fall Meeting Abstracts, 2015

II.8 C-SWEPA Progress on Understanding the Propagation of ICMEs and the Development of Magnetic Complexity

In order to shed light on ICME propagation in the inner heliosphere, the members of the C-SWEPA team have used observations from the MErcury Surface, Space ENvironment, GEochemistry, and Ranging (MESSENGER) spacecraft, in orbit around Mercury, to investigate ICMEs near 0.3 AU. MESSENGER, the first spacecraft since the 1980s to make in-situ measurements at distances < 0.5 AU, presents a unique opportunity for observing the innermost heliosphere. It also allows studies of ICME evolution as they expand and propagate outward, interacting with the solar wind. In order to catalog ICME events observed by MESSENGER, we designed a strict set of selection criteria to identify them based on magnetic field observations only, since reliable solar wind plasma observations are not available from MESSENGER. We identified 61 ICME events observed by the MESSENGER Magnetometer between 2011 and 2014, and conducted statistical analyses of ICME properties at Mercury. In addition, using existing datasets of ICMEs at 1 AU we investigated key ICME property changes from Mercury to 1 AU. We find good agreement with previous studies for the magnetic field strength dependence on heliospheric distance, *r*. We have also established three different lines of evidence that ICME deceleration continues beyond the orbit of Mercury: 1) we find a shallow decrease with distance of $\sim r^{-0.45}$ for the ICME shock speed from Mercury to 1 AU, 2) the average transit speed from the Sun to Mercury for ICMEs in our catalog is ~20% faster than the average speed from the Sun to 1 AU, 3) the ICME transit time to 1 AU has a weaker dependence on the CME initial coronagraphic speed, as compared to what we predict based on our MESSENGER ICME catalog. Based on our results, future ICME propagation studies should account for ICME speed changes beyond Mercury's heliocentric distances to improve ICME arrival time forecasting. Our ICME

database will also prove particularly useful for multipoint spacecraft studies of recent ICMEs, as well as for model validation of ICME properties.

Illustrating the benefit of our ICME database, we used data on an ICME seen by MESSENGER and STEREO A starting from 29 December 2011 in a near-perfect longitudinal conjunction (within 3◦) to study changes in the ICME's structure via interaction with the solar wind in less than 0.6 AU. From force-free field modeling we infer that the orientation of the underlying flux rope has undergone a rotation of ~80◦ in latitude and ~65◦ in longitude. Based on both spacecraft measurements as well as ENLIL model simulations of the steady state solar wind, we find that interaction involving magnetic reconnection with corotating structures in the solar wind dramatically altered the ICME magnetic field. In particular, we observed a highly turbulent region with distinct properties within the flux rope at STEREO A (see Figure II.8.1), not observed at MESSENGER, which we attribute to interaction between the ICME and a heliospheric plasma sheet/current sheet during propagation. The short duration, multiple successions of bi-directional and uni-directional suprathermal electron flows in the turbulent region are indicative of the spacecraft traversing a succession of closed and open field lines within this short time frame. We infer that most likely the closed field lines of the ICME, interchange reconnected with the open field lines of the HPS in transit between ~0.4 and ~1 AU, thereby opening up some of the closed ICME field lines.

Our case study is a concrete example of a sequence of events that can increase the complexity of ICMEs with heliocentric distance even in the inner heliosphere. The results highlight the need for large-scale statistical studies of ICME events observed in conjunction at different heliocentric distances to determine how frequently significant changes in flux rope orientation occur during propagation. These results also have significant implications for space weather forecasting and should serve as a caution on using very distant observations to predict the geo-effectiveness of large interplanetary transients.

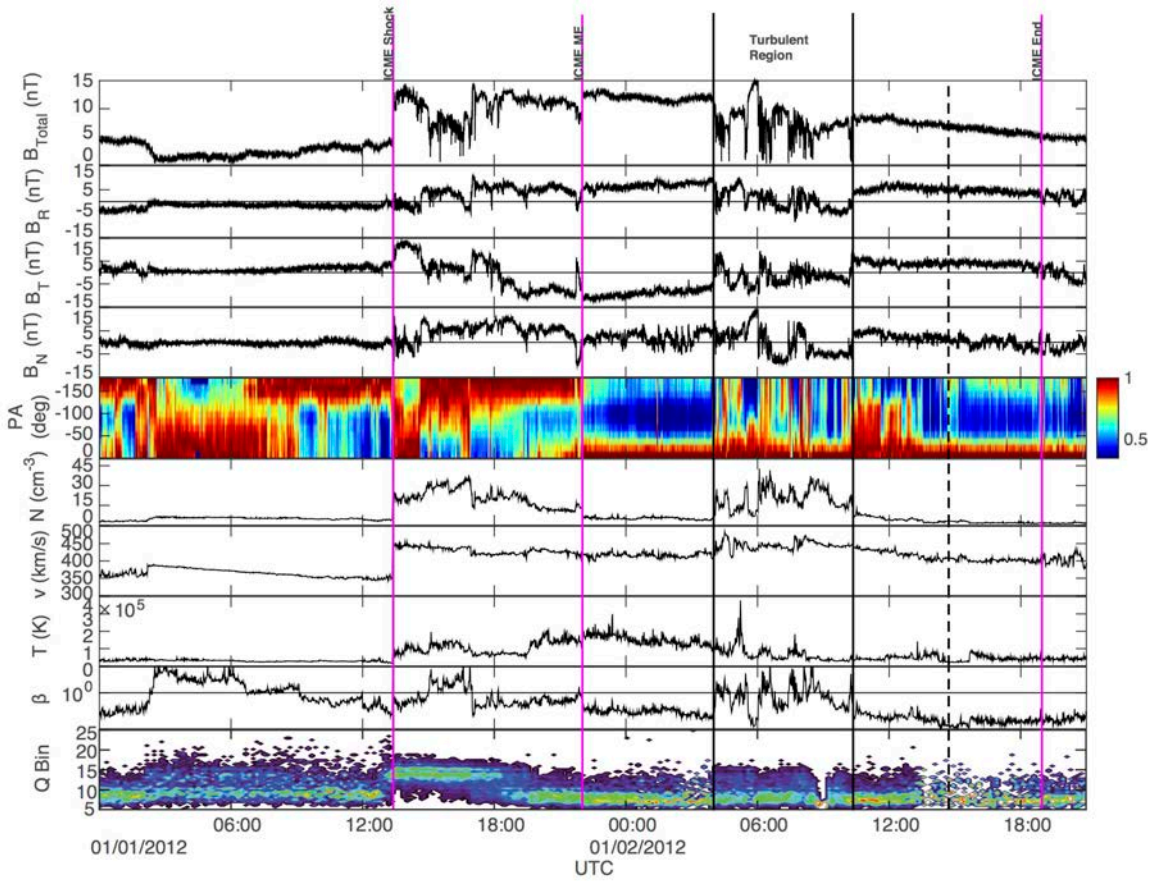

Figure II.8.1: *STEREO A magnetic field and plasma data of the ICME on days 1-2 January 2012. From top to bottom: the magnetic field magnitude, the magnetic field vector components in RTN coordinates, suprathermal electron pitch angle distributions, the proton density, velocity, temperature, the plasma β, and the 10-minute averaged iron charge state distribution over the time period. Vertical magenta lines denote the crossing time of the ICME shock, magnetic ejecta, and ICME end, while the black vertical lines denote the start and end of the turbulent region. The black dashed line indicates the time of the return to bi-directional electron flows in the magnetic ejecta.*

Lugaz et al. (2016) studied the interaction between Earth's magnetic field and the solar wind results in the formation of a collisionless bow shock 60,000-100,000 km upstream of our planet, as long as the solar wind fast magnetosonic Mach (hereafter Mach) number exceeds unity. Here, we present one of those extremely rare instances, when the solar wind Mach number reached steady values <1 for several hours on 17 January 2013. Simultaneous measurements by more than ten spacecraft in the near-Earth environment reveal the evanescence of the bow shock, the sunward motion of the magnetopause and the extremely rapid and intense loss of electrons in the outer radiation belt. This study allows us to directly observe the state of the inner magnetosphere, including the radiation belts during a type of solar wind-magnetosphere coupling which is unusual for planets in our solar system but may be common for close-in extrasolar planets.

Relevant Publications:

. Winslow, R. M., N. Lugaz, L. C. Philpott, N. A. Schwadron, C. J. Farrugia, B. J. Anderson, and C. W. Smith (2015), Interplanetary coronal mass ejections from MESSENGER orbital observations at Mercury, *J. Geophys. Res. Space Physics*, *120*, doi:10.1002/2015JA021200.

. Winslow, R. M., Lugaz, N., Schwadron, N. A., Farrugia, C. J., Yu, W., Raines, J. M., Mays, M. L., Galvin, A. B., and Zurbuchen, T. H., Longitudinal conjunction between MESSENGER and STEREO A: Development of ICME complexity through stream interactions, Journal of Geophysical Research (Space Physics), 121, 6092, 2016

. Lugaz, N., Farrugia, C. J., Huang, C.-L., Winslow, R. M., Spence, H. E., and Schwadron, N. A., Earth's magnetosphere and outer radiation belt under sub-Alfvénic solar wind, Nature Communications, 7, 13001, 2016

Relevant Presentations

. Winslow, R., Anderson, B. J., Schwadron, N., Lugaz, N., Farrugia, C., Philpott, L., and Paty, C., Interplanetary coronal mass ejections at Mercury: Database and effects on the magnetosphere, 41st COSPAR Scientific Assembly, 41, 2016

. Lugaz, N., Al-haddad, N., Schwadron, N., Riley, P., Farrugia, C., and Winslow, R., The Geo-Effectiveness of CME-Driven Shocks and Sheaths, 41st COSPAR Scientific Assembly, 41, 2016

. Lugaz, N., Huang, C.-L., Schwadron, N., Spence, H., Farrugia, C., and Winslow, R., Losses of Energetic Electrons in Earth's Outer Radiation Belt During Unusual Coronal Mass Ejections, 41st COSPAR Scientific Assembly, 41, 2016

. Winslow, R. M., Lugaz, N., Philpott, L. C., Schwadron, N., Farrugia, C. J., Anderson, B. J., and Smith, C. W., Interplanetary Coronal Mass Ejections from MESSENGER Orbital Observations at Mercury, AGU Fall Meeting Abstracts, 2015

II.9 Can Solar Active Regions Harbor Energy for Superflares?

The question of whether so-called superflares (energies from 10^{33}-10^{35} ergs) could occur on the Sun is of great interest scientifically. There are also obvious practical (space weather) implications. Shibata et al. (2013) suggested that flares on the order of 10^{34} ergs could occur every 800 years on the Sun, while Schrijver et al. (2012) argued that the magnetic energy for such a flare would require a sunspot 20 times greater then ever observed, and that 10^{33} ergs was a practical upper limit for flares.

Major solar eruptions such as X-class flares and very fast coronal mass ejections originate in active regions on the Sun. The energy that powers these events is believed to be stored as free magnetic energy (E_F - energy above the potential field state) prior to eruption. Therefore, the maximum free energy (ME_F) that can be stored in an active region bounds the largest possible eruption that can emanate from it. Using line-of-sight or vector magnetograms, the maximum energy that can be stored in a region can be estimated with the aid of the Aly-

Sturrock theorem. We have investigated the active regions where the largest flares in the last 30 years have originated. Table 1 shows the ten largest ME_F values we found. Five of these active regions had an ME_F on the order of or greater than 10^{34} ergs. Our results suggest that 10^{34} ergs solar flares cannot be ruled out based on magnetic energy storage.

Maximum E_F of Selected Active Regions

AR	Magnetogram Date	Magnetic Flux (10^{22} Mx)	ME_F (10^{33} ergs)
10486	2003/10/30	9.28	21.10
5395	1989/3/12	10.23	19.82
12192	2014/10/24	9.51	14.43
6659	1991/6/9	7.14	12.09
10720	2005/1/19	4.76	9.47
11520	2012/7/12	5.53	6.41
5747	1989/10/18	4.95	5.31
9415	2001/4/6	3.29	4.58
9077	2000/7/14	3.81	4.28
8100	1997/11/5	3.73	4.11

Table II.9.1. Maximum Free Energy available in ten flare-productive active regions.

References

- Schrijver, C. J., Beer, J., Baltensperger, U., Cliver, E. W., Gudel, M., Hudson, H. S., McCracken, K. G., Osten, R. A., Peter, T., Soderblom, D. R., Usoskin, I. G., and Wolff, E. W. (2012). Estimating the frequency of extremely energetic solar events, based on solar, stellar, lunar, and terrestrial records. Journal of Geophysical Research (Space Physics), 117:A08103.
- Shibata, K., Isobe, H., Hillier, A., Choudhuri, A. R., Maehara, H., Ishii, T. T., Shibayama, T., Notsu, S., Notsu, Y., Nagao, T., Honda, S., and Nogami, D. (2013). Can Superflares Occur on Our Sun? PASJ, 65.

II.10 Data Sharing and Products

The MESSENGER ICME database is available online as the supplemental material of Winslow et al. [2015]. The database (http://spdf.gsfc.nasa.gov/pub/data/messenger/ and http://c-swepa.sr.unh.edu/icmecatalogatmercury.html) makes available the CME launch time at the Sun, the ICME arrival time and end time at MESSENGER, the max and mean magnetic fields, the estimated transit speed, and MESSENGER's heliocentric distance.

NASA's Virtual Energetic Particle Observatory (VEPO) provides enhanced access to energetic particle data sets of strong interest to C-SWEPA for comparison of time intensities and variously-averaged flux spectra from still-operational experiments on ACE, Stereo-A/B, Wind, SOHO, and GOES. Archival data are also available from Ulysses, IMP-8, Helios 1 & 2, Pioneer 10 & 11, and

Voyager 1 &2. Fluxes and spectra can be compared from various sources for omnidirectional protons, helium, and heavier ions. The latest addition includes full energy distributions for thermal to suprathermal protons and alphas from the Solar Wind Ion Composition Spectrometer on the ACE spacecraft. Future additions of similar distributions are planned from Wind and Ulysses. New Horizons solar wind plasma moments are already available from the related Coordinated Data Analysis Web (CDAWeb) service at cdaweb.gsfc.nasa.gov, and energetic particle flux data from the PEPSSI instrument will be added in the future.

VEPO enables C-SWEPA and other users to see selected fluxes and spectra averaged over user-selected time intervals. VEPO is very useful for comparison of evolving flux spectra from solar energetic particle (SEP) events as observed by multiple spacecraft sources in the heliosphere. A key motivation of these VEPO services is to enable cross-comparison of spectra from different sensors on the same spacecraft and from different locations to check flux calibrations. This function becomes maximally useful in the case of inner heliospheric "reservoir events" in which spatial gradients vanish during the decay phases of some SEP events. C-SWEPA Collaborator John Cooper at NASA Goddard Space Flight Center is the Principal Investigator for VEPO. The web site is accessible at vepo.gsfc.nasa.gov.

Cooper is continuing analysis of the VEPO data to define whether the more continuous record of energetic particle flux measurements at 1 AU can approximately represent the flux environment at Mars and its moons Phobos and Deimos. One method of studying this problem is to compare the flux spectra at 1 AU to those measured by the Ulysses spacecraft when it crossed the Mars orbital range during initial flight to Jupiter and the three subsequent polar orbits of the Sun. This comparison will similarly be done for the earlier one-time traversals of the Mars orbit by Pioneer 10 & 11, Voyager 1 & 2, and more recently by the planetary Galileo Orbiter, Cassini, and New Horizons spacecraft, all carrying energetic particle sensors. Thus far, the Ulysses comparison shows no significant radial variation of fluxes averaged over multiple solar particle events. A similar comparison was also done between fluxes at 1 AU and at perihelion passages of Helios 1 & 2 with the same result, no significant radial variation in the inner heliosphere. It appears that the cumulative effect of many solar events, adding to the more uniform fluxes of inwardly diffusing cosmic ray particles from the outer heliosphere, is to produce a reservoir of relatively uniform intensity averaged over time throughout the inner heliosphere.

Relevant Presentations

- James, A., M. Stevens, K. Korreck, The Heating of Helium Across Interplanetary Shocks in Front of Coronal Mass Ejections, AAS, 2014 (Drew from shock database)
- Korreck, K., M. Stevens, S. Lepri, J. Kasper, Heavy Ion Heating at Shocks in the Heliosphere, Fall AGU, 2014 (Drew from shock database)
- Mike Stevens gave a colloquium at MIT's Plasma Science and Fusion Center IAP "Space Weather Research: Scientific and Social Issues of Living Near a Star" on Jan 14, 2015. He detailed the use of the database for shocks and SEP events.
- McGuire, R. E., D. Bilitza, R. Candey, R. Chimiak, J. Cooper, L. Garcia, B. Harris, R. Johnson, T. Kovalick, N. Lal, H. Leckner, M. Liu, N. Papitashvili, D. A. Roberts, Multi-Point Observations of the Inner Magnetosphere from the Van Allen Probes and Related Missions at NASA's Space Physics Data Facility (SPDF), Poster SM23B-4187, Fall 2014 AGU Meeting, San Francisco, CA, 2014.

- John Cooper presented remotely via WebEx at the splinter session "Harmonisation of SEP Data Calibrations" at the European Space Weather Week 11 (2014) conference in Liège, Belgium. He spoke on new scatterplot correlation functionality being implemented with the OMNIWeb services of the NASA Space Physics Data Facility (SPDF) in collaboration with the Virtual Energetic Particle Observatory (VEPO). John is Chief Scientist for SPDF and Principal Investigator for VEPO. Robert McGuire is SPDF Project Scientist. Natasha Papitashvili maintains OMNIWeb and created the new services as part of the SPDF-VEPO collaboration.
- John Cooper, Steven Sturner, Nikolaos Paschalidis, Richard Wesenberg, and Edward Sittler presented the talk "Natural Environmental Shielding Impacts on Missions to Extreme Radiation Environments" at the Second International Workshop on Instrumentation for Planetary Missions at GSFC during November 4-7, 2014. This talk addressed how Total Ionization Dosage (TID) is computed for Europa orbiter and flyby mission scenarios, and how moon body, ionospheric, and surface topographic shielding can reduce the spacecraft shielding requirements.
- John Cooper presented the talk "Space Weathering Applications of the Virtual Energetic Particle Observatory" at the Fall science team meeting of the DREAM2 (Dynamic Response of the Environments at Asteroids, the Moon, and Moons of Mars) in Greenbelt (2015). Led by William Farrell (695), DREAM2 is an interdisciplinary science team of NASA's Solar System Exploration Research Virtual Institute (SSERVI). Cooper leads the Virtual Energetic Particle Observatory (VEPO) in collaboration with Goddard's Space Physics Data Facility and DREAM2.
- John Cooper presented the talk, "Space Weather Investigations Enabled by the Virtual Energetic Particle Observatory," to the SEP Intercalibration Workshop as part of the Space Weather Workshop in Boulder, CO (2014). The particular value of VEPO was discussed for intercomparison of solar energetic particle data sets for the purpose of identifying and correcting calibration anomalies was discussed. So-called "reservoir events" after the peak phase of long duration SEP events, when flux spectra throughout the inner heliosphere are most similar even at widely separated spacecraft, were noted as ideal times for this purpose.
- Cooper, J. F., N. E. Papitashvili, N. Lal, R. C. Johnson, and R. E. McGuire, Enhanced Spectral Analysis of SEP Reservoir Events by OMNIWeb Multi-Source Browse Services of the NASA Space Physics Data Facility and the Virtual Energetic Particle Observatory, Triennial Sun-Earth Summit, Indianapolis, Indiana, April 26-30, 2015.
- Cooper, J. F., Time-Averaged Proton-Helium Flux Spectra Comparison at 1 AU and the Orbit of Mars, Exploration Science Forum/SSERVI, NASA Ames Research Center, July 20-22, 2016.
- Cooper, J. F., Virtual Energetic Particle Observatory: Radiation Environment at Mars and its Moons, Physics Dept. Seminar, Howard University, Sept. 28, 2016.
- Cooper, J. F., and N. E. Papitashvili, Space Weathering Radiation Environment of the Inner Solar System from the Virtual Energetic Particle Observatory (VEPO) and the NASA Space Physics Data Facility (SPDF), Fall 2016 Meeting, American Geophysical Union, Dec. 12-16, 2016.

- Cooper, J. F., Solar Energetic Radiation Impacts on Space Weathering: Mercury to Mars, 7th Solar Orbiter Workshop / Exploring the Solar Environs, Granada, Spain, April 3-6, 2017.

III Modifications of Scope and Justification

The original C-SWEPA proposal was extremely cross-disciplinary covering a range of topics: solar wind acceleration, CME initiation, the propagation of disturbances in the solar wind, impact of these disturbances on the magnetosphere, and particle acceleration and radiation effects. The key point made in the proposal is that by coupling MHD codes with particle propagation, acceleration codes and radiation codes (EPREM and EMMREM), we are capable of probing the impacts of solar disturbances across an immense range of scales and physical phenomena. The original proposed project including funding to explore physical effects and perform validation in all of the wide-ranging areas of investigation.

The grant awarded for C-SWEPA was only the portion of the project covering the following areas:

- Particle acceleration and propagation
- Radiation modeling and validation

The awarded funds were roughly 35% of the funding proposed.

As demonstrated by the wide-ranging achievements of the C-SWEPA team, we have managed to progress in most of the originally proposed areas. This is a remarkable achievement given the reduced C-SWEPA budget.

Despite reduced funding, the team felt that it should remain whole. While many individuals within the project have received almost no funding, we have kept the avenues open to collaboration. This has allowed the project to leverage a more cross-disciplinary approach than would have been possible otherwise.

Another key decision made early on was to maintain the goal of coupling the Predictive Science MHD models (CORHEL and MAS) with EPREM to explore the origins of particle acceleration in the low corona. This turned out to be extremely fortuitous since recent research largely coming from the C-SWEPA team is demonstrating that large SEP events arise likely from a “sweet spot” in particle acceleration beneath 5 solar radii [see Schwadron et al., 2015]. Ongoing work by K. Kozarev in the coming year (2016-2017) will further quantify the importance of the low corona for particle acceleration.

In terms of deliverables, the team remains committed to providing the community with both data products and models that will be useful. PREDICCS, the CME propagation database developed by Winslow et al. [2015], VEPO, and the Wind shock database are all excellent examples of such products. The team has already delivered EPREM and PREDICCS to the CCMC and is currently in the process of delivering several key new models. First, EPREM has been coupled with ENLIL including an embedded shock finder and diffusive shock solver that is showing great promise for predicting SEP events. Second, an EPREM-based cone model is also being delivered. The latter

allows for solutions of SEP events from the very low corona (inside of 2 solar radii) and therefore will allow researchers to develop insights about the potential for development of large SEP events from coronal observations.

Thus, although descoped compared to the original plan, the C-SWEPA projects has delivered what we proposed, and in most cases, delivered far greater scientific impact than originally anticipated. The highly cross-disciplinary nature of the project has allowed a rare and exceedingly important leveraging of scientific investigations, which has resulted in synthesis between disparate models and observations. Indeed, this type of cross-disciplinary research is at the heart of LWS science.

Lastly, we emphasize the importance of C-SWEPA for future projects such as Solar Orbiter and Solar Probe Plus. C-SWEPA provides the ability to integrate observations into a much wider purview of solar phenomena than had been originally anticipated. This type of global context will be critical on SPP and Solar Orbiter for developing an understanding of observations and their relationship to the solar events that create them. Collaboration with the SPP and Solar Orbiter teams is in its infancy, but will clearly prove to be a significant legacy of the C-SWEPA project.

IV Management Structure and Changes in Collaboration

As emphasized in Section V, the structure of the C-SWEPA team was not changed despite the large reduction in our original budget. In addition, we have added new young team members Reka Winslow (PostDoc), Colin Joyce (recently graduated), Junhong Chen (recently graduated) and Philip Quinn (Graduate Student). Junhong Chen and Colin Joyce graduated in 2016. Very recently, we learned that Colin Joyce has won an extremely prestigious award at the University of New Hampshire: the Graduate Student Research/Scholarship/Creativity award (2016).

Another important addition to the C-SWEPA team is Leila Mays of the CCMC. Dr. Mays works closely with Matt Gorby (UNH) on the application of C-SWEPA models at the CCMC. She is enormously hard-working and her efforts have been extremely visible to the community as evidenced by the wide-ranging invited talks involving C-SWEPA she has received.